JETP LETTERS VOLUME 69, NUMBER 2 25 JAN. 1999

The running BFKL: resolution of Caldwell's puzzle

N. N. Nikolaev*
Institut für Kernphysik, Forschungszentrum Jülich,, D-52425 Jülich, Germany
V. R. Zoller**
Institute of Theoretical and Experimental Physics, 117218 Moscow, Russia

(Submitted 21 December 1998)
Pis'ma Zh. Éksp. Teor. Fiz. **69**, No. 2, 92–97 (25 January 1999)

The HERA data on the proton structure function $F_2(x,Q^2)$ at very small x and Q^2 show a dramatic departure of the logarithmic slope $\partial F_2/\partial \log Q^2$ from theoretical predictions based on the DGLAP evolution. We show that the running BFKL approach provides a quantitative explanation for the observed x and/or Q^2 dependence of $\partial F_2/\partial \log Q^2$. © *1999 American Institute of Physics.* [S0021-3640(99)00302-3]

PACS numbers: 14.20.Dh

Caldwell's presentation of the HERA data in terms of the logarithmic derivative $\partial F_2/\partial \log Q^2$ for the proton structure function (SF) $F_2(x,Q^2)$ exhibits a turn-over of the slope towards small x and/or Q^2 down to the currently attainable $x \sim 10^{-6}$ and $Q^2 \sim 0.1$ GeV^2 (Refs. 1 and 2). The DGLAP evolution[3] with GRV input[4] predicts a steady increase of the derivative

$$\frac{\partial F_T^{\mathrm{DGLAP}}}{\partial \log Q^2} \propto \alpha_S(Q^2) G^{\mathrm{DGLAP}}(x,Q^2) \tag{1}$$

with $1/x$, due to the growth of the gluon structure function $G^{\mathrm{DGLAP}}(x,Q^2) = xg^{\mathrm{DGLAP}}(x,Q^2)$. A slight systematic discrepancy of the DGLAP analysis with the small-x data on $\partial F_2/\partial \log Q^2$ was also found in Ref. 5.

The turn-over point is located at $x \sim 5\times 10^{-4}$ and $Q^2 \sim 5$ GeV^2, values commonly believed to lie in a legitimate pQCD domain. Thus the phenomenon occurs at the boundary between ''soft'' and ''hard'' physics. Its explanation within the color dipole approach is based on two observations:[1)]

i) specific smallness of the $\log Q^2$ derivative of the subleading terms of the BFKL–Regge expansion of F_2 at the turn-over point, which is due to the nodal structure of the running BFKL eigen-SFs;

ii) a significant contribution to the small-Q^2 proton SF coming from the nonperturbative component of the BFKL pomeron.

The s-channel approach to the BFKL equation[7] was developed in terms of the color dipole cross section $\sigma(x,r)$ (Refs. 8 and 9; hereafter $\mathbf{r}$ is the color dipole moment). A positive feature of the color dipole picture, which will be referred to as the running BFKL approach, is the consistent incorporation of the two crucial properties of QCD: i) asymptotic freedom (AF), i.e., the running QCD coupling $\alpha_S(r)$, and ii) the finite propagation radius R_c of perturbative gluons.

The BFKL equation for the interaction cross section $\sigma(x,r)$ of the color dipole $\mathbf{r}$ with the target reads

$$\frac{\partial\sigma(x,r)}{\partial\log(1/x)}=\mathcal{K}\otimes\sigma(x,r)$$

$$=\frac{3}{8\pi^3}\int d^2\boldsymbol{\rho}_1|\boldsymbol{\mathcal{E}}(\boldsymbol{\rho}_1)-\boldsymbol{\mathcal{E}}(\boldsymbol{\rho}_2)|^2[\sigma(x,\rho_1)+\sigma(x,\rho_2)-\sigma(x,r)]. \tag{2}$$

Here the kernel $\mathcal{K}$ is related to the squared wave function of the color-singlet $q\bar{q}g$ state with the Weizsäcker–Williams (WW) soft gluon. The quantity

$$\boldsymbol{\mathcal{E}}(\boldsymbol{\rho})=-g_S(\rho)\boldsymbol{\nabla}_\rho K_0(\mu_G\rho)=g_S(\rho)\mu_G K_1(\mu_G\rho)\boldsymbol{\rho}/\rho, \tag{3}$$

where $R_c=1/\mu_G$ and $K_\nu(x)$ is the modified Bessel function, describes a Yukawa screened transverse chromoelectric field of the relativistic quark, and $|\mathcal{E}(\boldsymbol{\rho}_1)-\mathcal{E}(\boldsymbol{\rho}_2)|^2$ describes the flux (the modulus of the Poynting vector) of WW gluons in the $q\bar{q}g$ state, in which $\mathbf{r}$ is the $\bar{q}$–q separation and $\boldsymbol{\rho}_{1,2}$ are the q–g and $\bar{q}$–g separations in the two-dimensional impact parameter plane. Our numerical results are for the Yukawa screening radius $R_c=0.27$ fm. Recent fits to the lattice QCD data on the field strength correlators suggest similar values of R_c (Ref. 10).

The asymptotic freedom of QCD uniquely prescribes that the chromoelectric field be computed with the running QCD charge $g_S(r)=\sqrt{4\pi\alpha_S(r)}$ taken at the shortest relevant distance in the $q\bar{q}g$ system, $R_i=\min\{r,\rho_i\}$. Although the running coupling thus introduced does not necessarily exhaust all NLO effects, it correctly describes the crucial enhancement of long-distance, and suppression of short-distance effects by the AF.

The properties of the running color dipole BFKL equation responsible for the observed Q^2 dependence of $\partial F_2/\partial\log Q^2$ are as follows.[11,12] The spectrum of the running BFKL equation is a series of moving poles in the complex j plane, with eigenfunctions

$$\sigma_n(x,r)=\sigma_n(r)\exp[\Delta_n\log(1/x)], \tag{4}$$

which are solutions of

$$\mathcal{K}\otimes\sigma_n=\Delta_n\sigma_n(r). \tag{5}$$

The leading eigenfunction $\sigma_0(r)$ is node-free. The subleading $\sigma_n(r)$ has n nodes. The intercepts Δ_n closely, to better than 10%, follow the law $\Delta_n=\Delta_0/(n+1)$ suggested earlier by Lipatov.[13] The intercept of the leading pole trajectory, with the above specific choice of R_c, is $\Delta_0\equiv\Delta_{\mathbf{P}}=0.4$. The subleading eigenfunctions σ_n (Refs. 11 and 12) are very close to Lipatov's quasi-classical solutions[13] for $n\gg1$. For our specific choice of the infrared regulator, R_c, the node of $\sigma_1(r)$ is located at $r=r_1\simeq0.05$–0.06 fm, for larger n the first node moves to a somewhat larger value $r\sim0.1$ fm.

The color dipole factorization[14] in conjunction with the explicit form of the $q\bar{q}$ light-cone wave function $\Psi_{qq}(z,r)$ relates the dipole cross sections $\sigma_n(r)$ with the eigen-SF $f_n(Q^2)$,

$$f_n(Q^2)=\frac{Q^2}{4\pi^2\alpha_{em}}\sum_{q=u,d,c,s}\int_0^1 dz\int d^2\mathbf{r}|\Psi_{qq}(z,r)|^2\sigma_n(r). \tag{6}$$

The BFKL–Regge expansion

$$\sigma(x,r)=\sigma_0(r)(x_0/x)^{\Delta_0}+\sigma_1(r)(x_0/x)^{\Delta_1}+\sigma_2(r)(x_0/x)^{\Delta_2}+\dots \tag{7}$$

gives the BFKL–Regge expansion for the SF:

$$F_2(x,Q^2)=\sum_n f_n(Q^2)(x_0/x)^{\Delta_n}. \tag{8}$$

The remarkable finding of Refs. 15, 11, and 12 is a good description of the HERA data on the proton SF starting with the Born two-gluon cross section $\sigma_B(r)$ as a boundary condition for the running BFKL equation (2) at $x_0=0.03$. With such a boundary condition, which could well be excessively restrictive, the expansion (7) fixes uniquely the normalization of the eigen-SFs.

The Bjorken variable $x=Q^2/2m_p\nu$ is commonly used for the presentation of experimental data even for $Q^2\lesssim m_\rho^2$, way beyond the kinematical region $Q^2\gg m_\rho^2$ it was originally devised for. At small Q^2, the relevant Regge parameter is $2m_p\nu/(Q^2+m_\rho^2)$ rather than $1/x$. Consequently, in the small-Q^2 region the Regge parameter x_0/x in Eqs. (7) and (8) must be replaced by $(x_0/x)(1+m_\rho^2/Q^2)$.

One more remark on kinematics is in order. The BFKL–Regge expansion (8) holds at small $x\lesssim 10^{-2}$. In order to model the sea contribution at larger x we multiply (8) by the familiar factor $(1-x)^m$, with $m=5$. This factor does not affect the diffraction region but strongly suppresses the production of gluons with $x\gtrsim 0.1$.

In applications it is convenient to work with $f_n(Q^2)$ represented in an analytical form. For the leading singularity we have

$$f_0(Q^2)=a_0\frac{R_0^2Q^2}{1+R_0^2Q^2}[1+c_0\log(1+r_0^2Q^2)]^{\gamma_0}, \tag{9}$$

which has the large-Q^2 asymptotic form[16,9]

$$f_0(Q^2)\propto[\alpha_s(Q^2)]^{-\gamma_0},\quad \gamma_0=\frac{4}{3\Delta_0}. \tag{10}$$

For $n\geq 1$ the functions $f_n(Q^2)$ can be approximated by

$$f_n(Q^2)=a_nf_0(Q^2)\frac{1+R_0^2Q^2}{1+R_n^2Q^2}\prod_{i=1}^{n_{\max}}\left(1-\frac{z}{z_n^{(i)}}\right), \tag{11}$$

where

$$z=[1+c_n\log(1+r_n^2Q^2)]^{\gamma_n}-1,\quad \gamma_n=\gamma_0\delta_n \tag{12}$$

and $n_{\max}=\min\{n,2\}$.

Since the relevant variable is a power of the inverse gauge coupling, the nodes of $f_n(Q^2)$ are spaced by 2–3 orders of magnitude on the Q^2 scale, and only the first two of them are in the accessible range of Q^2 (Refs. 11 and 12). The first nodes of subleading

TABLE I.

n	a_n	c_n	r_n^2, GeV^{-2}	R_n^2, GeV^{-2}	$z_n^{(1)}$	$z_n^{(2)}$	δ_n	Δ_n
0	0.0232	0.3261	1.1204	2.6018				0.40
1	0.279	0.1113	0.8755	3.4648	2.4773		1.0915	0.220
2	0.195	0.0833	1.5682	3.4824	1.7706	12.991	1.2450	0.148
3	0.471	0.0653	3.9567	2.7756	1.4963	6.9160	1.2284	0.111

$f_n(Q^2)$ are located at $Q^2\sim 20$–60 GeV^2, the second nodes of $f_2(Q^2)$ and $f_3(Q^2)$ are at $Q^2\simeq 5\times 10^3$ GeV^2 and $Q^2\simeq 2\times 10^4$ GeV^2, respectively. The parametrization tuned to reproduce the numerical results for $f_n(Q^2)$ at $Q^2\lesssim 10^5$ GeV^2 is given by Eq. (11). For $n=3$ we take a simplified form with only the first two nodes, because the third node of $f_3(Q^2)$ is at $\sim 2\times 10^7$ GeV^2, way beyond the reach of accelerator experiments at small x. The found parameters are listed in Table I.

Asymptotically, at $1/x\to\infty$, the expansion (8) is dominated by the term $f_0(Q^2)\times(x_0/x)^{\Delta_0}$. At moderately small x the subleading terms are equally important since $\Delta_n\sim 1/n$. However, as was pointed out in Refs. 11 and 12, for $Q^2\lesssim 10^4$ GeV^2 all $f_n(Q^2)$ with $n\geqslant 3$ are very similar in shape. Then we arrive at the truncated expansion

$$F_2(x,Q^2)=\sum_{n=0}^{3} f_n(Q^2)(x_0/x)^{\Delta_n}+F_2^{\mathrm{soft}}(Q^2)+F_2^{\mathrm{val}}(x,Q^2), \tag{13}$$

where the term $f_3(Q^2)(x_0/x)^{\Delta_3}$ with the properly adjusted weight factor a_3 stands for all terms with $n\geqslant 3$. The addition of this ''background'' term in Eq. (13) improves significantly the agreement with the data for large Q^2, thus expanding the applicability region of Eq. (13) over the whole small-x kinematical domain of HERA.

The need for a soft pomeron contribution F_2^{soft} in addition to the perturbative BFKL SFs described previously arises from phenomenological considerations. A viable BFKL phenomenology of the rising component of the proton structure function over the whole range of Q^2 studied at HERA (real photoabsorption included) is obtained if one starts with the Born dipole cross section $\sigma_B(r)$ as a boundary condition for the BFKL evolution at $x_0=0.03$.[17,12] However, such a purely perturbative input, $\sigma_B(r)$, with $R_c=0.27$ fm strongly underestimates the cross sections of soft processes and the proton SF at moderate $Q^2\sim 1$ GeV^2. Therefore, at $r\gtrsim R_c$ the above-described perturbative BFKL dipole cross section $\sigma_{\mathrm{pt}}(x,r)$ must be complemented by the contribution from the nonperturbative soft pomeron, $\sigma_{\mathrm{npt}}(x,r)$. In terms of the relationship[17] between $\sigma(x,r)$ and the gluon structure function of the proton, $G(x,Q^2)$, the nonperturbative dipole cross section $\sigma_{\mathrm{npt}}(r)$ at $r\gtrsim R_c$ must be associated with soft nonperturbative gluons in the conventional $G(x,Q^2)$. The contribution to $G(x,Q^2)$ from the nonperturbative transverse momenta $k^2\lesssim Q_0^2\sim m_\rho^2$ persists at all Q^2 and must not be subjected to the DGLAP evolution.

Because the BFKL rise of $\sigma(x,r)$ is due to the production of s-channel perturbative gluons, which does not contribute to $\sigma_{\mathrm{npt}}(r)$, we have argued[17,12] that to a first approximation one should consider an energy-independent $\sigma_{\mathrm{npt}}(r)$ and additivity of the scattering amplitudes from both the hard BFKL and soft nonperturbative mechanisms. For recent suggestions that our $\sigma_{\mathrm{npt}}(r)$ be identified with the soft pomeron of the two-

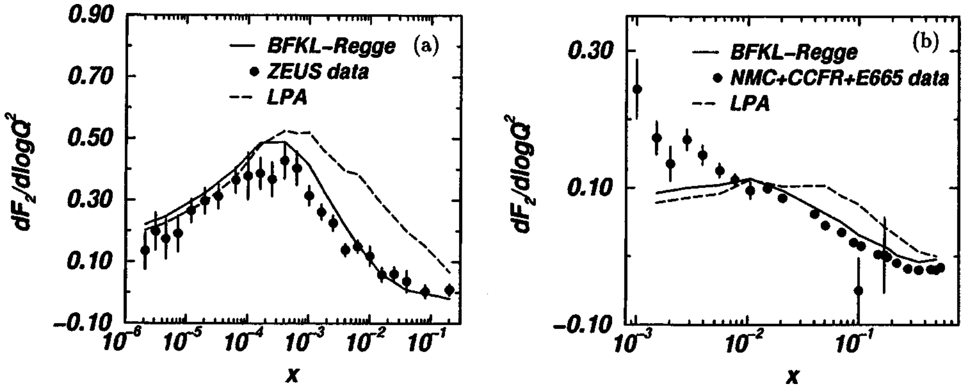

FIG. 1. Caldwell's plot of $\partial F_2/\partial \log Q^2$ for the ZEUS data[2] (a) and fixed target data[1] (b). Our predictions (BFKL–Regge) are shown by the solid lines. Shown by the dashed lines is the leading BFKL pole approximation (LPA).

pomeron picture see Refs. 18 and 19. In the models of soft scattering via polarization of the nonperturbative QCD vacuum,[20,21] $\sigma_{\rm npt}(r)$ is interpreted in terms of the nonperturbative gluon distributions.

In our opinion, the recently encountered troubles with the small-Q^2 extrapolations of the DGLAP evolution[5] and the failure of DGLAP fits in the Caldwell plot[1,2] are due to illegitimate imposing of the DGLAP evolution upon the nonperturbative glue.

The nonperturbative term $F_2^{\rm soft}(Q^2)$ in Eq. (13) calculated from Eq. (6) with $\sigma = \sigma_{\rm npt}(r)$ from Ref. 22 can be parametrized as follows:

$$F_2^{\rm soft}(Q^2)=b\frac{R^2Q^2}{1+R^2Q^2}[1+c\log(1+r^2Q^2)], \tag{14}$$

where $b=0.1077$, $c=0.0673$, $R^2=6.6447\ {\rm GeV}^{-2}$, and $r^2=7.0332\ {\rm GeV}^{-2}$. Thus its $\log Q^2$ derivative levels off at very small $Q^2\sim 0.15\ {\rm GeV}^2$ and does not contribute to the observed growth of $\partial F_2/\partial \log Q^2$.

In Fig. 1 we compare our estimates to both the HERA data and the fixed target data. In Ref. 2 the logarithmic slope $\partial F_2/\partial \log Q^2$ is derived from the data by fitting $F_2=a+b\log Q^2$ in bins of fixed x. The average value of Q^2 in each x-bin, $\langle Q^2\rangle$, is derived from the F_2-weighted mean value of $\log Q^2$ in that bin.

As we have noted above, at moderately small $x\sim 10^{-2}$–10^{-3} the contribution of the subleading poles to $F_2(x,Q^2)$ is still substantial (the relative weight factors, a_n, with $n\geqslant 1$ are presented in Table I), but toward the region of $x\sim 10^{-6}$ the leading pole contribution starts to prevail. At small Q^2 the ratio of $\log Q^2$ derivatives, $r_n=f'_n/f'_0$, can be estimated as

$$r_n\simeq a_n\frac{\Lambda_0^2}{\Lambda_n^2}\left(\frac{x}{x_0}\right)^{\Delta_0-\Delta_n}, \tag{15}$$

where

$$\Lambda_n^2\simeq 1/(R_n^2-c_0\gamma_0 r_0^2). \tag{16}$$

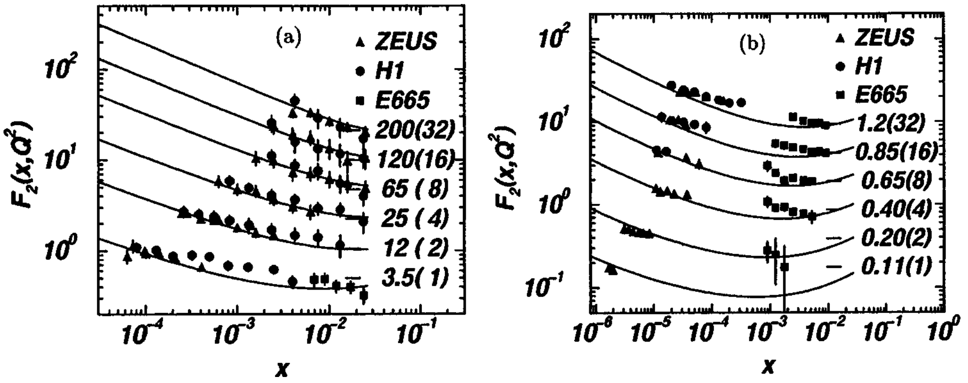

FIG. 2. Description of the H1, ZEUS and E665 $F_2(x,Q^2)$ data by the BFKL–Regge expansion (13): a — the large-Q^2 data ($Q^2=3.5$, 12, 25, 65, 120 and 200 GeV^2); b — the small-Q^2 data ($Q^2=0.11$, 0.20, 0.40, 0.65, 0.85 and 1.2 GeV^2). For display purposes we have multiplied F_2 by the numbers shown in brackets.

Because the subleading SFs $f_n(Q^2)$ have a node at $Q^2\sim 20$–60 GeV^2 (Refs. 11 and 12), their contribution to the slope $\partial F_2/\partial\log Q^2$ vanishes at $Q^2\sim 5-10$ GeV^2, which is very close to the turn-over point in the HERA data. Hence $\partial F_2/\partial\log Q^2$ at small Q^2 follows closely $\partial f_0/\partial\log Q^2$. From (9) it follows that at small Q^2, $f_0(Q^2)$ behaves like $\sim Q^2/(\Lambda_0^2+Q^2)$, with $\Lambda_0^2\simeq 0.72$ GeV^2 coming from (16). Therefore, $\partial F_2/\partial\log Q^2$ rises with Q^2 up to $Q^2\sim 1$ GeV^2 and then levels off. Only at large Q^2, when the sub-leading terms enter the game, $\partial F_2/\partial\log Q^2$ decreases and even becomes negative-valued at large x. Our estimates shown in Fig. 1a are in good agreement with HERA data.[2] The curves are somewhat wiggly because the x–$\langle Q^2\rangle$ correlation of the experimental data is non-monotonic.

In Fig. 1b we compare our predictions with the fixed target data.[1] Variation of the slope in this case is less pronounced, since the starting value of $\langle Q^2\rangle$ is $\langle Q^2\rangle\simeq 0.54$ GeV^2 at $x\simeq 10^{-3}$ (compare with $Q^2=0.12$ GeV^2 at $x=2.1\times 10^{-6}$ at HERA). It can easily be seen that the derivative $\partial f_0/\partial\log Q^2$ at such Q^2 is a rather slow function of Q^2. The agreement of our estimates with the fixed target data is quite reasonable, though there is a systematic discrepancy at small x. We recall that there is a certain mismatch between the E665 and H1/ZEUS data on $F_2(x,Q^2)$ in the close (x,Q^2) bins (see Fig. 2a and 2b).

*e-mail: kph154@ikp301.ikp.kfa-juelich.de

**e-mail: zoller@heron.itep.ru

[1)] The preliminary results have been reported at the DIS'98 Workshop.[6]

---

[1] A. Caldwell, *DESY Theory Workshop*, DESY, October 1997.

[2] ZEUS Collaboration, J. Breitweg *et al.*, Report # DESY-98-162.

[3] V. N. Gribov and L. N. Lipatov, Sov. J. Nucl. Phys. **15**, 438 (1972); G. Altarelli and G. Parisi, Nucl. Phys. B **126**, 298 (1977); Yu. L. Dokshitzer, Sov. Phys. JETP **46**, 641 (1977).

[4] M. Glück, E. Reya, and A. Vogt, Z. Phys. C **67**, 433 (1995).

[5] A. D. Martin, R. G. Roberts, W. J. Stirling, and R. S. Thorne, Report # DTP-98-10; RAL-TR-98-029.

[6] V. R. Zoller, in *Proceedings of the 6th International Workshop on DIS and QCD (DIS 98)*, Brussels, 1998; Report # FZ-IKP(TH)-1998-5.

[7] E. A. Kuraev, L. N. Lipatov and V. S. Fadin, Sov. Phys. JETP **44**, 443 (1976); **45**, 199 (1977); Ya. Ya. Balitskii and L. N. Lipatov, Sov. J. Nucl. Phys. **28**, 822 (1978).

[8] N. N. Nikolaev, B. G. Zakharov, and V. R. Zoller, JETP Lett. **59**, 8 (1994).
[9] N. N. Nikolaev, B. G. Zakharov, and V. R. Zoller, JETP **78**, 806 (1994).
[10] E. Meggiolaro, Report # HD-THEP-98-34.
[11] V. R. Zoller, in *Proceedings of the 5th International Workshop on DIS and QCD (DIS 97)*, Chicago, Ill., 1997.
[12] N. N. Nikolaev, B. G. Zakharov, and V. R. Zoller, JETP Lett. **66**, 138 (1997).
[13] L. N. Lipatov, Sov. Phys. JETP **63**, 904 (1986).
[14] N. N. Nikolaev and B. G. Zakharov, Z. Phys. C **49**, 697 (1991).
[15] N. N. Nikolaev and B. G. Zakharov, Phys. Lett. B **333**, 250 (1994).
[16] N. N. Nikolaev and B. G. Zakharov, Phys. Lett. B **327**, 157 (1994).
[17] N. N. Nikolaev and B. G. Zakharov, Phys. Lett. B **327**, 149 (1994).
[18] A. Donnachie and P. V. Landshoff, Phys. Lett. B **437**, 408 (1998).
[19] K. Golec-Biernat and M. Wüsthoff, Report # DTP-98-50.
[20] P. V. Landshoff and O. Nachtmann, Z. Phys. C **35**, 405 (1987).
[21] H. G. Dosch, T. Gousset, G. Kulzinger *et al.*, Phys. Rev. D **55**, 2602 (1997).
[22] J. Nemchik, N. N. Nikolaev, E. Predazzi *et al.*, JETP **86**, 1054 (1998).

Published in English in the original Russian journal. Edited by Steve Torstveit.

JETP LETTERS VOLUME 69, NUMBER 2 25 JAN. 1999

Four-wave mixing under conditions of Doppler-free resonance induced by strong radiation

A. K. Popov* and A. S. Baev

Institute of Physics, Siberian Branch of the Russian Academy of Sciences; Krasnoyarsk State Technical University, 660036 Krasnoyarsk, Russia

(Submitted 11 December 1998)
Pis'ma Zh. Éksp. Teor. Fiz. **69**, No. 2, 98–103 (25 January 1999)

The possibilities of enhancing the nonlinear optical response of a gaseous medium and the radiation conversion efficiency in four-wave mixing processes through the use of atomic coherence effects and the induced elimination of the Doppler broadening of resonances are investigated. Numerical illustrations of the effects are given for experiments in progress. © *1999 American Institute of Physics.* [S0021-3640(99)00402-8]

PACS numbers: 42.65.Hw

1. A great deal of attention is being devoted to experimental and theoretical investigations of resonant coherent interaction of electromagnetic fields on quantum transitions (see, for example, Refs. 1 and 2). This is explained by the favorable possibilities of studying quantum interference phenomena that in turn form the basis for the manipulation of the nonlinear optical properties of atomic–molecular systems and resonant conversion of laser radiation. There are substantially fewer publications on the characteristic features of the coherent interaction at Doppler-broadened transitions, which strongly influence the manifestation of the processes indicated. Our objective in the present letter is to show that new resonances in the nonlinear susceptibility, which are free of Doppler broadening, can be produced using auxiliary strong fields and atomic coherence. A substantial increase in the quantum efficiency of conversion is achieved even though the absorption of the initial radiations increases at the same time. A model corresponding to the experimental conditions of Ref. 1 is used for numerical illustrations. The elementary physical processes on which the proposed method is based and which consist of a change in the frequency-correlation properties of multiphoton processes in strong electromagnetic fields are discussed in greater detail in Ref. 3.

2. Consider the interaction scheme presented in Fig. 1. The wave $\mathbf{E}_3(t,\mathbf{r})$, interacting with the transition 2–3, consists of two components, $E_3^+(t,\mathbf{r})$ and $E_3^-(t,\mathbf{r})$, having the same frequencies but propagating in opposite directions. The wave vector of the component E_3^+ and the wave vector of the component E_3^- are parallel and antiparallel, respectively, to the wave vectors $\mathbf{k}_1$ and $\mathbf{k}_2$. It is assumed that only the lower level is occupied, and the radiation field at the 0–1 transition is so weak that the change in the population of this level can be neglected. The component E_3^+ of the field at the frequency ω_3 is also

© 1999 American Institute of Physics

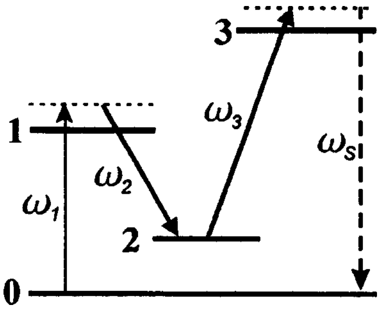

FIG. 1. Resonant four-wave interaction scheme.

weak, and the component E_3^- and the field E_2, interacting with the transition 1–2, can be of arbitrary intensity.

The system of equations for the density matrix in the interaction representation has the form

$$L_{03}\rho_{03}=i\{\rho_{00}V_{03}+\rho_{02}(V_{23}^{+}+V_{23}^{-})\},\quad L_{01}\rho_{01}=i\{\rho_{00}V_{01}+\rho_{02}V_{21}\},$$

$$L_{02}\rho_{02}=i\{\rho_{01}V_{12}+\rho_{03}(V_{32}^{+}+V_{32}^{-})\}, \tag{1}$$

where

$$L_{ij}=\partial/\partial t+\mathbf{v}\cdot\boldsymbol{\nabla}+\Gamma_{ij},\quad V_{ij}=G_{ij}\exp\{i(\Omega_i t-k_i z)\},$$

$$V_{23}^{\pm}=G_{23}^{\pm}\exp\{i(\Omega_3 t\mp k_3 z)\},\quad G_{ij}=-E_j d_{ij}/2\hbar,\quad \text{and}\quad G_{23}^{\pm}=-E_3^{\pm}d_{23}/2\hbar$$

are the Rabi frequencies characterizing the interaction, Ω_i is the detuning from resonance for the corresponding resonant field (for example, $\Omega_1=\omega_1-\omega_{01}$), and Γ_{ij} are the homogeneous half-widths of the transitions.

Thus, the induced atomic coherence ρ_{02} is a source of new components in the polarizations responsible for the absorption and generation of radiation. We shall represent the off-diagonal elements ρ_{01}, ρ_{02}, and ρ_{03} as products of amplitude and phase factors:

$$\rho_{01}=r_{01}\exp\{i(\Omega_1-k_1 z)\}+r_{01}^{-}\exp\{i[\Omega_1 t-(k_2+k_3+k_4)z]\},$$

$$\rho_{02}=r_{02}\exp\{i[(\Omega_1-\Omega_2)t-(k_1-k_2)z]\}+r_{02}^{-}\exp\{i[(\Omega_1-\Omega_2)t-(k_3+k_4)z]\},$$

$$\rho_{03}=r_{03}\exp\{i[\Omega_4 t-k_4 z]+\tilde{r}_{03}^{+}\exp\{i[(\Omega_1-\Omega_2+\Omega_3)t-(k_1-k_2+k_3)z]\}$$

$$+\tilde{r}_{03}^{-}\exp\{i[(\Omega_1-\Omega_2+\Omega_3)t-(k_1-k_2-k_3)z]\}.$$

Substituting these expressions into Eq. (1) and solving the system of algebraic equations for the amplitudes of the off-diagonal elements of the density matrix, we obtain expressions for the off-diagonal element r_{03} characterizing absorption and refraction of the wave E_4 in the presence of the strong fields E_2 and E_3^- and for the off-diagonal element $\tilde{r}_{03}^{+}$ responsible for nonlinear polarization and susceptibility at the generated frequency $\omega_S=\omega_1-\omega_2+\omega_3$:

$$r_{03}=i\frac{G_{03}}{P_{03}}\frac{P_{01}^{-}P_{02}^{-}+|G_{12}|^{2}}{P_{01}^{-}\{P_{02}^{-}+|G_{23}^{-}|^{2}/P_{03}+|G_{12}|^{2}/P_{01}^{-}\}}, \tag{2}$$

$$\tilde{r}_{03}^{+}=r_{01}\frac{G_{12}G_{23}^{+}}{P_{02}P_{03}^{+}}\frac{1}{1+|G_{23}^{-}|^{2}/P_{03}^{-}P_{02}}\frac{1}{1+|G_{23}^{-}|^{2}/P_{03}^{+}P_{02}^{-}}, \tag{3}$$

where

$$P_{02}=\Gamma_{02}+i[\Omega_1-\Omega_2-(k_1-k_2)v], \quad P_{02}^{-}=\Gamma_{02}+i[\Omega_1-\Omega_2-(k_3+k_4)v],$$

$$P_{03}=\Gamma_{03}+i(\Omega_4-k_4v),$$

$$P_{03}^{-}=\Gamma_{03}+i(\Omega_1-\Omega_2+\Omega_3-k_S^{-}v), \quad P_{03}^{+}=\Gamma_{03}+i(\Omega_1-\Omega_2+\Omega_3-k_S^{+}v),$$

$$P_{01}^{-}=\Gamma_{01}+i[\Omega_1-(k_2+k_3+k_4)v], \quad k_S^{-}=k_1-k_2-k_3, \quad k_S^{+}=k_1-k_2+k_3,$$

and v is the projection of the velocity of the atom on the z direction.

The solution for the off-diagonal element r_{01}, characterizing absorption and refraction of the E_1 wave in the presence of the strong fields E_2 and E_3^{-}, has the form[4]

$$r_{01}=-i\frac{G_{01}}{P_{01}}\frac{P_{02}P_{03}^{-}+|G_{23}^{-}|^{2}}{P_{03}^{-}\{P_{02}+|G_{23}^{-}|^{2}/P_{03}^{-}+|G_{12}|^{2}/P_{01}\}}, \tag{4}$$

where $P_{01}=\Gamma_{01}+i(\Omega_1-k_1v)$. Using it, in lowest order of perturbation theory in G_{23}^{+} we obtain from Eq. (3) the solution for the off-diagonal element $\tilde{r}_{03}^{+}$:

$$\tilde{r}_{03}^{+}=\frac{i}{P_{01}}\frac{G_{01}G_{12}G_{23}^{+}}{(P_{02}+|G_{23}^{-}|^{2}/P_{03}^{-}+|G_{12}|^{2}/P_{01})(P_{03}^{+}+|G_{23}^{-}|^{2}/P_{02}^{+})}. \tag{5}$$

As the intensity of the interacting radiations increases, the nonlinear polarization at first increases and then saturates. The higher the intensity, the larger the detunings from the resonances and the higher the polarizations at which saturation occurs. Intensities corresponding to resonant or quasiresonant optimal conditions are characteristic for continuous-wave lasers. In gaseous media which possess sharper and stronger resonances than condensed media, on account of Doppler effects only a small fraction of the atoms is in one of the resonances.

We shall show that this limitation can be overcome by making use of the effects considered above. For detunings from the unperturbed resonances substantially greater than the corresponding Doppler widths, $|G|^2/P \approx |G|^2/p - ikv|G|^2/p^2$, where p are the corresponding P factors at $v=0$. Thus, together with a shift and broadening of the resonances, strong fields induce additional Doppler shifts.[3,5] Since $\mathrm{Re}\{|G|^2/p^2\}<0$, $k_S^{-}<0$, it follows from Eq. (5) that there can be total compensation of the Doppler shifts and elimination of the inhomogeneous broadening of a two-photon resonance modified by strong fields. Since in the process all atoms, irrespective of their velocities, are simultaneously entrapped in the indicated resonance, a substantial increase of the nonlinear susceptibility and a simultaneous decrease of the saturation of nonlinear polarization can be expected. Using the indicated procedure, the cofactor, describing the modified two-photon resonance, in the denominator of Eq. (5) can be represented in the form

$$\begin{aligned}\tilde{P}_{02} &\equiv P_{02}+|G_{12}|^2/P_{01}+|G_{23}^-|^2/P_{03}^- \\ &\approx \tilde{\Gamma}_{02}+i\tilde{\Omega}_{02}-i\left\{\left(1+\frac{|G_{23}^-|^2}{\Omega_4^2}\right)(k_1-k_2)+\frac{|G_{12}|^2}{\Omega_1^2}k_1-\frac{|G_{23}^-|^2}{\Omega_4^2}k_3\right\}v,\end{aligned} \tag{6}$$

where $\tilde{\Gamma}_{02}$ and $\tilde{\Omega}_{02}$ are the half-width and the position of the resonance with the field-induced broadening and shift taken into account. The conditions for eliminating the dependence on v and therefore the Doppler broadening of the induced resonance follow from Eq. (6).

We underscore that all effects considered here and below are in no way due to the motion of populations, but rather they are a consequence of the appearance of coherent superpositions of quantum states as a result of the modulation of the wave functions in strong fields.[3] This is reflected in the appearance of traveling waves of coherence (described by the off-diagonal elements of the density matrix) on forbidden transitions and in the modification of their spectral dependences.

In contrast to the absorption and refraction processes studied in Ref. 3, where the relative directions of propagation of the interacting waves can be arbitrary, frequency-mixing processes require wave matching. This dictates only parallel directions of propagation of the parametrically interacting waves. The strong counterpropagating wave E_3^- does not participate directly in the photon conversion process. It only perturbs the quantum system. The effect can also be interpreted as a contribution of higher-order resonance processes, in which the number of absorbed and emitted counterpropagating photons is the same, so that this does not result in momentum nonconservation for the photons undergoing conversion. The resonances of the system and the degree of their inhomogeneous broadening can be manipulated by making use of the counterpropagating wave, and in this manner the conversion of radiations can be improved by making the correct choice of their intensity and frequency.

In contrast to cascade schemes, for transitions of the Raman scattering type k_1 is always greater than k_2. Induced elimination of the Doppler broadening of a quasi-two-photon transition by the strong field E_2 is impossible. The proposed method, which is based on the use of an additional counterpropagating wave E_3^-, makes it possible to overcome this limitation.

3. We shall illustrate the results of averaging with a Maxwellian velocity distribution and the effect of eliminating the Doppler broadening of the induced resonances on the absorption and the nonlinear susceptibility. For numerical analysis, we employ the parameters of the transitions of the sodium dimer molecule with the following wavelengths:[1] $\lambda_{01}=661$ nm, $\lambda_{12}=746$ nm, $\lambda_{23}=514$ nm, and $\lambda_{03}=473$ nm. The corresponding homogeneous half-widths of the transitions are 20.69, 23.08, 18.30, and 15.92 MHz, and the Doppler half widths are 0.678, 0.601, 0.873, and 0.948 GHz.

Figure 2 shows the normalized squared modulus of the velocity-averaged nonlinear susceptibility ($\tilde{\chi}$) that determines the four-wave interaction of the radiations versus the probe-field detuning normalized to the Doppler half-width ($\Delta\omega_{1D}$) of its transition. Normalization was performed for the value of the same quantity in the frequency range of interest in the absence of the counterpropagating wave. The strong field of the counterpropagating wave produces a substantial shift and narrowing of the resonance in the

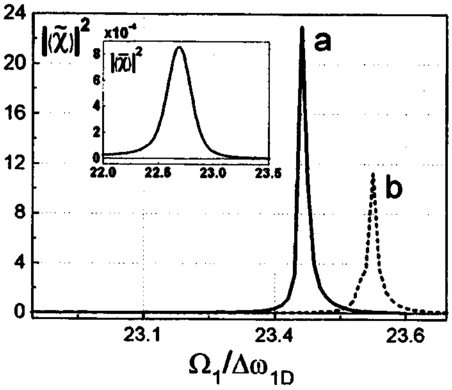

FIG. 2. Doppler-free resonance induced in the nonlinear susceptibility by the strong radiation of a counterpropagating wave. $\langle\tilde{\chi}\rangle$ is the velocity-averaged value of the normalized nonlinear susceptibility: a — under conditions of complete compensation of the Doppler broadening of the transition 0–2; b — under conditions of partial compensation, $\langle\bar{\chi}\rangle$ is the same, in the absence of the counterpropagating wave.

nonlinear susceptibility. This follows from a comparison of the curve in the inset, showing the spectral dependence of the same quantity in the absence of the counterpropagating wave and normalized to the corresponding value with simultaneous exact one- and multiphoton resonances in vanishingly weak fields. The Rabi frequency and detuning of the field E_2 are 2.35 GHz and 18.46 GHz $(27.2\cdot\Delta\omega_{1D})$, and the detuning of the field E_3^- is 1.83 GHz $(2.7\cdot\Delta\omega_{1D})$. Curve (a) corresponds to the optimal Rabi frequency, 0.89 GHz, of the field E_3^- in which Doppler broadening of the transition 0–2 is eliminated. For curve (b) the Rabi frequency, 1.06 GHz, is higher than the optimal value. The half-width of the resonance in the inset is approximately 80 MHz, which corresponds to a Doppler width of the unperturbed Raman transition of 7.8 MHz for resonance (a) and 8.4 MHz for resonance (b).

The formulas for the absorption coefficients have the form

$$\alpha_1(\Omega_1)=\alpha_{01}\,\mathrm{Re}\left\{\frac{\Gamma_{01}}{P_{01}}\,\frac{P_{02}P_{03}^-+|G_{23}^-|^2}{P_{03}^-\{P_{02}+|G_{23}^-|^2/P_{03}^-+|G_{12}|^2/P_{01}\}}\right\}, \tag{7}$$

$$\alpha_3(\Omega_S)=\alpha_{03}\,\mathrm{Re}\left\{\frac{\Gamma_{03}}{P_{03}}\,\frac{P_{01}^-P_{02}^-+|G_{12}|^2}{P_{01}^-\{P_{02}^-+|G_{23}^-|^2/P_{03}+|G_{12}|^2/P_{01}^-\}}\right\}. \tag{8}$$

Analysis of these velocity-averaged expressions shows that the maxima of the absorption and nonlinear susceptibility as a function of Ω_1 do not coincide with each other.

4. Let us consider the combined effect of induced Doppler-free resonances in the absorption and nonlinear polarization on the generation of radiation. We seek a solution in the form

$$E^j(z,t)=\mathrm{Re}\{E_j(z)\exp[i(\omega_j t-k_j z)]\}, \tag{9}$$

where k_j is the complex wave number at the corresponding frequency $k_j=k_j'-i\alpha_j/2$.

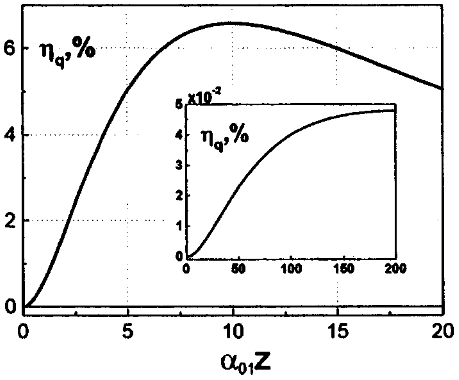

FIG. 3. Increase in the quantum efficiency of the conversion of E_1 into E_S radiation as a result of an induced Doppler-free resonance (α_{01z} is the optical thickness of the medium at frequency ω_{01}).

We shall confine our attention to the case of relatively small conversion factors, such that the fields E_2 and $E_3^{\pm}$ can be assumed to be constant throughout the medium, and only exponential absorption is taken into account for E_1. Then the truncated equation for $E_S(z)$ has the form

$$dE_S(z)/dz = i2\pi k'_S \chi_S^{(3)} E_1(0) E_2^* E_3 \exp(-i\Delta kz), \tag{10}$$

where $\chi_S^{(3)}$ is the effective nonlinear susceptibility, investigated above, for the four-wave parametric process $\omega_S = \omega_1 - \omega_2 + \omega_3$, $\Delta k = k_S - k_1 + k_2 - k_3$. The quantum conversion efficiency (QCE) for conversion of E_1 into E_S radiation at the exit from the medium is given by the formula

$$\eta_{\mathrm{q}} = (\omega_1/\omega_S)|E_S(z)/E_1(0)|^2 \exp(-\alpha_S z). \tag{11}$$

From Eq. (10) we obtain

$$\eta_{\mathrm{q}}(z) = (\omega_1/\omega_S)(|2\pi\chi_S^{(3)} E_2 E_3|^2/|\Delta k|^2)\exp(-\alpha_S z)|\exp(-i\Delta kz) - 1|^2. \tag{12}$$

Figure 3 shows the QCE versus the optical thickness of the medium with probe-field detuning corresponding to the peak of the nonlinear susceptibility under the conditions of phase matching ($\Delta k' = 0$) and compensation of Doppler broadening of the transition 0–2. The Franck–Condon factors for the transitions considered in the sodium dimer were used in the calculation. The inset shows the same dependence but with $E_3^- = 0$, in which case the conditions for the elimination of Doppler broadening are not satisfied. Comparing these curves shows a large increase in the conversion efficiency, which solves the problem posed in this work.

This work was supported by the Ministry of Education of the Russian Federation (Grant for Research in the Fundamental Natural Sciences) and the Russian Fund for Fundamental Research (Grants 97-02-00016G and 97-02-16092).

*e-mail: popov@cc.krascience.rssi.ru

---

[1] S. Babin, U. Hinze, E. Tiemann, and B. Wellegehausen, Opt. Lett. **21**, 1186 (1996).

[2] M. D. Lukin *et al.*, Phys. Rev. Lett. **81**, 2675 (1998).

[3] A. S. Baev and A. K. Popov, JETP Lett. **67**, 1018 (1998); A. K. Popov and V. M. Shalaev, Phys. Rev. A (1999), to be published; T. Ya. Popov, A. K. Popov, S. G. Rautian, and A. A. Feoktistov, Zh. Eksp. Teor. Fiz. **57**, 444 (1969) [Sov. Phys. JETP **30**, 243 (1970)].

[4] A. K. Popov, Izv. Ross. Akad. Nauk, Ser. Fiz. **60**, 99 (1996).

[5] C. Cohen-Tannoudji *et al.*, Opt. Commun. **27**, 71 (1978); S. Reynaud *et al.*, Phys. Rev. Lett. **42**, 756 (1979); S. Reynaud *et al.*, Opt. Commun. **42**, 39 (1982); G. Vemuri, G. S. Agarwal, and B. Rao, Phys. Rev. A **53**, 2842 (1996).

Translated by M. E. Alferieff

JETP LETTERS VOLUME 69, NUMBER 2 25 JAN. 1999

Intensity fluctuations in the presence of weak localization of light in a disordered medium

D. B. Rogozkin
Moscow Engineering-Physics Institute, 115409 Moscow, Russia

(Submitted 28 October 1998; resubmitted 10 December 1998)
Pis'ma Zh. Éksp. Teor. Fiz. **69**, No. 2, 104–109 (25 January 1999)

It is shown that the intensity fluctuations in the speckle pattern arising when light is reflected from a disordered sample are negatively correlated. The relative amplitude of the correlations is two times larger in the exactly backward direction than far from this direction. © *1999 American Institute of Physics.* [S0021-3640(99)00502-2]

PACS numbers: 42.25.Dd, 42.25.Hz

The interference of waves propagating in opposite directions along the same trajectory leads to weak localization, which is manifested in the form of coherent amplification of backscattering in the reflection of light from disordered samples.[1,2] A coherent backscattering peak is observed against the background of the speckle pattern — a strongly fluctuating dependence of the intensity on the observation angle.[2,3] A speckle pattern arises because the phase of the elastically scattered waves is related with the random arrangement of the nonuniformities of the medium. The strongest fluctuations are observed near the exactly backward direction — in the coherent backscattering cone.[3]

One of the main problems studied in investigations of fluctuations in a speckle pattern is the analysis of correlations between different spots in the pattern, i.e., angular or intermodal correlations. Correlations of this kind are determined by long propagation trajectories of waves in the medium, and they are of the same nature as the universal fluctuations of the electronic conductance of small metallic samples.[4] They are responsible for the deviation of the intensity fluctuations from Rayleigh statistics.[5] Neglecting weak localization, angular correlations have been discussed in greatest detail for transmission geometry[5–10] and to a lesser extent for reflection.[6,7,11] Correlations near the exactly backward direction, where weak localization is strongly manifested, have been studied only in Ref. 7. The contribution of time-reversed trajectories was estimated in Ref. 7 by the random-matrix method in the approximation of δ-correlated fluctuations (i.e., in the limit $k_0 l \rightarrow \infty$, where k_0 is the wave number and l is the mean free path).

In the present letter, the manifestation of interference of time-reversed trajectories in intermodal correlations of the intensity of light reflected from disordered samples is discussed. The results of diagrammatic calculations of the angular correlation function for purely elastic scattering from a system of small-radius centers are reported. It is shown that for a small difference between the directions of observation, the correlation function of the backscattered intensity possesses a triangular dip. Fluctuations in different spots of a speckle pattern are negatively correlated, and if at least one direction of observation is

© 1999 American Institute of Physics

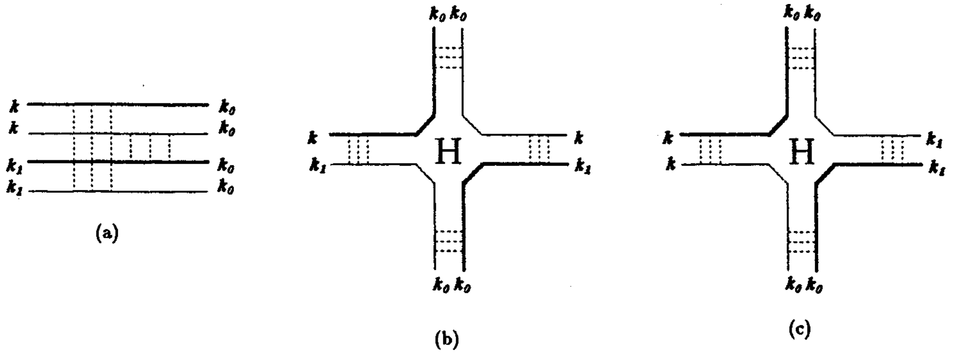

FIG. 1.

exactly backward, the amplitude of the correlations is doubled. This law is also manifested in correlations between backscattered and transmitted radiation intensities.

To calculate the correlation function

$$C(\mathbf{k},\mathbf{k}_1)=\langle I(\mathbf{k}|\mathbf{k}_0)I(\mathbf{k}_1|\mathbf{k}_0)\rangle-\langle I(\mathbf{k}|\mathbf{k}_0)\rangle\langle I(\mathbf{k}_1|\mathbf{k}_0)\rangle\,,$$

where $\mathbf{k}_0$ and $\mathbf{k},\mathbf{k}_1$ are the wave vectors of the incident and backscattered waves, we shall use an expansion in terms of the multiplicity of interference of ''ladders.''[8] This approach is valid if the total number of propagation modes $N=k_0^2A/4\pi$ (A is the surface area of the sample) is large, $Nl/L\gg 1$ (L is the thickness of the sample), and one-dimensional localization of waves does not occur.

Far from the exactly backward direction ($|\mathbf{k}+\mathbf{k}_0|$, $|\mathbf{k}_1+\mathbf{k}_0|\gg 1/l$, where l is the mean free path) the diagrams without time-reversed wave lines (see Fig. 1) make the leading-order contribution to the expansion in terms of the small parameter $1/k_0^2A$. The disconnected ''ladders'' give the contribution C_1 (Fig. 1), which is nonzero only for $\mathbf{k}=\mathbf{k}_1$ (Ref. 8), $C_1(\mathbf{k},\mathbf{k}_1)=(4\pi^2/A)\langle I(\mathbf{k}|\mathbf{k}_0)\rangle^2\delta(\mathbf{k}_\parallel-\mathbf{k}_{1\parallel})$, where $\mathbf{k}_\parallel$ and $\mathbf{k}_{1\parallel}$ are the wave-vector components parallel to the surface; $C_1(\mathbf{k}=\mathbf{k}_1)=\langle I(\mathbf{k}|\mathbf{k}_0\rangle^2$.

The correlations between different spots in a speckle pattern are determined by the value of $C(\mathbf{k},\mathbf{k}_1)$ for $\mathbf{k}\neq\mathbf{k}_1$. In this case, two diagrams, corresponding to a single interaction of the ''ladders'' (Fig. 1b and 1c), make the main contribution to the correlation function. The quantity H in these diagrams is the Hikami vertex[12] (see also Refs. 8, 11, and 13). The contribution of the first diagram, C_2', is a sharp function of $\mathbf{k}$ and $\mathbf{k}_1$ with characteristic variation scale $|\mathbf{k}_\parallel-\mathbf{k}_{1\parallel}|\sim 1/l$. The contribution of the second diagram, C_2'', on the contrary, is a smooth function of $\mathbf{k}$ and $\mathbf{k}_1$, which on the scales of variation of C_2' can be taken as constant. For $\mathbf{k}=\mathbf{k}_1$ the contributions of C_2' and C_2'' are equal. If only the rapid variation of the correlation function on scales of the order of $|\Delta\mathbf{k}_\parallel|\sim 1/l$ is of interest, then we can write

$$C_2(\mathbf{k},\mathbf{k}_1)=C_2'+C_2''=C(\mathbf{k}_\parallel-\mathbf{k}_{1\parallel},-\mathbf{k}_\parallel+\mathbf{k}_{1\parallel}|0,0)+C(0,0|0,0), \tag{1}$$

where $C(\mathbf{q}_1,\mathbf{q}_2|\mathbf{q}_3,\mathbf{q}_4)(\mathbf{q}_1+\mathbf{q}_2+\mathbf{q}_3+\mathbf{q}_4=0)$ denotes the contribution of one correlation diagram with different values of $\Delta\mathbf{k}_\parallel$ of the incident and backscattered waves.

Near the exactly backward direction ($|\mathbf{k}+\mathbf{k}_0|,|\mathbf{k}_1+\mathbf{k}_0|\leqslant 1/l$), in addition to the ladder diagrams shown in the figure, it is also necessary to consider diagrams with one or two time-reversed wave lines (the time-reversal transformation corresponds to the substitutions $\mathbf{k}_0\rightarrow-\mathbf{k}$, $\mathbf{k}\rightarrow-\mathbf{k}_0$ or $\mathbf{k}_0\rightarrow-\mathbf{k}_1$, $\mathbf{k}_1\rightarrow-\mathbf{k}_0$ at the ends of a wave line). Such diagrams take into account the weak localization effect[1,2] — the interference of waves propagating in opposite directions along the same trajectories.

In this case C_1 is the sum of four diagrams.[14] The equality $C_1(\mathbf{k}=\mathbf{k}_1)=\langle I(\mathbf{k}|\mathbf{k}_0\rangle^2$ remains valid if the average intensity is calculated with the coherent component included, $\langle I\rangle=\langle I^{\mathrm{inc}}+I^{\mathrm{c}}\rangle$.

The correlation function C_2 is now determined by the contribution of 16 diagrams. The eight diagrams arising when a combination of fields with one reversed wave is averaged and the six diagrams arising in the case of two reversed waves are added to the two diagrams considered above (see Fig. 1). This becomes clear if different contributions to the correlation function $\langle\,\delta(I^{\mathrm{inc}}+I^{\mathrm{c}})\,\delta(I^{\mathrm{inc}}+I^{\mathrm{c}})_1\rangle$ are analyzed. The correlations of incoherent intensities $\langle\,\delta I^{\mathrm{inc}}\delta I_1^{\mathrm{c}}\rangle$ are determined by four diagrams: near the exactly backward direction, two more diagrams with pairwise reversed wave lines are added to the two diagrams considered above. The correlations between the incoherent and coherent intensities $\langle\,\delta I^{\mathrm{inc}}\delta I_1^{\mathrm{c}}\rangle$ are likewise determined by four diagrams. Finally, an equal number of diagrams contribute to the correlation function $\langle\,\delta I^{\mathrm{c}}\delta I_1^{\mathrm{c}}\rangle$ of coherent intensities. The result is

$$\begin{aligned}C_2(\mathbf{k},\mathbf{k}_1)=&\,C(\mathbf{q},-\mathbf{q}|0,0)+C(0,0|0,0)+2C^{\mathrm{c}}(\mathbf{q}_0,0|-\mathbf{q}_0,0)+2C^{\mathrm{c}}(-\mathbf{q}_1,-\mathbf{q}|\mathbf{q}_0,0)\\&+2C^{\mathrm{c}}(\mathbf{q}_1,0|-\mathbf{q}_1,0)+2C^{\mathrm{c}}(-\mathbf{q}_0,\mathbf{q}|\mathbf{q}_1,0)+2C^{\mathrm{cc}}(-\mathbf{q}_0,\mathbf{q}_1|\mathbf{q},0)\\&+C^{\mathrm{cc}}(0,0|\mathbf{q}_0,-\mathbf{q}_0)+C^{\mathrm{cc}}(-\mathbf{q}_1,\mathbf{q}_1|0,0)+2C^{\mathrm{cc}}(-\mathbf{q}_0,-\mathbf{q}_1|\mathbf{q}_0,\mathbf{q}_1),\end{aligned}\qquad(2)$$

where C^{c} and C^{cc} are the contributions of diagrams with one and two reversed wave lines, $\mathbf{q}=(\mathbf{k}-\mathbf{k}_1)_\parallel$, $\mathbf{q}_0=(\mathbf{k}+\mathbf{k}_0)_\parallel$, and $\mathbf{q}_1=(\mathbf{k}_1+\mathbf{k}_0)_\parallel$. In the absence of interactions which destroy T invariance, C, C^{c}, and C^{cc} differ only as a result of the multiplicity of scattering (there are at least two collisions per reversed line).

The function $C(\mathbf{q}_1,\mathbf{q}_2|\mathbf{q}_3,\mathbf{q}_4)$ in Eqs. (1) and (2) decreases rapidly with increasing $q_i(i=1\ldots4)$ on scales of the order of $q_i\sim1/l$. For this reason, for $q_0,q_1\gg1/l$ we return from Eq. (2) immediately to Eq. (1). It also follows from Eq. (2) that the correlation function between the intensity values in the coherent backscattering cone ($q_0<1/l$) and far from it ($q_1\gg1/l$) is described by the expression

$$C_2(\mathbf{k},\mathbf{k}_1)=C(0,0|0,0)+2C^{\mathrm{c}}(\mathbf{q}_0,0|-\mathbf{q}_0,0)+C^{\mathrm{cc}}(0,0|\mathbf{q}_0,-\mathbf{q}_0).\qquad(3)$$

We shall present the results of a calculation of the correlation function C_2 for the reflection of a plane wave from a disordered system of small-radius centers (we neglect terms containing the small factor l/L).

The diagrams shown in Fig. 1b and 1c and similar diagrams with reversed wave lines can be easily calculated in a general form using a coordinate–angle representation and the transport equation for intensity propagators. The technique for such calculations is presented in Refs. 11 and 13. In the reflection geometry, spatial scales of the order of the mean free path l play an important role, and in this connection the contribution of diagrams in which one or two propagators correspond to the unscattered intensity must be singled out. These diagrams make a contribution of the same order as the diagrams containing the multiply scattered intensity (in the calculations in Ref. 6 the contribution of the unscattered intensity was neglected, and in consequence the results are qualitatively incorrect; see Refs. 11 and 13 for a discussion). The diffusion approximation can be used to calculate the intensity of multiply scattered light for small q_i $(q_i \ll 1/l)$.

As a result, we obtain that for $q_i \ll 1/l$ the function $C(\mathbf{q}_1,\mathbf{q}_2|\mathbf{q}_3,\mathbf{q}_4)$ is linear:

$$C(\mathbf{q}_1,\mathbf{q}_2|\mathbf{q}_3,\mathbf{q}_4)=\frac{1}{\pi k_0^2 A}\left(-a+\frac{1}{2}(|\mathbf{q}_1|+|\mathbf{q}_2|+|\mathbf{q}_3|+|\mathbf{q}_4|)l \;\; b\right), \tag{4}$$

where the coefficients a and b for normal incidence and reflection of the waves are $a \simeq 3.72$, $b \simeq 19.82$ for diagrams without reversed lines[11] and $a^{\mathrm{c}} \simeq 3.33$, $b^{\mathrm{c}} \simeq 18.77$ for diagrams with one and $a^{\mathrm{cc}} \simeq 2.93$, $b^{\mathrm{cc}} \simeq 17.73$ for diagrams with two reversed wave lines. The ratio b/a characterizes the multiplicity of scattering and is maximum for the contribution with two reversed waves.

According to Eq. (4), fluctuations of the reflected radiation are always negatively correlated. Physically, this is due to the conservation of the radiation flux in elastic scattering. In the conservation condition

$$\langle(\delta R)^2\rangle=\sum_{\mathbf{k},\mathbf{k}_1}[C_1(\mathbf{k},\mathbf{k}_1)+C_2(\mathbf{k},\mathbf{k}_1)+\ldots]=0, \tag{5}$$

where $\langle(\delta R)^2\rangle$ is the variance of the total reflection coefficient, among the components of C_2 the component C_2'' makes the main contribution. This is explained by the smooth dependence of C_2'' on $\mathbf{k}$ and $\mathbf{k}_1$. Therefore it follows from Eq. (5) that $C_2''<0$. The other components of C_2 are identical with C_2'' if $q_i=0$ (to within small differences due to the contribution of low-multiplicity scattering). The fact that the correlation function C_2 possesses a triangular dip near $q_i=0$ attests to the predominant role of long wave propagation trajectories.

In accordance with Eqs. (2) and (4), the correlation function of intensity fluctuations near the backward direction $(q,q_0,q_1 \ll 1/l)$ has the form

$$\begin{aligned}C_2(\mathbf{k},\mathbf{k}_1)=\frac{1}{\pi k_0^2 A}&(-(2a+8a^{\mathrm{c}}+6a^{\mathrm{cc}})+ql(b+2b^{\mathrm{c}}+b^{\mathrm{cc}})\\&+4(q_0+q_1)l\;\;(b^{\mathrm{c}}+b^{\mathrm{cc}})).\end{aligned} \tag{6}$$

The angular dependence of the correlations is equally determined by the difference in the observation directions and their deviation from the backward direction.

It is interesting that while weak localization does not change the relative magnitude of the fluctuations in a spot of the speckle pattern, $\langle(I-\langle I\rangle)^2\rangle/\langle I\rangle^2=1$ for $\mathbf{k}=\mathbf{k}_1=-\mathbf{k}_0$ (Ref. 14), it strongly influences the intermodal correlations of the fluctuations. The relative amplitude of the correlations in the coherent backscattering cone is approximately two times larger than outside the cone:

$$\frac{C_2(\mathbf{k}=\mathbf{k}_1)}{\langle I(\mathbf{k}|\mathbf{k}_0)\rangle^2}\simeq-\frac{8\pi}{k_0^2 A}\begin{cases}2, & q_0=q_1\ll 1/l\\ 1, & q_0=q_1\gg 1/l\end{cases}. \tag{7}$$

If **k** and $\mathbf{k}_1$ differ strongly in direction, then the correlation function no longer depends on the angle between them. The amplitude of the correlations likewise doubles in this case, when one direction (**k** or $\mathbf{k}_1$) coincides with the backward direction:

$$\frac{C_2(\mathbf{k},\mathbf{k}_1)}{\langle I(\mathbf{k}|\mathbf{k}_0)\rangle\langle I(\mathbf{k}_1|\mathbf{k}_0)\rangle} \simeq -\frac{4\pi}{k_0^2A}\begin{cases} 2, & q_0 \ll 1/l, \quad q_1 \gg 1/l \\ 1, & q_0, \quad q_1 \gg 1/l \end{cases}. \tag{8}$$

Let us compare the above-obtained expressions with the computational results obtained by the random-matrix method.[7] A contribution of the order of $1/k_0^2A$, corresponding to the function C_2, can also be discerned in the correlation function found in Ref. 7. Since the calculations in Ref. 7 were performed in the limit $k_0l \to \infty$ (i.e., the fluctuations were assumed to be δ-correlated with respect to directions), we can compare not the correlation functions C_2 themselves, but rather only their values when the q_i are either large or zero. In the three cases $q,q_0,q_1 \gg 1/l$; $q=0,q_0,\ q_1 \gg 1/l$; and $q_0=0,q,q_1 \gg 1/l$ our results and those of Ref. 7 are in quantitative agreement (within the limits of accuracy of the approximation used in Ref. 7). For scattering in the exactly backward direction $(q=q_0=q_1=0)$, the results differ by a factor of 1.5 (according to Ref. 7, in the first row of Eq. (7) the number 1.5 should appear instead of 2).

We note that the results of Ref. 7 and the results obtained above differ radically from the results of Ref. 6, where reflection far from the backward direction was studied and positive correlations were predicted. The results obtained in Ref. 6 are at variance with flux conservation (the inaccuracy of the results obtained in Ref. 6 is shown in Refs. 11 and 13).

The final results (7) and (8) remain valid even if strong internal reflection occurs at the boundaries of the medium. In recent years there has been great interest in the multiple-scattering of light in such a system.[15] Internal reflection from boundaries changes only the explicit form of the function $C(\mathbf{q}_1,\mathbf{q}_2|\mathbf{q}_3,\mathbf{q}_4)$. In the strong reflection limit ($1-r \ll 1, r$ is the reflection coefficient) a direct calculation of the correlation diagram gives the following result, which is asymptotically exact in the large parameter $(1-r)^{-1}$:

$$C(\mathbf{q}_1,\mathbf{q}_2|\mathbf{q}_3,\mathbf{q}_4) = -\frac{4}{\pi k_0^2A(1+(4/3)q_1l/(1-r))\ldots(1+(4/3)q_4l/(1-r))}. \tag{9}$$

According to Eq. (9), the presence of internal reflection influences only the angular scale of the correlations and does not change the qualitative form of the correlation function (in contrast to spatial correlations for $1-r \ll 1$).[16]

It is interesting that weak localization should also be manifested in correlations between the values of the intensity of backscattered and transmitted radiation. The amplitude of the correlations doubles when the backscattered wave propagates in the backward direction. In our situation the contribution C_1 is absent and the leading contribution is C_2, for which Eq. (3) remains valid. Instead of Eq. (8), now we shall have ($\mathbf{k}_1$ refers to the transmitted wave)

$$\frac{C_2(\mathbf{k},\mathbf{k}_1)}{\langle I(\mathbf{k}|\mathbf{k}_0)\rangle\langle I(\mathbf{k}_1|\mathbf{k}_0)\rangle} \simeq -\frac{4\pi}{k_0^2A}\begin{cases} 4/3, & q_0 \ll 1/l \\ 2/3, & q_0 \gg 1/l \end{cases}. \tag{10}$$

The negative sign of the correlations is dictated by the condition of flux conservation, which in the present case has the form

$$\langle \delta R\ \delta T\rangle = \sum_{\mathbf{k},\mathbf{k}_1} [C_2(\mathbf{k},\mathbf{k}_1) + \ldots] = -\langle (\delta T)^2\rangle,$$

where $\langle (\delta T)^2\rangle$ is the variance of the transmission coefficient.

In conclusion, let us indicate how the characteristic features of the correlations reflect on the distribution function of the intensity $P(I)$. According to Ref. 5, on account of the effect of correlations, the complete distribution function $P(I)$ should deviate from the Rayleigh law $P_R(I) = (1/\langle I\rangle)\exp(-I/\langle I\rangle)$, where $\langle I\rangle$ is the average intensity in a given direction. The character of the deviation is determined by the value of $C_2(\mathbf{k},\mathbf{k})$, and for negative correlations it is described by the formula[11]

$$\frac{P(I)}{P_R(I)} \simeq \exp\left(-\frac{I^2}{4\langle I\rangle^4} |C_2(\mathbf{k},\mathbf{k})| \right). \tag{11}$$

The deviations from the Rayleigh law have opposite signs for transmission[5] and reflection.[11] Flux conservation, which leads to negative correlation, suppresses strong intensity fluctuations of the intensity of the reflected radiation. Since the ratio $C_2(\mathbf{k},\mathbf{k})/\langle I\rangle^2$ for the exactly backward direction is two times larger than far from this direction, the deviation of the fluctuations in the coherent back-scattering cone from Rayleigh statistics is more pronounced.

I take this opportunity to thank E. E. Gorodnichev and A. I. Kuzovlev for their interest in this work and for valuable suggestions. This work was supported by the Russian Fund for Fundamental Research (Project 96-02-17518) and the Ministry of General and Professional Education of the Russian Federation (Project 95-0-5.4-137).

[1] Yu. N. Barabanenkov, Yu. A. Kravtsov, V. D. Ozrin, and A. I. Saichev, Prog. Opt. **29**, 65 (1991).

[2] V. L. Kuz'min and V. P. Romanov, Usp. Fiz. Nauk **166**, 247 (1996).

[3] S. Etemad, R. Thompson, and M. J. Andrejco, Phys. Rev. Lett. **57**, 575 (1986); M. Kaveh, M. Rosenbluh, I. Edrei, and I. Freund, Phys. Rev. Lett. **57**, 2049 (1986).

[4] R. Berkovits and S. Feng, Phys. Rep. **238**, 135 (1994).

[5] E. Kogan, M. Kaveh, R. Baumgartner, and R. Berkovits, Phys. Rev. B **48**, 9404 (1993); Th. M. Nieuwenhuizen and M. C. W. van Rossum, Phys. Rev. Lett. **74**, 2674 (1995).

[6] M. J. Stephen and G. Cwillich, Phys. Rev. Lett. **59**, 285 (1987); L. Wang and S. Feng, Phys. Rev. B **40** 8284 (1989).

[7] P. A. Mello, E. Akkermans, and B. Shapiro, Phys. Rev. Lett. **61**, 459 (1988).

[8] S. Feng, C. Kane, P. A. Lee, and A. D. Stone, Phys. Rev. Lett. **61**, 834 (1988).

[9] M. C. W. van Rossum and Th. M. Nieuwenhuizen, Phys. Lett. A **177**, 452 (1993); M. C. W. van Rossum, J. F. de Boer, and Th. M. Nieuwenhuizen, Phys. Rev. E **52**, 2053 (1995).

[10] A. Z. Genack and N. Garcia, Europhys. Lett. **21**, 753 (1993); J. F. de Boer, M. P. van Albada, Th. M. Nieuwenhuizen *et al.*, Phys. Rev. Lett. **73**, 2567 (1994); M. Stoitchev and A. Z. Genack, Phys. Rev. Lett. **79**, 309 (1997).

[11] D. B. Rogozkin, Phys. Lett. A **236**, 159 (1997).

[12] S. Hikami, Phys. Rev. B **24**, 2671 (1981).

[13] D. V. Rogozkin and M. Yu. Cherkasov, JETP Lett. **58**, 585 (1993); Phys. Rev. B **51**, 12256 (1995).

[14] R. Berkovits and M. Kaveh, Phys. Rev. B **41**, 2635 (1990).

[15] J. H. Li and A. Z. Genack, Phys. Rev. E **49**, 4530 (1994); E. Amic, Th. M. Nieuwenhuizen, and J. M. Luck, J. Phys. A **29**, 4915 (1996).

[16] L. V. Korolev and D. B. Rogozkin, Zh. Éksp. Teor. Fiz. **113**, 291 (1998) [JETP **86**, 164 (1998)].

Translated by M. E. Alferieff

JETP LETTERS VOLUME 69, NUMBER 2 25 JAN. 1999

Effect of a pulsed magnetic field on the microhardness of C_{60} single crystals

Yu. A. Osip'yan, R. K. Nikolaev, and S. Z. Shmurak
Institute of Solid-State Physics, Russian Academy of Sciences, 142432 Chernogolovka, Moscow Region, Russia

Yu. I. Golovin, D. V. Lopatin, and R. B. Morgunov
G. R. Derzhavin Tambov State University, 392622 Tambov, Russia

(Submitted 4 December 1998)
Pis'ma Zh. Éksp. Teor. Fiz. **69**, No. 2, 110–113 (25 January 1999)

Magnetic-field pulses with induction greater than 10 T were observed to influence the microhardness of C_{60} single crystals. It was established that the magnetic field reversibly alters the bulk properties of the material. © *1999 American Institute of Physics.* [S0021-3640(99)00602-7]

PACS numbers: 81.05.Tp, 81.40.Lm, 62.20.Qp

Investigations of the changes induced in the mechanical properties of real crystals by external magnetic fields (MFs) can yield important information, which is inaccessible by other methods, about physical processes in the structural-defects subsystem.[1–3] In the last few years it has been reliably established that even energetically weak MFs with induction $\sim 1-10$ T can give rise to lasting residual changes in the plastic properties of diamagnetic dielectric crystals and polymers.[1] In Refs. 4 and 5 it was shown that this can be explained by the influence of MFs on the kinetics and yield of spin-dependent reactions in the paramagnetic-structural-defects subsystem, which influences dislocation mobility. In Ref. 6, a modified EPR method was used to obtain direct experimental confirmation of this hypothesis. It is important to investigate the effect of MFs on the mechanical properties of new materials, such as fullerites. However, the first investigations of the plastic properties of fullerites[7–9] established that their plasticity is determined by dislocation mechanisms and that structural defects exhibit paramagnetic properties.[10–12] This suggests that the magnetoplastic effects observed in ionic and covalent crystals can also occur in fullerites.

In the present work we investigated the possibility that after fullerites are pretreated in a MF residual changes occur in their microhardness. Single-crystal C_{60} samples of high purity (99.95% C_{60}) with an average linear dimension $\sim 3-5$ mm, grown from the vapor phase and possessing the faceting natural for face-centered cubic crystals, were used to investigate the sensitivity of the microhardness to MFs. Picein was used to secure the crystals to glass in a manner so that the face under investigation would be accessible for indentation and was parallel to the platform of the PMT-3 microhardness meter. Indentation was conducted over 5 s with a 20 g load on the indenter. It is known that as a result of photostimulated oxidation of the surface, the microhardness of C_{60} changes as the

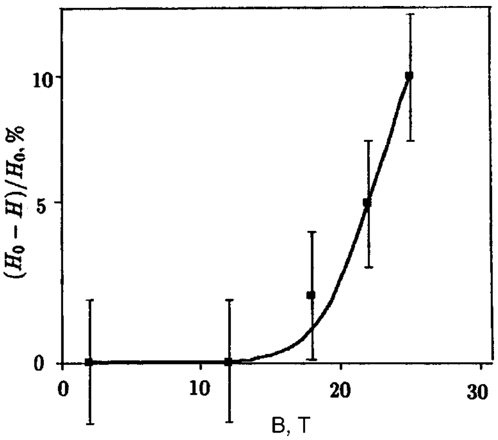

FIG. 1. Relative difference $(H_0 - H)/H_0$ of the microhardness H and H_0 of C_{60} crystals which have and have not been exposed to a magnetic field versus the amplitude B of the field pulses.

samples age in air,[9,13] so that to slow down oxidation all experimental procedures were performed in the dark, except for the measurements of the dimensions of the indentations, which were performed in weak red light. In the absence of MFs, this made it possible to maintain the microhardness of the crystals constant for ~10 days at the value obtaining immediately after the crystals are extracted from the evacuated capsule. Each point on the plots (Figs. 1 and 2) was obtained by averaging the dimensions of 15–20 indentations produced under identical conditions. The magnetic-field pulses were close in shape to a single half-period of a sinusoid with amplitude B up to 24 T and duration 140 μs, and they were generated in a few-turn solenoid by discharging a capacitor bank.

The effect of the pretreatment of the crystals in a pulsed MF on their microhardness H was investigated in the experiments. The microhardness of the samples that were not exposed to MFs (i.e., in the control experiments) was $H_0 = 210 \pm 4$ MPa, which is close to the data obtained in Ref. 8 for ''as grown'' crystals. In crystals exposed to a single MF pulse, the microhardness H measured 1 min after treatment in a field was lower than in

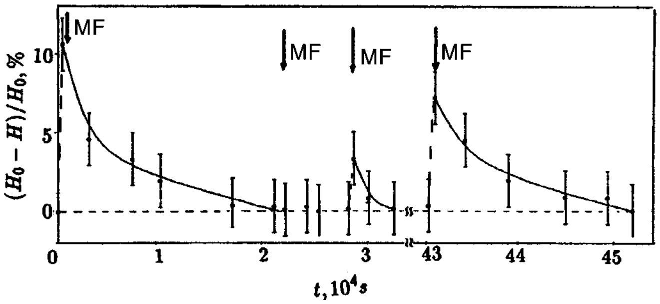

FIG. 2. Relative difference $(H_0 - H)/H_0$ of the microhardness H and H_0 of C_{60} crystals which have and have not been exposed to a magnetic field versus the time interval t between the first MF pulse and subsequent measurements of the microhardness H. The arrows mark the times when the additional MF pulses were switched on. The amplitude of the MF pulses is $B = 24$ T.

the control experiments: $(H_0 - H)/H_0 = 10 \pm 2\%$ (Fig. 1). After the MF pulse, the crystal was ground in order to remove a 100–300 μm thick layer, after which the microhardness on the freshly formed surface was measured. The microhardness differed from H_0 by the same amount as the microhardness H measured on the initial surface. Therefore not only the subsurface but also the interior layers of the material were affected by the MFs. A change in microhardness after the crystals were exposed to a MF was reliably detected only for $B > 10$ T and was not observed in weaker fields B (Fig. 1).

When a sample was subjected to repeated indentation for several hours after the first treatment of the crystal in a MF, it was observed that as the time between the MF pulse and measurement of the microhardness increased, the value of H increased and reached the level H_0 after ~ 6 h, i.e., the softening effect $(H_0 - H)/H_0$ dropped to zero (Fig. 2).

Switching on a second MF pulse immediately after H was restored to H_0 did not change the microhardness of the crystal, but the third and fourth field pulses, applied 8 and 120 h, respectively, after the first one, once again decreased the microhardness, the decrease being somewhat less than that due to the first MF pulse (Fig. 2). Therefore there is a time interval during which the crystal is insensitive to repeated MF pulses.

A separate series of experiments established that exposure of crystals for 20 s and 2 min to a constant MF with induction $B = 2$ T does not change H within the limits of the experimental error. In addition, it was verified that the electric field of the current leads to the solenoid does not influence the microhardness of the crystals.

It follows from the results of the experiments described above that a MF pulse gives rise to a reversible decrease of the microhardness of crystals, but these data do not permit judging the degree of reversibility of the changes produced by a MF in the structural-defects subsystem at the microlevel, since, as was established in Ref. 1, reversibility of the macroplastic properties does not always attest to reversibility of internal restructurings. This is because in the course of relaxation structural defects can pass through a series of states with increasingly lower thermodynamic potential,[1] and depending on the configuration of the defects in each state the dislocation mobility and plasticity can be lower or higher than the initial value.[1]

Simple estimates show that the ponderomotive forces arising in diamagnetic crystals (including C_{60}) in MFs are many orders of magnitude weaker than the forces required to reliably detect changes in the plastic properties. The attempt to link the influence of an MF on the microhardness with a change in the electronic state of stable defects encounters the following conflict. Magnetic-field-induced changes in the microhardness remain for quite a long time after the field is switched off, while the energy imparted by the field to the electron spin moment is only 20% of the average thermal energy kT at the experimental temperature $T \sim 300$ K. For this ratio of the magnetic and thermal energies, a MF cannot excite equilibrium defects and the electronic subsystem of the crystal as a whole.

Just as in ionic crystals,[1–3] the objects in C_{60} that are affected by MFs are probably nonequilibrium point defects as well as dislocations (the density of the latter in the experimental crystals was $\sim 10^6$ cm^2). In the fullerites used in our experiments the simple cubic and fcc phases coexist, and the simple cubic modification is metastable. It can be inferred that, as in II–VI compounds, the transformation of the cubic phase to the fcc phase, energetically favorable at room temperature, is accompanied by a displacement of twinning dislocations. For this reason, a change in H could be stimulated by the field-induced motion of dislocations.

In addition, the MF-induced change in H in molecular crystals could occur for reasons that are similar to those that explain the plastification of polymers in MFs. For example, it is known that C–O bonds exhibit substantial anisotropy of the magnetic susceptibility, which results in reorientation of the macromolecules in polymers in MFs.[14,15] The presence of such bonds in C_{60} molecules can explain the change in H as being due to reorientation of individual molecules in a MF.

In summary, a magnetoplastic effect was observed in C_{60} crystals. This effect consists in a change of the microhardness of the crystals after exposure to a MF pulse. Further investigations are required in order to establish the nature of this phenomenon.

This work was supported by the Russian Fund for Fundamental Research (Grant 97-02-16074).

[1] Yu. I. Golovin and R. B. Morgunov, Chem. Rev. **24**, 1 (1998).
[2] A. A. Urusovskaya, V. I. Al'shits, A. E. Smirnov, and N. N. Bekkauer, JETP Lett. **65**, 497 (1997).
[3] É. P. Belozerova, A. A. Svetashev, and V. L. Krasnikov, Izv. Akad. Nauk SSSR, Ser. Fiz. **61**, 291 (1997).
[4] M. I. Molotskii, R. E. Kris, and V. N. Fleurov, Phys. Rev. B **51**, 12531 (1995).
[5] V. I. Al'shits, E. V. Darinskaya, and O. L. Kazakova, Zh. Éksp. Teor. Fiz. **111**, 615 (1997) [JETP **84**, 1338 (1997)].
[6] Yu. I. Golovin, R. B. Morgunov, V. E. Ivanov, and S. E. Zhulikov, JETP Lett. **68**, 426 (1998).
[7] Yu. A. Ossipian, V. S. Bobrov, Yu. S. Grushko *et al.*, Appl. Phys. A: Solids Surf. **56**, 1 (1993).
[8] V. S. Bobrov, R. A. Dilanian, L. S. Fomenko *et al.*, J. Supercond. **8**, 1 (1995).
[9] V. I. Orlov, V. I. Nikitenko, R. K. Nikolaev *et al.*, JETP Lett. **59**, 704 (1994).
[10] S. K. Misra and V. Petkov, Appl. Magn. Reson. **8**, 277 (1995).
[11] J. Stankovski, W. Kempinski, A. Koper, and J. Martinek, Appl. Magn. Reson. **6**, 145 (1994).
[12] Y. Ksari and G. Chouteau, Fullerene Sci. Technol. **4**, 1227 (1996).
[13] I. Manika and J. Maniks, Fullerene Sci. Technol. **5**, 149 (1997).
[14] G. Maret and K. Dransfeld, in *Strong and Ultrastrong Magnetic Fields and Their Applications*, edited by F. Herlach, Springer-Verlag, New York, 1985, pp. 143–204.
[15] G. K. Deshpande and M. L. Khare, Indian J. Pure Appl. Phys. **17**, 143 (1979).

Translated by M. E. Alferieff

JETP LETTERS VOLUME 69, NUMBER 2 25 JAN. 1999

Effect of a magnetic field on the plasticity and photo- and electroluminescence of ZnS single crystals

Yu. I. Golovin, R. B. Morgunov, A. A. Baskakov, and M. V. Badylevich
G. R. Derzhavin Tambov State University, 392622 Tambov, Russia

S. Z. Shmurak
Institute of Solid-State Physics, Russian Academy of Sciences, 142432 Chernogolovka, Moscow Region, Russia

(Submitted 10 December 1998)
Pis'ma Zh. Éksp. Teor. Fiz. **69**, No. 2, 114–118 (25 January 1999)

It is found that a ~10 T magnetic field influences the microhardness and the photo- and electroluminescence of ZnS single crystals containing microtwins. It is established that a magnetic field irreversibly changes the properties of the crystal, leading to relaxation of the metastable states of structural defects. © *1999 American Institute of Physics.* [S0021-3640(99)00702-1]

PACS numbers: 81.05.Dz, 81.40.Lm, 62.20.Qp, 81.40.Tv, 78.60.Fi, 78.55.Et

It has now been reliably established that an energetically weak magnetic field (MF) with induction $B\sim 1$ T is capable of effectively influencing physical processes in organic crystals at room temperature: fluorescence,[1–3] photoconductivity,[4,5] chemical reactions,[6,7] polymerization,[8] and others. The nature of these effects is linked to the fact that a MF affects the evolution of the paramagnetic particles during a brief (1–10 ns) intermediate stage, during which there is not enough time for spin–lattice relaxation to occur. At the magnetic inductions typical for these experiments, $B=0.1$–1 T, the duration of spin conversion is 10^{-11}–10^{-10} s. For all intents and purposes, up to now the elementary processes accompanying the plastic flow of crystals have not been investigated with nanosecond time resolution, which would make it possible to judge such short-lived processes. For this reason, the effect of MFs on the dislocation mobility in ionic crystals which was observed at room temperature in Ref. 9 with an induction $B\sim 1$ T is paradoxical at first glance. Experimental investigations performed in the last few years show convincingly that the parameters of plastic flow of ionic crystals are an indicator of the effect of MFs on the spin state of short-lived (~1 ns) states of complexes of structural defects in the process of their relaxation.[10–14] The use of conventional parameters, such as dislocation mobility, macroplastic flow rate, microhardness, and so on, for the interpretation of the events occurring at atomic and electronic levels often encounters serious difficulties because of the complicated and often ambiguous relation between the magnetic properties and the spin and molecular dynamics. For this reason, the observation of the effect of MFs on some other macrophysical characteristics of crystals would open up new possibilities for interpreting the effect of MFs on electronic processes accompanying plastic flow. A possible influence of MFs on the plasticity of crystals with covalent bonds

© 1999 American Institute of Physics

is of great interest, and because of the wider spectrum of the spin-dependent events accompanying the plastic deformation of these materials it can be even more diverse than in ionic crystals.

The objective of the present work was to produce experimental conditions for observing and investigating the influence of MFs on the plastic properties and the photo- and electroluminescence of ionic-covalent semiconductor diamagnetic ZnS crystals.

The experiments were performed on $2\times2\times4$ mm ZnS single crystals, containing microtwins and 10^{-3} at. % Cu as an impurity and possessing (1210) and (1011) faceting in hexagonal notation. In experiments of all types, the crystals were exposed to a MF pulse in the form of a half period of a sinusoid with amplitudes $B=7$ T (10 ms duration) or $B=24$ T (140 μs duration). Three different characteristics were used as a response to possible field-induced changes in the crystals: 1) the microhardness H measured with a 100 g load acting on an indenter for 10 s; 2) the intensity I of photoluminescence excited by monochromatic light with wavelength $\lambda_{EX}=380$ nm and measured in different parts of the optical spectrum with a DM-4 monochromator and an FÉU-106 photomultiplier; and, 3) the spectrum-integrated intensity Q of electroluminescence excited by an ac electric voltage with amplitude 2.2 kV and frequency 800 Hz. The voltage was applied to silver contacts deposited on a (1210) face of the crystal or on the plates of an air-filled capacitor into which the sample was inserted.

Each characteristic was measured before the MF was switched on. The values of H_0,I_0, and Q_0 measured before the MF pulse were used as controls. The variations of H, I, and Q caused by exposure of the samples to a MF served as a quantitative measure of the residual field-induced changes in the crystals. We emphasize that the measurements of each quantity were made in the absence of magnetic field, so there could not have been an influence of MF on the measurement procedure or the operating regimes of the instruments, i.e., it was the aftereffect of the MF which was studied.

Special attention was devoted to the photosensitivity of the experimental crystals and the possibility that they retain a definite light sum. For this reason, the crystals were protected from stray illumination, which could change each measured parameter, and the intensity and duration of the light fluxes required for the measurements were monitored. Control experiments showed that the electric field inevitably arising from the current leads to the solenoid when the MF pulse is produced does not in itself influence H, I, or Q. The maximum intensity of the induced electric field (1 V/mm) was incomparably less than the intensity of the field from the current leads and the field exciting the electroluminescence. In all experiments, the temperature of the sample in the solenoid was monitored with a thermocouple and was constant to within ± 0.1 K.

The effect of a MF on the microhardness was investigated in the first series of experiments. It was found that one MF pulse with $B=24$ T increases H by 5–10% (Fig. 1). Each point in Fig. 1 was obtained by averaging 100–200 individual measurements of the size of the indentation. The hardening initiated by the field pulse remains for a long time after the pulse (Fig. 1), and the superposition of repeated field pulses does not lead to any appreciable additional change in the microhardness. This attests to the fact that a MF stimulates an irreversible process in the crystals, i.e., it gives rise to relaxation of long-lived metastable states of the crystal.

In the second series of experiments, we investigated the effect of a MF on the

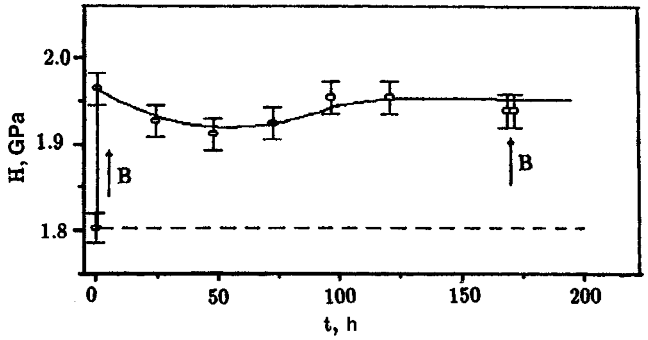

FIG. 1. Microhardness H of a crystal versus the running time t. The arrows mark the moments when MF pulses with amplitude $B = 24$ T are switched on. The dashed line shows the microhardness H_0 before the crystals are exposed in a MF.

photoluminescence. It was observed that the luminescence spectrum changes after a MF pulse (with both $B = 7$ and 24 T). The change in the spectrum consists in a decrease of the peak intensity at 525 nm (Fig. 2). It was established that the gradual buildup of luminescence due to the successive filling of electronic traps (see inset in Fig. 2) is different in the control and field-treated samples. This means that the change that we detected in the luminescence intensity is not due to an incompetent comparison of values of I measured at different stages of trap filling. The changes that could be brought about by the spectrum measurement procedure did not change the form of the spectrum with repeated measurements, provided that there was no MF between the measurements.

Definite changes after exposure of a crystal to a MF are also observed in the excitation spectrum of the luminescence detected at $\lambda = 525$ nm (Fig. 3). They consist in a

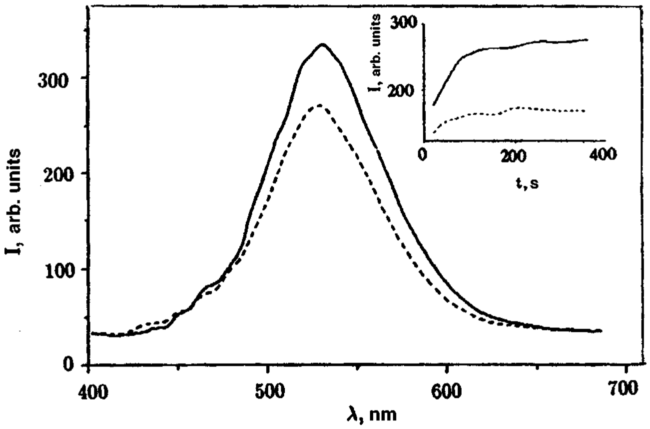

FIG. 2. Photoluminescence spectra excited by light with $\lambda_{EX} = 380$ nm: Solid lines — before the MF pulse; dashed lines — after a MF pulse with amplitude $B = 7$ T. Inset: Corresponding dependences of the photoluminescence intensity I at $\lambda = 525$ nm versus the duration t of photoexcitation. The measurement error in I with repeated insertion of a sample into and removal of the sample from the measuring cell does not exceed one arbitrary unit.

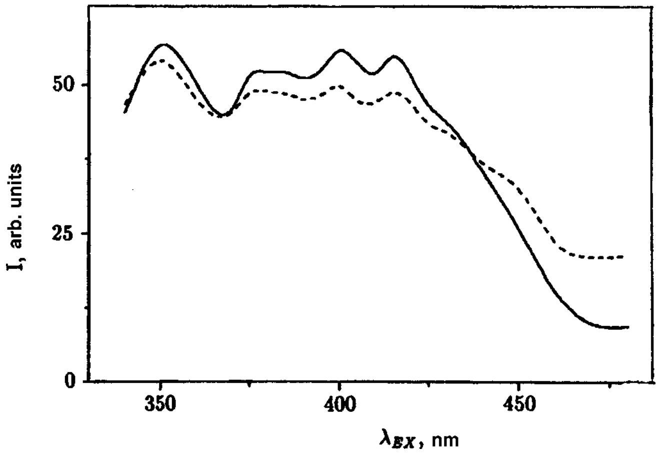

FIG. 3. Excitation spectra of photoluminescence at $\lambda = 525$ nm: Solid line — before the MF pulse, dashed line — after a MF pulse with amplitude $B = 7$ T. The measurement error in I with repeated insertion of the sample into and removal of the sample from the measuring cell does not exceed 0.5 arbitrary units.

simultaneous decrease of I at $\lambda_{EX} = 350$–425 nm and an increase in I for $\lambda_{EX} > 425$ nm. The field-induced changes in the luminescence and excitation spectra persisted for several days, as did the changes in the microhardness.

The measurements of H and I were performed on 300 samples. Of these, six did not show sensitivity to a MF. This can be explained by the fact that the state was different and the impurity distribution in the boule from which the samples were cut was nonuniform. An unambiguous correlation between the magnitude of the effect of a field on the microhardness and on the photoluminescence was observed: The luminescence spectra remained unchanged only in the samples for which the microhardness also remained unchanged. Therefore the observed magnetoplastic and magnetooptic effects could be a consequence of the same process occurring in the crystal.

In the third series of experiments it was observed that the spectrum-integrated intensity Q of the electroluminescence of the crystals increases by a factor of 10 after the crystals are exposed to a MF (Fig. 4). Therefore Q is a more sensitive characteristic of the effect of a MF on the state of the crystals than is H or I. The possibility repeatedly affecting the electroluminescence with a MF attests to this (Fig. 4). However, no effect of the MF on the electroluminescence was observed in crystals where H and I were also insensitive to MFs. Therefore the existence of metastable states in a crystal is also important for the manifestation of an effect of MFs on the electroluminescence.

In Ref. 12 it was shown that the changes in the plastic properties of ionic crystals in MFs can have at least two explanations: 1) the effect of a MF on the degree of aggregation of metastable complexes of point defects, and 2) the effect of a MF on the interaction between dislocations and paramagnetic point defects. Both effects can occur in ZnS crystals also.

Point defect known to exist as complexes containing doubly charged S vacancies, are responsible for the photoluminescence detected at 525 nm in the experiments described above.[15] However, a change in I does not mean that the effect of a MF consists

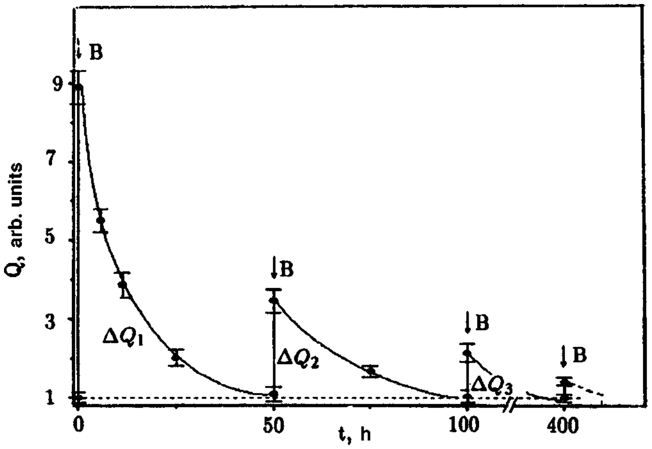

FIG. 4. Spectrum-integrated intensity Q of electroluminescence versus time t. The arrows mark the moments when the MF pulses with amplitude $B=7$ T are switched on; ΔQ_i are the jumps arising in the electroluminescence intensity as a result of the exposure of the crystals in a MF. Q was measured in the process of switching on an electric field for a short time (1–5 min).

in modification of these complexes. It is possible that they play only the role of an indicator that is sensitive to a MF-induced redistribution of electrons between other point defects. The bimolecular character of the kinetics of luminescence decay that we observed, signifying that the luminescence arises when conduction electrons recombine with sulfur complexes and also the changes occurring in the excitation spectra (Fig. 3) attest to this.

The states of point defects in a MF could change for the following reason. In the experimental crystals, dislocation motion is accompanied by a transition of the polytypic hexagonal phase to the cubic phase and is thermodynamically favorable.[16,17] Magnetic-field-induced depinning of dislocations from obstacles (for example, by the scheme described in Refs. 18 and 19) and displacement of the dislocations could result in the relaxation of the metastable phase in our experiments and could influence the state of point defects present in the phase transition regions and which are responsible for the photo- and electroluminescence.

In summary, a magnetoplastic effect was observed in ZnS crystals. It was established that the change in the plastic properties of crystals in a MF is accompanied by a change in their photo- and electroluminescence also. The results of the experiments described attest to the possibility of nonthermal control of metastable states in a crystal by means of a MF. A procedure of normalizing the different parts of a sample in a MF can be used to prevent aging of luminophores.

The results obtained open up a fundamental possibility for investigating the nature of the magnetoplastic effect using modern experimental means, making it possible to judge, with high temporal resolution, the course of electronic processes in crystals and the change in their kinetics in a magnetic field.

This work was supported by the Russian Fund for Fundamental Research (Grants Nos. 97-02-16074 and 98-02-16644).

[1] E. L. Frankevich, Zh. Éksp. Teor. Fiz. **50**, 1226 (1966) [JETP **23**, 814 (1966)].
[2] E. L. Frankevich, A. I. Pristupa, and V. M. Kobryanskiĭ, JETP Lett. **40**, 733 (1984).
[3] E. L. Frankevich, V. I. Lesin, and A. I. Pristupa, Zh. Éksp. Teor. Fiz. **75,** 415 (1978) [Sov. Phys. JETP **48**, 208 (1978)].
[4] A. E. Sokolik and E. L. Frankevich, Usp. Fiz. Nauk **111,** 261 (1973) [Sov. Phys. Usp. **16**, 687 (1974)].
[5] E. L. Frankevich and E. I. Balabanov, JETP Lett. **1**, 169 (1965).
[6] A. L. Buchachenko and I. V. Khudyakov, Usp. Khim. **60**, 1105 (1991).
[7] A. L. Buchachenko, Usp. Khim. **62**, 1139 (1993).
[8] Ya. L. Zel'dovich, A. L. Buchachenko, and E. L. Frankevich, Usp. Fiz. Nauk **155**, 3 (1988) [Sov. Phys. Usp. **31**, 385 (1988)].
[9] V. I. Al'shits, E. V. Darinskaya, T. M. Perekalina, and A. A. Urusovskaya, Fiz. Tverd. Tela (Leningrad) **29**, 467 (1987) [Sov. Phys. Solid State **29**, 265 (1987)].
[10] V. I. Al'shits, E. V. Darinskaya, and O. L. Kazakova, Zh. Éksp. Teor. Fiz. **111**, 615 (1997) [JETP **84**, 338 (1997)].
[11] Yu. I. Golovin, R. B. Morgunov, V. E. Ivanov *et al.*, JETP Lett. **68**, 426 (1998).
[12] Yu. I. Golovin and R. B. Morgunov, Zh. Éksp. Teor. Fiz. **115**, 1 (1999) [*sic*].
[13] Yu. I. Golovin and R. B. Morgunov, Chem. Rev. **24**, 1 (1998).
[14] Yu. I. Golovin, R. B. Morgunov, A. I. Tyurin, and V. I. Ivolgin, Dokl. Akad. Nauk **361**, 352 (1998).
[15] A. N. Georgobiani and M. B. Kotlyarevskiĭ, in *The Physics of II–IV Compounds* [in Russian], edited by M. K. Sheĭnkman, Nauka, Moscow, 1986.
[16] V. I. Klimenko, S. A. Omel'chenko, and S. Z. Shmurak, Fiz. Tverd. Tela (Leningrad) **30**, 1803 (1988) [Sov. Phys. Solid State **30**, 1036 (1988)].
[17] V. I. Klimenko, A. M. Muradyan, A. V. Solov'ev, and S. Z. Shmurak, Fiz. Tverd. Tela (Leningrad) **33**, 562 (1991) [Sov. Phys. Solid State **33**, 319 (1991)].
[18] M. I. Molotskii and V. N. Fleurov, Phys. Rev. B **52**, 15829 (1995).
[19] M. I. Molotskii, R. E. Kris, and V. N. Fleurov, Phys. Rev. B **51**, 12531 (1995).

Translated by M. E. Alferieff

JETP LETTERS VOLUME 69, NUMBER 2 25 JAN. 1999

Self-organization of the critical state in a two-dimensional multijunction SQUID under closed boundary conditions

S. L. Ginzburg and N. E. Savitskaya

*St. Petersburg Institute of Nuclear Physics, Russian Academy of Sciences,
188350 Gatchina, Russia*

(Submitted 16 December 1998)
Pis'ma Zh. Éksp. Teor. Fiz. **69**, No. 2, 119–125 (25 January 1999)

A model of a closed system with self-organization is presented. This is a simplified model of a multijunction SQUID in an ac magnetic field. In our closed system, a self-organized critical state is realized on account of the fact that current dumping, which gives rise to self-organization in open systems, is replaced here by a fundamentally different mechanism — annihilation of the currents. © *1999 American Institute of Physics.* [S0021-3640(99)00802-6]

PACS numbers: 85.25.Dq, 05.65.+b

The concept of self-organized criticality (SOC), which was proposed in 1987[1] and is now undergoing intensive development, is used to describe the behavior of a wide class of dissipative dynamical systems. As such systems evolve, they reach a critical state which becomes self-maintaining and structurally consists of a set of metastable states that pass into one another by an avalanche effect arising as a result of a local external perturbation of the system. Such a critical state is said to be self-organized, and the criterion for the existence of SOC in a system is taken to be power-law behavior of the probability density of the size of the avalanche.

In Ref. 2 it was shown that an interesting physical example of a system with SOC are granular superconductors (GSCs) with a large value of the fundamental parameter of the system $V \sim j_c a^3/\Phi_0$ (j_c is the critical intergranular contact current, a is the size of a granule, and Φ_0 is a the quantum of magnetic flux). In Ref. 2, using the physical features of the behavior of GSCs for $V \gg 1$, simplified models were introduced for various types of GSCs. It was found that a simplified model of a two-dimensional multijunction SQUID with positive current injection into a randomly chosen junction under open boundary conditions is equivalent to the Abelian sandpile model (ASM) — one of the basic mathematical models for studying SOC.[3] However, on account of its physical nature the multijunction SQUID model possesses a number of new properties and makes it possible to study a system under conditions which did not arise previously for the ASM and other systems with SOC.

Thus, to study the critical state of a GSC in practice a superconductor is placed in an ac magnetic field, and in this case closed boundary conditions, under which self-organization does not exist in any of the previously known models for studying SOC, are

© 1999 American Institute of Physics

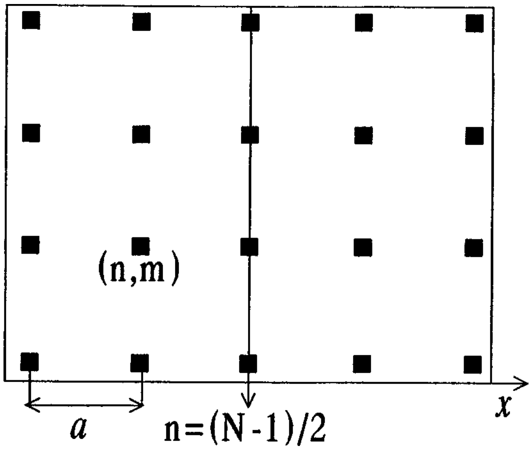

FIG. 1. Section of a two-dimensional multijunction SQUID by the (x,y) plane.

natural. In the present letter we show that SOC is realized under closed boundary conditions in the model of a multijunction SQUID in an ac magnetic field.

The possibility of self-organization in our model under closed boundary conditions is due to a number of physical features of GSCs that distinguish them from previously known systems with SOC.

In the first place, in a GSC an ac magnetic field excites both positive and negative currents simultaneously. This makes it necessary to take into account the second (negative) threshold value for currents in the current–voltage characteristic of the junctions, which was unimportant under the conditions of Ref. 2, where only a positive current was injected into the system. We note that in the ASM there is only a positive threshold, since all quantities are positive by definition.

Secondly, currents with opposite signs can annihilate each other, and the annihilation process replaces the process of current dumping outside the system which makes it possible for SOC to exist under open boundary conditions.

Our two-dimensional multijunction SQUID consists of two superconducting plates arranged parallel to each other and connected by Josephson junctions. We shall assume that a magnetic field is directed along the y axis, $\mathbf{h_{ex}}=h_{\text{ex}}\mathbf{e_y}$. Junctions with dimensions $l\times l$ are arranged at the sites of an $N\times M$ lattice having a period a and lying in the (x,y) plane. A Josephson current flows along the z axis (Fig. 1). Using the resistive model of a Josephson junction, we can write a system of equations[4,5] for the gauge-invariant phase differences $\varphi_{n,m}$,

$$V\sin\varphi_{n,m}+\tau\frac{d\varphi_{n,m}}{dt}=\Delta_{n,m}(\varphi)+2\pi F_{n,m},$$

$$V=\frac{2\pi j_c}{j_\varphi},\quad j_\varphi=\frac{\phi_0}{8\pi l^2\lambda_L},\quad F_{n,m}=\frac{j_{1n,m}}{j_\varphi},\quad \tau=\frac{\Phi_0}{\rho_0 j_\varphi},\tag{1}$$

$$\Delta_{n,m}(\varphi)=\varphi_{n+1,m}+\varphi_{n-1,m}+\varphi_{n,m-1}+\varphi_{n,m+1}-4\varphi_{n,m},$$

where j_c is the critical current density, λ_L is the London penetration depth, Φ_0 is the flux quantum, ρ_0 is the surface resistance of a junction, $j_{1n,m}$ is the injection current density, and $\Delta_{n,m}$ is the two-dimensional discrete Laplacian.

In what follows we shall assume that $V \gg 1$. This condition allows for the existence of a large number of metastable states for each SQUID in our system.[4] In this case, to investigate the critical state of a multijunction SQUID we shall employ a simplified model introduced in Ref. 2 for a GSC. The model is described by a system of mappings (equations with discrete time) for the dimensionless currents flowing through the junctions,

$$z_{n,m} = z_c \sin \varphi_{n,m} + \frac{\tau}{2\pi} \frac{\partial \varphi_{n,m}}{\partial t},$$

where $z_c = V/2\pi$:

$$\begin{aligned} z_{n,m}(k+1) - z_{n,m}(k) = {} & [\theta(z_{n+1,m}(k) - z_c) - \theta(-z_{n+1,m}(k) - z_c] \\ & + [\theta(z_{n-1,m}(k) - z_c) - \theta(-z_{n-1,m}(k) - z_c)] \\ & + [\theta(z_{n,m-1}(k) - z_c) - \theta(-z_{n,m-1}(k) - z_c)] \\ & + [\theta(z_{n,m+1}(k) - z_c) - \theta(-z_{n,m+1}(k) - z_c)] \\ & - 4[\theta(z_{n,m}(k) - z_c) - \theta(-z_{n,m}(k) - z_c)] + \xi_{n,m}(k), \end{aligned} \tag{2}$$

$$\xi_{n,m}(k) = F_{n,m}(k+1) - F_{n,m}(k),$$

where $\theta[x]$ is the Heaviside theta function, k is the discrete time, and $F_{n,m}$ is the dimensionless injection current, the same as in Eq. (1). Although in the present case current is not injected directly into the system, it can be shown[2] that the effect of an external magnetic field $\mathbf{h}_{\text{ex}}$ effectively reduces to the injection of a positive current at all sites of the right-hand boundary of the SQUID and of a negative current of exactly the same magnitude at all sites of the left-hand boundary of the SQUID. Thus the total current in the system is conserved and is zero.

Therefore $\xi_{n,m}(k) = 0$ for sites inside the lattice $(1 < n < N, 1 < m < M)$ and at the top and bottom boundaries of the lattice $(m = M, 1 < n < N$ and $m = 1, 1 < n < N)$. At the left-hand boundary of the lattice $(1 \leqslant m \leqslant M, n = 1)$

$$\xi_{n,m}(k) = \frac{2\lambda_L a}{\Phi_0} (h_{\text{ex}}(k) - h_{\text{ex}}(k+1)), \tag{3}$$

and at the right-hand boundary of the lattice $(n = N, 1 \leqslant m \leqslant M)$

$$\xi_{n,m}(k) = \frac{2\lambda_L a}{\Phi_0} (h_{\text{ex}}(k+1) - h_{\text{ex}}(k)). \tag{4}$$

In addition, as we have said more than once, closed boundary conditions are realized in the system (see Ref. 2 for a more detailed discussion). Thus Eqs. (2) take the following form at the boundaries of the lattice, for example, at the left-hand boundary:

$$\begin{aligned} z_{n,m}(k+1)-z_{n,m}(k)=&[\theta(z_{n+1,m}(k)-z_c)-\theta(-z_{n+1,m}(k)-z_c]\\ &+[\theta(z_{n,m-1}(k)-z_c)-\theta(-z_{n,m-1}(k)-z_c)]\\ &+[\theta(z_{n,m+1}(k)-z_c)-\theta(-z_{n,m+1}(k)-z_c)]\\ &-3[\theta(z_{n,m}(k)-z_c)-\theta(-z_{n,m}(k)-z_c)]+\xi_{n,m}(k). \end{aligned} \tag{5}$$

At the corner junctions of the lattice, for example, at (1, 1), we have

$$\begin{aligned} z_{n,m}(k+1)-z_{n,m}(k)=&[\theta(z_{n,m+1}(k)-z_c)-\theta(-z_{n,m+1}(k)-z_c]\\ &+[\theta(z_{n+1,m}(k)-z_c)-\theta(-z_{n+1,m}(k)-z_c)]\\ &-2[\theta(z_{n,m}(k)-z_c)-\theta(-z_{n,m}(k)-z_c)]+\xi_{n,m}(k). \end{aligned} \tag{6}$$

The system of mappings (2), (5), and (6) with the corresponding $\xi_{n,m}(k)$ can be written in the form of the algorithms that are ordinarily used to describe the dynamics of systems with SOC, specifically, ASM. The analog of the heights in this case is the value of the current $z_{n,m}$, and the main difference from the ASM, aside from the closed boundary conditions, is the possibility that negative currents exist in the system and a second (negative) threshold $-z_c$ is present.

Computer simulation of the system described by Eqs. (2), (5), and (6) was done with $z_c=9.5$ in the standard manner for systems with SOC.

1. Starting with an empty lattice (all $z_{n,m}(0)=0$), we excited a current in the system according to the rule

$$\xi_{N,p}(k)=1, \quad \xi_{1,l}(k)=-1, \tag{7}$$

where p and l are random and independent. We note that the excitation rules (7) are different from the rules (3) and (4) described previously and ordinarily realized in an experiment. However, they do not destroy the main physical requirement that the total current injected into the system is zero. We chose the perturbation method (7) because in the case of the rules (3) and (4) the system degenerates into a set of one-dimensional strips, and it is well known that SOC does not exist in a one-dimensional situation.[1]

2. After current excitation, the system relaxes according to Eqs. (2), (5), and (6). During the relaxation process $\xi_{n,m}(k)=0$ for all the junctions, all the way out to the complete stopping of the dynamics.

3. After the dynamics stops, i.e., when all $|z_{n,m}|<z_c$, a current is once again excited in the system according to the rules (7), and the process is repeated according to steps 2 and 3.

After a transient process, the system reaches a critical state which consists of a collection of metastable states which pass into one another, in each of which the currents on the left-hand side of the lattice are negative and the currents on the right-hand side are positive.

Here and below, the division of the lattice into right- and left-hand parts is different for even and odd values of N. For even N the left-hand part of the lattice consist of junctions with $1\leqslant n\leqslant N/2$ and the right-hand part consists of junctions with $N/2+1\leqslant n \leqslant N$. For odd N the left-hand part of the lattice consists of junctions with $1\leqslant n$

$\leqslant (N-1)/2$ and the right-hand part consists of junctions with $(N-1)/2+2 \leqslant n \leqslant N$, i.e., in the case of odd N the right- and left-hand parts of the lattice are separated by a column of junctions with $n=(N-1)/2+1$.

We term the process of current excitation followed by relaxation an avalanche, and we shall enumerate the avalanches with the index i. The following quantities were calculated in each avalanche in the stationary critical state:

1. The current averaged over the ''positive'' subsystem at the moment the *i*th avalanche ends (the analog of the mass of the system in the ASM[6])

$$z_i^+ = \frac{1}{S} \sum_{m=1}^{M} \sum_{n=N_1}^{N} z_{n,m}(k_i), \tag{8}$$

where k_i is the moment at which the *i*th avalanche ends, and S is the size of the subsystem. For even N, $N_1 = N/2+1$ and $S=MN/2$, while for the odd N, $N_1=(N-1)/2+2$ and $S=M(N-1)/2$.

2. The voltage averaged over the corresponding subsystem over the time of the *i*th avalanche (the analog of the size of an avalalanche in the ASM[6]). For the ''positive'' subsystem

$$u_i^+ = \frac{1}{S} \sum_{k=k_{i-1}+1}^{ki} \sum_{m=1}^{M} \sum_{n=N_1}^{N} [\theta(z_{n,m}(k)-z_c) - \theta(-z_{n,m}(k)-z_c)]. \tag{9}$$

For the ''negative'' subsystem

$$u_i^- = \frac{1}{S} \sum_{k=k_{i-1}+1}^{ki} \sum_{m=1}^{M} \sum_{n=1}^{N_2} [-\theta(-z_{n,m}(k)-z_c) + \theta(z_{n,m}(k)-z_c)], \tag{10}$$

where $N_2 = N/2$ for even N and $N_2=(N-1)/2$ for odd N.

We shall characterize the critical state, which arises, by the probability densities of the voltages $\rho(u_i^+)$ and $\rho(|u_i^-|)$. They are displayed in Fig. 2. These quantities demonstrate a power-law dependence $\rho(u) \sim u^{-\alpha}$, $\alpha \approx 1$. Therefore a self-organized critical state exists in the ''positive'' and ''negative'' parts of our *closed* system.

The existence of SOC in a closed system becomes possible because of the existence of currents which have opposite signs and can annihilate each other. For $z_c = 9.5$ and the system geometry described above, the annihilation process occurs on junctions located at the boundary of the ''positive'' and ''negative'' subsystems. For odd N, this is the central column of junctions with $n=(N-1)/2+1$, and for even N these are columns of junctions with $n=N/2$ and $n=N/2+1$.

The junctions on which annihilation occurs effectively play the role of a reservoir for the current collected from the ''positive'' and ''negative'' subsystems. According to the definition of the right- and left-hand parts of the lattice and Eqs. (8)–(10), these junctions are taken into account in the calculations only for even N. Therefore it can be conjectured that for odd N the properties of the ''positive'' subsystem are completely equivalent to the properties of a system of corresponding size with one open boundary.

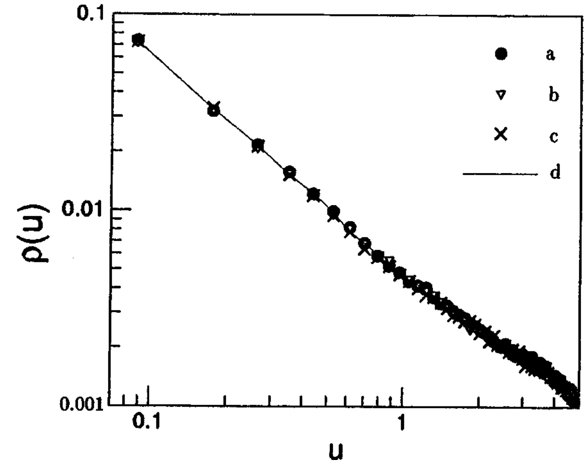

FIG. 2. Voltage probability density for: a) the "positive" part of a 42×21 system with annihilation, b) the "negative" part of a 42×21 system with annihilation, c) the "positive" part of a 43×21 system with annihilation, and d) a 21×21 system with an open boundary.

To check this, we compared the "positive" subsystem with an $N_2\times M$ multijunction SQUID, with $N_2=N/2$ for even N and $N_2=(N-1)/2\times M$ for odd N. The right-hand, top, and bottom boundaries of this SQUID are closed and the left-hand boundary is open.

We studied a system with one open boundary in the same regime as previously for the system with annihilation. A positive current was injected into a randomly chosen site of the right-hand boundary, thereby giving rise to an avalanche. The next current injection was made after the system reached the next metastable state. In this case it is sufficient to include only the positive threshold in the equations describing the current dynamics. Then, as was shown in Ref. 2, these equations are completely identical to the rules for the addition and toppling of sand in the ASM with the corresponding boundary conditions and with the addition of sand at the right-hand boundary.

Just as for the "positive" subsystem, for the system with an open boundary we shall determine for each avalanche in the stationary critical state the system-averaged current at the moment the ith avalanche ends (Eq. (8) with n ranging from 1 to N_2) and the system-averaged voltage over the time of the ith avalanche (Eq. (9) with n ranging from 1 to N_2 and in the absence of the second term arising as a result of the second threshold).

We compared the "positive" subsystem and a system with an open boundary not only with respect to the voltage probability density but also with respect to the power spectra $S_z(f)$ and $S_u(f)$ of the currents and voltages, respectively. As was shown in Ref. 6, these spectra are the characteristics that are most sensitive to the features of the system:

$$S_z(f)=2\sum_{j=-\infty}^{j=\infty}[\langle z_{j_0}z_{j_0+j}\rangle-\langle z\rangle^2]e^{-i2\pi fj}, \tag{11}$$

where $\langle\dots\rangle$ denotes averaging over the avalanche number. The formula for $S_u(f)$ is similar.

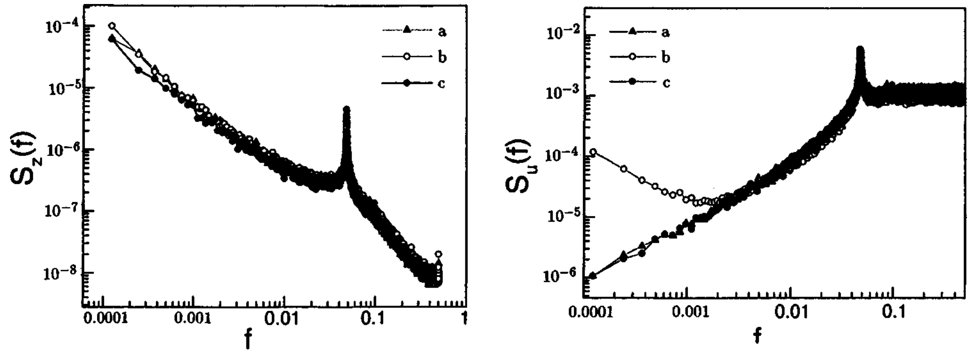

FIG. 3. Power spectra $S_z(f)$ and $S_u(f)$ of the currents and voltages, respectively, for: a) the ''positive'' part of a 43×21 system with annihilation, b) the ''positive'' part of a 42×21 system with annihilation, and c) a 21×21 system with an open boundary.

It is evident from the data presented in Figs. 2 and 3 that for odd N the properties of the critical state of a system with annihilation and an open boundary are completely equivalent; their voltage probability densities are identical over a wide interval, and the power spectra of the currents and voltages behave identically. For even N, however, a difference at low frequencies is observed in the power spectra of the voltages for the systems investigated. Calculations performed for systems with different dimensions established that the discrepancy in the behavior of the spectra for even and odd N is first observed at a frequency $f_p \sim 1/M^2$.

In conclusion, we note that in the case of both a system with annihilation and a system with an open boundary the spectra contain a peak which indicates the presence of a quasiperiodic process in the system. Calculations were also performed for systems with different dimensions, and it was established that the frequency of this peak is $f_0 \sim 1/M$.

In summary, the main results of this letter can be formulated as follows. A model of a closed system with SOC was proposed: this is a simplified model of a multijunction SQUID in an ac magnetic field. The magnetic field induces in the system both positive and negative currents. Current dumping, which makes possible the existence of SOC in open systems, is replaced by a fundamentally different mechanism: the annihilation of currents having opposite signs. It was also shown that if the junctions on which annihilation occurs are neglected in the calculations, then the properties of the critical state for a system with annihilation will be completely equivalent to those of a system of the corresponding size with one open boundary. When annihilation is taken into account, a difference is observed between the two systems only in the power spectra of the voltages at low frequencies.

We thank M. A. Pustovoĭt and O. V. Gerashchenko for an involved discussion of the problems and for valuable remarks.

This work was supported by the Scientific Council on ''Superconductivity'' of the program ''Topical Problems in Condensed-Matter Physics'' and was performed as part of Project 96021 ''Profil'.'' This work was also supported by the subprogram ''Statistical Physics'' of the Government Scientific and Technical Program ''Physics of Quantum and

Wave Processes'' as part of Project VIII-3 and the Government Program ''Neutron Studies of Matter.''

[1] P. Bak, C. Tang, and K. Wiesenfeld, Phys. Rev. Lett. **59**, 381 (1987).
[2] S. L. Ginzburg, Zh. Éksp. Teor. Fiz. **106**, 607 (1994) [JETP **79**, 334 (1994)].
[3] D. Dhar, Phys. Rev. Lett. **64**, 1613 (1990).
[4] K. K. Likharev, *Introduction to the Dynamics of Josephson Junctions*, Nauka, Moscow, 1985.
[5] A. Barone and G. Paternò, *Physics and Applications of the Josephson Effect*, Wiley, New York, 1982; Mir, Moscow, 1984.
[6] S. L. Ginzburg, M. A. Pustovoit, and N. E. Savitskaya, Phys. Rev. E **57**, 1319 (1998).

Translated by M. E. Alferieff

JETP LETTERS VOLUME 69, NUMBER 2 25 JAN. 1999

Green's function of a 2D Fermi system undergoing a topological phase transition

V. P. Gusynin and V. M. Loktev*⁾

N. N. Bogolyubov Institute of Theoretical Physics, Ukrainian National Academy of Sciences, 252143 Kiev, Ukraine

S. G. Sharapov

N. N. Bogolyubov Institute of Theoretical Physics, Ukrainian National Academy of Sciences, 252143 Kiev, Ukraine;
Department of Physics, University of Pretoria, 0002 Pretoria, South Africa

(Submitted 16 December 1998)
Pis'ma Zh. Éksp. Teor. Fiz. **69**, No. 2, 126–131 (25 January 1999)

An explicit expression is obtained for the single-particle Green's function of a 2D metallic system with attraction between carriers. It is shown that as a result of transverse phase fluctuations, this function is pole-free throughout the entire region of finite temperatures (both above and below the topological phase transition point) corresponding to a nonzero modulus of the complex order field describing the transition from a nonsuperconducting (in this case normal) state to a superconducting state, whose appearance in the 2D case is not accompanied by spontaneous breaking of charge symmetry. © *1999 American Institute of Physics.* [S0021-3640(99)00902-0]

PACS numbers: 74.20.Mn, 74.25.Jb

1. Since the discovery of high-temperature superconductors (HTSCs) the already considerable attention devoted to low-dimensional systems has increased even more. Many of their properties, the electronic properties first and foremost, are so anisotropic (see, e.g., the review[1]) that they can be described on the basis of 2D models. This is especially nontrivial with respect to the critical temperature T_c, since its high values (up to $\sim 10^2$ K), which are maintained practically down to monolayers[2] (in terms of the number of cuprate planes), are apparently a two-dimensional phenomenon and not a consequence of any three-dimensionalizing interactions. Moreover, as a rule, experiments attest to exceptional smoothness of the transition (especially in lightly doped samples) between the normal and superconducting (SC) states of HTSCs,1) making it possible to classify the latter as a crossover transition rather than an ordinary second-order phase transformation. To some extent, this could explain why the study of low-dimensional electronic liquids has become one of the important problems of condensed-matter physics (see the review by Wiegmann[6]).

One method of describing them was proposed in Refs. 7–9, which treated simple models of a 2D metal with arbitrary carrier density n_f or, equivalently, arbitrary Fermi energy ϵ_F of noninteracting fermions (the equivalency follows from the fact that for them

$\epsilon_F = \pi n_f / m$, where m is the effective mass of the carrier) . It was shown that the temperature T_{BKT} of the Berezinskiĭ–Kosterlitz–Thouless topological transition plays a critical role in this case. As is well known, here there is no order parameter in the usual sense, but nonetheless the temperature of the transformation of the normal to the superconducting state can be calculated by introducing a complex order field $\Phi(x)$, for which $\langle \Phi(x) \rangle = 0$. While the SC model is of the same universality class as the 2D XY model,[10,11] the two models are not identical. A specific property of the latter model is that the ''two-component vector'' $\Phi(x)$ is not a unit vector — its modulus is not conserved as the temperature is raised above T_{BKT}: it decreases sharply near and above the mean-field temperature T_c^{MF}, which is always higher than T_{BKT}. In addition, both temperatures are functions of n_f.

However, the spectral characteristics of SC states both above and below $T_c(T_{\mathrm{BKT}})$ are of no less interest. Moreover, photoemission or tunneling experiments admit a direct determination of the spectral function $A(\omega,\mathbf{k})$ of the SC state, which is directly related by the expression $A(\omega,\mathbf{k}) = \pi^{-1} \mathrm{Im}\, G(\omega + i0,\mathbf{k})$ to the single-particle Green's function (GF), which for HTSCs is ordinarily written on the basis of phenomenological or, to one degree or another, qualitative considerations.[12–14] Essentially, the only exception is Ref. 15, where an attempt was made to calculate analytically the GF of the 2D Hubbard model with attraction, but the question of the behavior of the spectrum near the phase transition was actually not considered in that model because the T-matrix approach was used. In this connection, there is a need to calculate the GF on the basis of a simple but nontrivial model containing a topological transition. As far as we know, such a calculation has not yet been done.

2. Just as in Refs. 7 and 8, we shall employ a very simple Hamiltonian for 2D attracting fermions ($\hbar = k_B = 1$)

$$\mathcal{H} = \psi_\sigma^\dagger(x)(-\nabla^2/2m - \mu)\psi_\sigma(x) - V\psi_\uparrow^\dagger(x)\psi_\downarrow^\dagger(x)\psi_\downarrow(x), \tag{1}$$

where $x = \mathbf{r},\tau$ are the spatial and imaginary-time variables; $\psi_\sigma(x)$ is the Fermi field with spin $\sigma = \uparrow,\downarrow$; μ is the chemical potential, which fixes n_f; and, V is the effective attraction. The subsequent steps in the calculation involve introducing Nambu spinors and treating the fermions as composite objects consisting of spin and charge parts:

$$\Psi^\dagger(x) = (\psi_\uparrow^\dagger(x), \quad \psi_\downarrow(x)) = \Upsilon^\dagger(x)\exp[-i\tau_3\theta(x)/2], \tag{2}$$

where $\Upsilon^\dagger(x)$ corresponds to the Nambu spinor for neutral fermions. Taking into account that, according to the standard definition of the GF,

$$G(x) = \langle \Psi(x)\Psi^\dagger(0) \rangle, \tag{3}$$

and substituting expressions (2) into Eq. (3), we arrive at the expression

$$G_{\alpha\beta}(x) = \sum_{\alpha_1\beta_1} \mathcal{G}_{\alpha_1\beta_1}(x) \langle [\exp(i\tau_3\theta(x)/2)]_{\alpha\alpha_1} [\exp(-i\tau_3\theta(0)/2)]_{\beta_1\beta} \rangle, \tag{4}$$

whence one can see that the GF of charged (observable) Fermi particles is a product of the GFs

$$\mathcal{G}_{\alpha\beta}(x) = \langle \Upsilon(x)_\alpha \Upsilon^\dagger(0)_\beta \rangle \tag{5}$$

of the neutral fermions and a correlation function of the phases $\langle \exp(i\tau_3\theta(x)/2) \times \exp(-i\tau_3\theta(0)/2)\rangle$, which corresponds to the charged degrees of freedom. Fourier transforming expression (4) gives

$$G(i\omega_n,\mathbf{k}) = T\sum_{m=-\infty}^{\infty}\int\frac{d^2p}{(2\pi)^2}\sum_{\alpha,\beta=\pm} P_\alpha\mathcal{G}(i\omega_m,\mathbf{p})P_\beta D_{\alpha\beta}(i\omega_n-i\omega_m,\mathbf{k}-\mathbf{p}), \tag{6}$$

where the projection operators are $P_\pm \equiv (1/2)(I+\tau_3)$, I and τ_i are the unit and Pauli matrices, $\omega_n = (2n+1)\pi T$ are the Matsubara Fermi frequencies; $D_{\alpha\beta}(i\Omega_n,\mathbf{q})$, which is the Fourier transform of $D_{\alpha\beta}(x) = \langle \exp(i\alpha\theta(x)/2)\exp(-i\beta\theta(0)/2)\rangle$, contains, as one can see, only even (bosonic) frequencies.

The neutral-particle GF (5) was calculated in Refs. 7 and 8, where it was shown that in a 2D metal the form of the function corresponds to that based on Bogolyubov's BCS theory,

$$\mathcal{G}(i\omega_n\mathbf{k}) = -\frac{i\omega_n\hat{I}+\tau_3\xi(\mathbf{k})-\tau_1\rho}{\omega_n^2+\xi^2(\mathbf{k})+\rho^2}, \quad \xi(\mathbf{k}) = \frac{\mathbf{l}^2}{2m}-\mu, \tag{7}$$

where $|\langle\Phi(x)\rangle|$ has been replaced by $\langle|\Phi(x)|\rangle \equiv \rho$ and the approximation $\Phi(x) = \rho\exp(i\theta(x))$ is used, giving $\langle\Phi(x)\rangle = 0$ in two dimensions on account of the random transverse (consistent with the principle of conservation of the modulus[10]) fluctuations of the phase of the field $\Phi(x)$. It should be noted that the gap in the neutral-particle spectrum and, accorddingly, the existence of a neutral condensate are not associated with the so-called incoherent precursors (precursor pairs) that arise in the strong-coupling approximation above T_c irrespective of the dimension of the space.[12,13] In the approach proposed here, the appearance of a neutral order parameter ρ, generating a gap in the normal phase of a 2D metal, is simply a manifestation of the collective behavior of the system as a whole, changing its spectrum and properties.

3. The representation (6) with the known GF (7) shows that the resulting expression for the charged-particle GF is entirely determined by the correlation function $D(x) \equiv D_{\pm\pm}(x)$. Its quite general form can be represented by the expression

$$D(t,\mathbf{r}) = \exp(-\gamma t)(r/r_0)^{-T/8\pi J}\exp(-r/\xi_+(T)), \tag{8}$$

which follows from the theory of the BKT transition with the dynamics of vortex excitations taken into account.[10,11,16,17] In Eq. (8) γ is the temporal decay constant of phase correlations, which is introduced phenomenologically; $r_0 \equiv (2/T)(J/K)^{1/2}$ is the scale of algebraic decay of correlations in the BKT phase ($T < T_{\mathrm{BKT}}$); $\xi_+(T)$ is the correlation length in the region $T > T_{\mathrm{BKT}}$, and $\xi_+(T \to T_{\mathrm{BKT}}) \to \infty$. The constants J and K correspond to the ''transverse'' stiffness and compressibility of the neutral condensate, expressions for which are presented in Refs. 7 and 8. We shall examine below only the static ($\gamma = 0$) case, leaving the dynamic case for a separate exposition.

Then it can be shown that the Fourier transform of the static correlation function $D(x)$ has the form

$$D(i\Omega_n,\mathbf{q})=\int_0^{1/T}d\tau\int d\mathbf{r}\exp(i\Omega_n\tau-i\mathbf{q}\cdot\mathbf{r})(r/r_0)^{-T/8\pi J}\exp(-r/\xi_+(T))$$

$$=2\pi\delta_{n0}\frac{r_0^{2(1-\alpha)}\Gamma(2\alpha)}{(q^2+1/\xi_+^2)^\alpha}\,{}_2F_1\left(\alpha,-\alpha+\frac{1}{2};1;\frac{(q\xi_+)^2}{(q\xi_+)^2+1}\right),\tag{9}$$

where ${}_2F_1(a,b;c;z)$ is the hypergeometric function, in which

$$\alpha=1-\frac{T}{8\pi J}.\tag{10}$$

Since it is a weakly varying function of **q**, a good approximation of the function is the asymptotic expression in the limit $q\to\infty$, so that ultimately we have for Eq. (9)

$$D(i\Omega_n,\mathbf{q})=C\delta_{n0}\frac{\xi_+^{2\alpha}}{[(q\xi_+)^2+1]^\alpha},\quad C=2\pi\frac{\Gamma(\alpha)}{\Gamma(1-\alpha)}\left(\frac{2}{r_0}\right)^{2\alpha-2},\tag{11}$$

whence (see Eq. (6))

$$G(i\omega_n,\mathbf{k})=-C\int\frac{d^2q}{(2\pi)^2}\frac{i\omega_n+\tau_3\xi(\mathbf{q})}{\omega_n^2+\xi^2(\mathbf{q})+\rho^2}\frac{\xi_+^{2\alpha}}{[(\mathbf{k}-\mathbf{q})^2\xi_+^2+1]^\alpha}.\tag{12}$$

It is important to underscore that even for $T<T_{\mathrm{BKT}}$ the propagator (11) of the phase correlations does not exhibit the canonical behavior $\sim 1/q^2$ characteristic of, for example, the Bogolyubov mode in more than two dimensions. In 2D systems the presence of modes with a propagator $\sim 1/q^2$ would lead to strong infrared singularities, to avoid which the modes are ‘‘automatically’’ softened ($\sim 1/q^{2\alpha}$, since $\alpha<1$). We also note that the charged-fermion propagator (12), unlike the neutral-fermion propagator (7), does not contain terms proportional to the matrix τ_1, whose presence would lead to spontaneous breaking of charge symmetry, in contradiction to the general theorem of the impossibility of such breaking in two dimensions.[18]

The integral in Eq. (12) can be calculated exactly, yielding

$$G(i\omega_n,\mathbf{k})=-\frac{Cm\xi_+^{2\alpha}}{2\pi\alpha}\left[\frac{A}{(u_1u_2)^\alpha}F_1\left(\alpha,\alpha,\alpha;\alpha+1;\frac{u_1-1}{u_1},\frac{u_2-1}{u_2}\right)\right.$$

$$\left.+\left(\sqrt{\omega_n^2+\rho^2}\to-\sqrt{\omega_n^2+\rho^2}\right)\right],\tag{13}$$

where F_1 is the Appel function of two variables,[19]

$$A=\frac{1}{2}\left(\tau_3-\frac{\omega_n}{\sqrt{\omega_n^2+\rho^2}}\right),\quad u_{1,2}=m\xi_+^2(u_0\pm\sqrt{D}),$$

$$D=u_0^2+\frac{2}{m\xi_+^2}\left(\mu-i\sqrt{\omega_n^2+\rho^2}\right),\quad u_0\equiv\frac{k^2\xi_+^2+1}{2m\xi_+^2}-\mu+i\sqrt{\omega_n^2+\rho^2}.\tag{14}$$

Expression (13) more or less completes the analytical calculation of the desired GF of a 2D metal in the entire important range of temperatures.

4. To find the spectral density, however, it is necessary to know the retarded GF, which is obtained by the Matsubara substitution $i\omega_n \to \omega + i0$, so that $\sqrt{\omega_n^2+\rho^2} \to i\sqrt{\omega^2-\rho^2}$. Ultimately, we obtain from Eq. (13)

$$G(\omega,\mathbf{k}) = -\frac{Cm\xi_+^{2\alpha}}{2\pi\alpha}\left[\frac{\mathcal{A}}{(v_1v_2)^\alpha}F_1\left(\alpha,\alpha,\alpha;\alpha+1;\frac{v_1-1}{v_1},\frac{v_2-1}{v_2}\right)\right.$$
$$\left. + (\sqrt{\omega^2-\rho^2} \to -\sqrt{\omega^2-\rho^2})\right], \tag{15}$$

where now

$$\mathcal{A} = \frac{1}{2}\left(\tau_3 + \frac{\omega}{\sqrt{\omega^2-\rho^2}}\right), \quad v_{1,2} = m\xi_+^2(v_0 \pm \sqrt{D}),$$

$$D = v_0^2 + \frac{2}{m\xi_+^2}(\mu + \sqrt{\omega^2-\rho^2}), \quad v_0 = \frac{k^2\xi_+^2+1}{2m\xi_+^2} - \mu - \sqrt{\omega^2-\rho^2}, \tag{16}$$

Let us consider first the region $T < T_{\mathrm{BKT}}$, where $\xi_+ = \infty$. In this case, one argument of the Appel function becomes 1 and the GF can be expressed in terms of the hypergeometric function ${}_2F_1$:

$$G(\omega,\mathbf{k}) = -\Gamma^2(\alpha)\left(\frac{2}{mr_0^2}\right)^{\alpha-1}\left[\frac{\mathcal{A}}{(-z)^\alpha}\,{}_2F_1\left(\alpha,\alpha;1;\frac{k^2}{2mz}\right)\right.$$
$$\left. + (\sqrt{\omega^2-\rho^2} \to -\sqrt{\omega^2-\rho^2})\right], \tag{17}$$

where $z = \mu + \sqrt{\omega^2-\rho^2}$. It is easy to check the limit $T=0$. In this case $D(\mathbf{r}) \to 1$ (i.e., long-range order is established in the system), $\alpha = 1$, and therefore

$$G_{11}(\omega,\mathbf{k}) = \frac{\omega + \xi(\mathbf{k})}{\omega^2 - \xi^2(\mathbf{k}) - \rho^2}, \tag{18}$$

and the spectral function can be expressed in terms of the standard sum of two δ peaks corresponding to quasiparticle energies[2)] $E(\mathbf{k}) = \pm\sqrt{\xi^2(\mathbf{k}) + \rho_0^2}$ $(\rho_0 = \rho(T=0))$.

From formula (15) one can see that the GF is real in the region $|\omega| < \rho$; in other words, there is no spectral weight in this frequency range, or a gap remains in the spectrum throughout the entire range of T, including the nonsuperconducting region, where $\rho \neq 0$.

However, a more interesting fact is that the GF (15) has a pole-free structure. Indeed, for $T < T_{\mathrm{BKT}}$, where it has the form (17), it is easy to see that near the quasiparticle state, where $\omega \approx \pm E(\mathbf{k})$, the argument of the hypergeometric function is close to 1. Using this, as well as the relation between the hypergeometric functions,[19] we find

$$G(\omega,\mathbf{k})\sim-\Gamma^2(\alpha)\left(\frac{2}{mr_0^2}\right)^{\alpha-1}\frac{\mathcal{A}}{[-(\mu+\sqrt{\omega^2-\rho^2})]^{\alpha}}$$
$$\times\left\{\frac{\Gamma(1-2\alpha)}{\Gamma^2(1-\alpha)}+\frac{\Gamma(2\alpha-1)}{\Gamma^2(\alpha)}\frac{1}{(1-z_1)^{2\alpha-1}}\right\}, \qquad (19)$$

where $z_1\equiv k^2/2mz=(k^2/2m)/(\mu+\sqrt{\omega^2-\rho^2})\simeq 1$.

The expansion found is of an unusual form, because it contains a cut rather than a pole. It is obvious that the difference of the GF (19) from the standard function is entirely due to the phase fluctuations, which lead to a parameter $\alpha\neq 1$ [see Eq. (10)]. Although in the region $T\leqslant T_{\mathrm{BKT}}$ it is small, the pole-free (or equivalently the non-Fermi liquid) behavior of the GF is of fundamental importance. In addition, this parameter increases either with T or, since $J\sim n_f$ (Refs. 7 and 8), with decreasing carrier density, and one would therefore expect the most salient qualitative features in the properties of superconducting 2D metals to appear as the doping decreases, as is in fact observed in HTSCs.

Space limitations do not permit us to present in this letter a more detailed analysis of the formulas obtained for the GF. But even the results presented above show that both the spectral function and the corresponding density of single-particle states, to which the GFs written out above in the static approximation lead, will contain a gap so long as ρ is finite. Filling of the gap and the transformation of the gap into a pseudogap require at least taking into account the temporal decay of the γ correlations in Eq. (8). This in turn will lead to damping of charged fermions. As a rule, the latter is introduced artificially in the charged-fermion GFs (see, for example, Refs. 12 and 14) in order to obtain and thereby describe the pseudogap behavior of the normal state of HTSCs. As we have shown above, the non-Fermi character of the GF is not directly related with the temporal decay and is found to be characteristic of 2D metallic systems in the static approximation for the correlation function of the phase fluctuations. Despite the fact that a 2D superconducting system was studied above, the pole-free behavior obtained for the GFs is quite general and can be extended to other physical situations where long-wavelength excitations of a composite type can exist.

Finally, it can also be expected that there exists a region of parameters (fermion density, probability of interplanar tunneling of fermions, and so on) where the characteristic features found will also remain for the GFs of quasi-2D systems, such as are real layered compounds, including HTSCs.

*)e-mail: vloktev@bitp.kiev.ua

1)As an example, the uniform magnetic susceptibility,[3] specific heat,[4] and NMR relaxation rate[5] often do not respond at all to T_c. The change in the resistance remains quite sharp, and correspondingly the transition remains narrow.

2)To obtain the off-diagonal components G_{12} and G_{21}, the correlation functions $D_{-+}(\mathbf{r})$ and $D_{+-}(\mathbf{r})$, which are nonzero at $T=0$, must be reconstructed.

---

[1] V. M. Loktev, Fiz. Nizk. Temp. **22**, 3 (1996) [Low Temp. Phys. **22**, 1 (1996)].

[2] K. Saito and M. Kaise, Phys. Rev. B **57**, 11786 (1998).

[3] Y. Itoh *et al.*, Phys. Soc. Jpn. **65**, 3751 (1996).

[4] J. W. Loram *et al.*, Physica C **235-240**, 134 (1994).

[5] A. V. Bondar' *et al.*, in *Physical Problems of High-Temperature Superconductors* [in Russian], edited by V. M. Loktev, Naukova Dumka, Kiev, 1990, p. 5.

[6] P. B. Wiegmann, http://xxx.lanl.gov/abs/cond-mat/9808004.

[7] V. P. Gusynin, V. M. Loktev, and S. G. Sharapov, JETP Lett. **65**, 182 (1997); JETP, at press.

[8] V. P. Gusynin, V. M. Loktev, and S. G. Sharapov, Fiz. Nizk. Temp. **23**, 816 (1997) [Low Temp. Phys. **23**, 612 (1997)]; Ibid. **23**, 1247 (1997) [Low Temp. Phys. **23**, 1936 (1997)].

[9] V. M. Loktev and V. M. Turkovskiĭ, Zh. Éksp. Teor. Fiz. **114**, 605 (1998) [JETP **87**, 329 (1998)].

[10] A. Z. Patashinskiĭ and V. L. Pokrovskiĭ, *Fluctuation Theory of Phase Transitions*, Pergamon Press, Oxford, 1979, 1st edition [Russian original, 2nd ed., Nauka, Moscow, 1983].

[11] Yu. A. Izyumov and Yu. N. Skryabin, *Statistical Mechanics of Magnetically Ordered Systems*, Nauka, Moscow, 1982.

[12] O. Tchernyshyov, Phys. Rev. B **56**, 3372 (1997).

[13] B. Janko, J. Mali, and K. Levin, http://xxx.lanl.gov/abs/cond-mat/9805018; I. Kostin *et al.*, Phys. Rev. B **58**, R5936 (1998).

[14] M. Franz and A. J. Millis, http://xxx.lanl.gov/abs/cond-mat/9705401; to appear in Phys. Rev. B.

[15] M. Yu. Kagan *et al.*, Phys. Rev. B **57**, 5995 (1998).

[16] M. Plischke and B. Bergersen, *Equilibrium Statistical Physics*, Prentice-Hall, New Jersey, 1989, p. 167.

[17] P. Minnhagen, Rev. Mod. Phys. **59**, 1001 (1987).

[18] N. D. Mermin and H. Wagner, Phys. Rev. Lett. **17**, 1113 (1966); P. C. Hohenberg, Phys. Rev. **158**, 383 (1967); S. Coleman, Commun. Math. Phys. **31**, 259 (1973).

[19] A. Erdélyi, *Higher Transcendental Functions (Bateman Manuscript Project),* Vols. 1–3, edited by A. Erdélyi, McGraw-Hill, New York, 1953, 1953, 1955; Vols. 1–3, Nauka, Moscow, 1965, 1966, 1967.

Translated by M. E. Alferieff

JETP LETTERS VOLUME 69, NUMBER 2 25 JAN. 1999

Electromagnetic waves in the nonlocal Josephson electrodynamics of a thin film of a magnetic superconductor

A. I. Lomtev*

Donetsk Physicotechnical Institute, Ukrainian National Academy of Sciences, 340144 Donetsk, Ukraine

(Submitted 16 December 1998)
Pis'ma Zh. Éksp. Teor. Fiz. **69**, No. 2, 132–138 (25 January 1999)

An integrodifferential equation describing the dynamics of the phase difference with spatial and temporal nonlocality is derived for a Josephson junction in a thin film of magnetic superconductor. It is shown that the magnetic subsystem renormalizes the spectrum of small-amplitude electromagnetic excitations and leads to their damping. © *1999 American Institute of Physics.* [S0021-3640(99)01002-6]

PACS numbers: 74.50.+r, 74.25.Nf

1. A large number of magnetic superconductors manifesting new, unique properties are now well known.[1–3] Besides ternary compounds,[4] the coexistence of superconductivity and magnetism has been established in high-temperature superconducting (HTSC) compounds of the type REBaCuO, RECuO, and others, where RE denotes a rare-earth ion. The strong antiferromagnetic correlation of copper spins in the CuO_2 planes in a superconducting state is one of the most important features of HTSC materials.[5]

The equations of nonlocal Josephson electrodynamics have now been obtained and investigated in five cases: 1) a tunnel junction at the interface between two superconducting ultrathin films, whose thicknesses are much less than the London length; 2) a tunnel junction between massive superconductors, whose thickness is much greater than the London length; 3) a tunnel junction between superconducting layers of finite thickness in a direction orthogonal to the magnetic field; 4) a ''butt-joined'' tunnel junction between superconducting plates of finite thickness along the magnetic field; and, 5) inclined (canted) Josephson junction between superconducting plates of finite thickness along the magnetic field.

Thus in Refs. 6–13 it is shown that nonlocality effects can be substantial even in junctions with large thickness d ($d \gg \lambda$, where λ is the London penetration depth) along the magnetic field (in the direction of the vortices), i.e., in situations previously studied in a local approximation. In the opposite limiting case of junctions in thin films, such that $d \gg \lambda$, the nonlocality is very substantial and becomes the determining factor. The corresponding equations have been derived and studied in Refs. 14–17. A Josephson junction between two superconducting layers of finite thickness in a direction orthogonal to the magnetic field of the vortices was studied in Ref. 18. In recent works[19,20] a ''butt-joined'' junction and an inclined (canted) junction, respectively, of finite thickness along the

© 1999 American Institute of Physics

magnetic field of the vortices with arbitrary ratio d/λ were studied.

2. It becomes all the more important to investigate the nonlocal electrodynamics of Josephson junctions in ultrathin films of magnetic superconductors for which $d \ll \lambda$. In this case, the problem can be reduced to that of an infinitely thin two-dimensional plane, such that the dependence of the physical characteristics of a junction on the coordinate z perpendicular to the plane of the film can be neglected.

We shall also assume that the system is two-dimensional with respect to its superconducting and magnetic properties, so that the magnetic permeability of the film can be represented in the form $\mu(\mathbf{r}-\mathbf{r}',t-t')=\mu(\boldsymbol{\rho}-\boldsymbol{\rho}',t-t')\delta(z-z')$, where $\mathbf{r}=(x,y,z)$ and $\boldsymbol{\rho}=(x,y)$.

The geometry of the problem is as follows: the film plane is the xy plane, the current propagates along the y axis, and the line of weak links lies on the x axis.

Following Refs. 21 and 22, we proceed from Maxwell's equations for the magnetic induction $\mathbf{B}(\mathbf{r},t)=\nabla\times\mathbf{A}(\mathbf{r},t)$ ($\mathbf{A}(\mathbf{r},t)$ is the vector potential), determined by the sum of the magnetic field $\mathbf{H}(\mathbf{r},t)$ produced by the nondecaying current $\mathbf{j}(\mathbf{r},t)$ and the magnetization $\mathbf{M}(\mathbf{r},t)$:

$$\nabla\times\mathbf{B}(\mathbf{r},t)=\frac{4\pi}{c}\mathbf{j}(\mathbf{r},t)+4\pi\nabla\times\mathbf{M}(\mathbf{r},t). \tag{1}$$

The relation between the current, potential, and phase of the order parameter $\Theta(\mathbf{r},t)$ (in the London gauge $\nabla\cdot\mathbf{A}(\mathbf{r},t)=0$) is determined by the expression

$$\mathbf{j}(\mathbf{r},t)=(c/4\pi\lambda^2)[\mathbf{S}(\boldsymbol{\rho},t)-\mathbf{A}(\mathbf{r},t)], \tag{2}$$

where the vector $\mathbf{S}(\boldsymbol{\rho},t)$ is determined by the gradient of the phase:

$$\mathbf{S}(\boldsymbol{\rho},t)=\frac{\Phi_0}{2\pi}\nabla\Theta(\boldsymbol{\rho},t), \tag{3}$$

where Φ_0 is the quantum of magnetic flux.

The phase of the order parameter satisfies the condition

$$\nabla\times\mathbf{S}(\boldsymbol{\rho},t)=-\hat{\mathbf{z}}\,\frac{\Phi_0}{2\pi}\,\frac{\partial\varphi(x,t)}{\partial x}\,\delta(y), \tag{4}$$

where $\hat{\mathbf{z}}$ is a unit vector in the direction of the z axis, and $\varphi(x,t)$ is determined by the phase difference of the order parameter at the junction

$$\varphi(x,t)=\Theta(x,+0,t)-\Theta(x,-0,t). \tag{5}$$

The system of equations (1) and (2) leads to the relation

$$\nabla\times\mathbf{H}(\mathbf{r},t)=\frac{c}{4\pi\lambda^2}[\mathbf{S}(\boldsymbol{\rho},t)-\mathbf{A}(\mathbf{r},t)], \tag{6}$$

which for an ultrathin film with $d\ll\lambda$ can be represented in the form

$$\nabla\times\mathbf{H}(\mathbf{r},t)=\lambda_{\text{eff}}^{-1}[\mathbf{S}(\boldsymbol{\rho},t)-\mathbf{A}(\mathbf{r},t)]\,\delta(z), \tag{7}$$

where $\lambda_{\text{eff}}=\lambda^2/d$ is the Peierls penetration depth and $\delta(z)$ is the Dirac delta function. The magnetic field $\mathbf{H}(\mathbf{r},t)$ is related with the magnetic induction $\mathbf{B}(\mathbf{r},t)$ by the integral relation

$$\mathbf{H}(\mathbf{r},t)=\int_{-\infty}^{t}dt'\int_{-\infty}^{\infty}d\boldsymbol{\rho}'\,\mu^{-1}(\boldsymbol{\rho}-\boldsymbol{\rho}',t-t')\mathbf{B}(\boldsymbol{\rho}',z,t'), \tag{8}$$

where $\mu(\boldsymbol{\rho}-\boldsymbol{\rho}',t-t')$ is the magnetic permeability of a two-dimensional superconducting film.

From the system (7) and (8) we obtain an equation for the vector potential

$$\begin{aligned}\nabla\times\left\{\int_{-\infty}^{t}dt'\int_{-\infty}^{\infty}d\boldsymbol{\rho}'\,\mu^{-1}(\boldsymbol{\rho}-\boldsymbol{\rho}',t-t')\nabla\times\mathbf{A}(\boldsymbol{\rho}',z,t')\right\}\\ =\lambda_{\text{eff}}^{-1}[\mathbf{S}(\boldsymbol{\rho},t)-\mathbf{A}(\boldsymbol{\rho},z,t)]\delta(z),\end{aligned} \tag{9}$$

expressing the vector potential in terms of the field of the source $\mathbf{S}(\boldsymbol{\rho},t)$. From the continuity equation $\nabla\cdot\mathbf{j}(\mathbf{r},t)=0$ and Eq. (2) follows $\nabla\cdot\mathbf{S}(\boldsymbol{\rho},t)=0$. Therefore the vector field $\mathbf{S}(\boldsymbol{\rho},t)$ can be expressed as the curl of the vector field $\mathbf{F}(\boldsymbol{\rho},t)$ in the form

$$\mathbf{S}(\boldsymbol{\rho},t)=\nabla\times\mathbf{F}(\boldsymbol{\rho},t), \tag{10}$$

where

$$\mathbf{F}(\boldsymbol{\rho},t)=\hat{\mathbf{z}}F(\boldsymbol{\rho},t). \tag{11}$$

Substituting expression (11) into relation (4), we obtain an equation describing the function $F(\rho,t)$ in the form

$$\nabla^2F(\boldsymbol{\rho},t)=\frac{\Phi_0}{2\pi}\frac{\partial\varphi(x,t)}{\partial t}\delta(y). \tag{12}$$

On the one hand, the density $j_y(x,0,t)$ of the current flowing through the Josephson junction is the sum of (for example) three terms: the densities of the Josephson supercurrent, the normal (quasiparticle) current, and the capacitive displacement current

$$j_y(x,0,t)=j_c\left[\sin\varphi(x,t)+\frac{\beta}{\omega_j^2}\frac{\partial\varphi(x,t)}{\partial t}+\frac{1}{\omega_j^2}\frac{\partial^2\varphi(x,t)}{\partial t^2}\right]d\,\delta(z), \tag{13}$$

where β is the dissipative parameter, and j_c and ω_j are the critical current and Josephson frequency, respectively. On the other hand, it follows from Eq. (2) that the same current density $j_y(x,0,t)$ can be expressed as

$$j_y(x,0,t)=\frac{c}{4\pi\lambda_{\text{eff}}}[S_y(x,0,t)-A_y(x,0,0,t)]\delta(z). \tag{14}$$

Equating the expressions for the current density (13) and (14), we see that

$$j_c\left[\sin\varphi(x,t)+\frac{\beta}{\omega_j^2}\frac{\partial\varphi(x,t)}{\partial t}+\frac{1}{\omega_j^2}\frac{\partial^2\varphi(x,t)}{\partial t^2}\right]=\frac{c}{4\pi\lambda^2}[S_y(x,0,t)-A_y(x,0,0,t)]. \tag{15}$$

To obtain a closed dynamical equation for the phase density $\varphi(x,t)$, a functional relation between

$$\Delta_y(x,t)=S_y(x,0,t)-A_y(x,0,0,t) \tag{16}$$

and $\varphi(x,t)$ must be found.

To solve the system of equations (9), we introduce the Fourier transform for the vectors $\mathbf{A}(\mathbf{r},t)$ and $\mathbf{S}(\boldsymbol{\rho},t)$ and the scalar function $\mu^{-1}(\boldsymbol{\rho},t)$ in the form

$$\mathbf{A}(\boldsymbol{\rho},z,t)=\int\frac{d^2q\,dp\,d\omega}{(2\pi)^4}\exp(i\mathbf{q}\cdot\boldsymbol{\rho}+ipz-i\omega t)\mathbf{A}(\mathbf{q},p,\omega), \tag{17}$$

$$\mathbf{S}(\boldsymbol{\rho},t)=\int\frac{d^2q\,d\omega}{(2\pi)^3}\exp(i\mathbf{q}\cdot\boldsymbol{\rho}-i\omega t)S(\mathbf{q},\omega), \tag{18}$$

and

$$\mu^{-1}(\boldsymbol{\rho},t)=\int\frac{d^2q\,d\omega}{(2\pi)^3}\exp(i\mathbf{q}\cdot\boldsymbol{\rho}-i\omega t)\mu^{-1}(\mathbf{q},\omega). \tag{19}$$

Using the relations (17) and (18), we represent $\Delta_y(x,t)$ as an integral in the form

$$\Delta_y(x,t)=\frac{1}{(2\pi)^2}\int_{-\infty}^{\infty}d\omega\int_0^{\infty}q\,dq\int_{-\pi}^{\pi}d\vartheta[S_y(\mathbf{q},\omega)-A_y(\mathbf{q},\omega)]$$
$$\times\exp(iqx\cos\vartheta-i\omega t), \tag{20}$$

where $q=(q_x^2+q_y^2)^{1/2}$, ϑ is the polar angle in the (q_x,q_y) plane, and

$$\mathbf{A}(\mathbf{q},\omega)=\int_{-\infty}^{\infty}\frac{dp}{2\pi}\mathbf{A}(\mathbf{q},p,\omega). \tag{21}$$

The solutions of Eq. (9) can now be represented in the form

$$\mathbf{A}(\mathbf{q},p,\omega)=\lambda_{\text{eff}}^{-1}\mu(q,\omega)(q^2+p^2)[\mathbf{S}(\mathbf{q},\omega)-\mathbf{A}(\mathbf{q},\omega)]. \tag{22}$$

As follows from Eqs. (21) and (22), we write a relation between $\mathbf{S}(\mathbf{q},\omega)$ and $\mathbf{A}(\mathbf{q},\omega)$ in the form

$$\mathbf{A}(\mathbf{q},\omega)=\frac{\mu(q,\omega)}{\mu(q,\omega)+2q\lambda_{\text{eff}}}\mathbf{S}(\mathbf{q},\omega), \tag{23}$$

and therefore

$$S_y(\mathbf{q},\omega)-A_y(\mathbf{q},\omega)=\frac{2q\lambda_{\text{eff}}}{\mu(\mathbf{q},\omega)+2q\lambda_{\text{eff}}}S_y(\mathbf{q},\omega). \tag{24}$$

To calculate $S_y(\mathbf{q},\omega)$ Eq. (12) must be differentiated with respect to the coordinate x, since $S_y(\boldsymbol{\rho},t)=-\partial F(\boldsymbol{\rho},t)/\partial x$. As a result, we have

$$\Delta S_y(\boldsymbol{\rho},t)=-\frac{\Phi_0}{2\pi}\frac{\partial^2\varphi(x,t)}{\partial x^2}\delta(y). \tag{25}$$

A consequence of this equation is

$$S_y(\mathbf{q},\omega)=\frac{\Phi_0}{2\pi q^2}\int_{-\infty}^{\infty}dx\int_{-\infty}^{\infty}dt\,\exp(-iq\cos\vartheta x+i\omega t)\,\frac{\partial^2\varphi(x,t)}{\partial x^2}. \tag{26}$$

Combining expressions (26), (24), (20), and (15), we obtain an integrodifferential equation for the dynamics of the phase difference at a Josephson junction in the presence of magnetic ordering of any type in a superconducting film:

$$\sin\varphi(x,t)+\frac{\beta}{\omega_J^2}\frac{\partial\varphi(x,t)}{\partial t}+\frac{1}{\omega_J^2}\frac{\partial^2\varphi(x,t)}{\partial t^2}$$
$$=l_J\int_{-\infty}^{\infty}dx'\int_{-\infty}^{\infty}dt'K\left(\frac{x-x'}{2\lambda_{\mathrm{eff}}},t-t'\right)\frac{\partial^2\varphi(x',t')}{\partial x'^2}, \tag{27}$$

where $l_J=\lambda_J^2/\lambda$, λ_J is the Josephson penetration depth, and the kernel $K((x-x')/2\lambda_{\mathrm{eff}},t-t')$, which is nonlocal with respect to the spatial and time variables, has the form

$$K\left(\frac{x-x'}{2\lambda_{\mathrm{eff}}},t-t'\right)=\int_0^{\infty}\frac{dq}{\pi}\int_{-\infty}^{\infty}\frac{d\omega}{2\pi}\,\frac{2\lambda_{\mathrm{eff}}J_0[q(x-x')]\exp[-i\omega(t-t')]}{\mu(\mathbf{q},\omega)+2q\lambda_{\mathrm{eff}}}. \tag{28}$$

Here J_0 is a zeroth-order Bessel function. The temporal nonlocality of Eq. (27) is due to the frequency dispersion of the magnetic permeability $\mu(\mathbf{q},\omega)$.

3. Since $\lambda\gg a$ (a is the crystal lattice constant), it is natural to use a hydrodynamic description of the magnetic subsystem. Staying in the paramagnetic temperature range, we have for the magnetic permeability the expression[23]

$$\mu(\mathbf{q},\omega)=1+i4\pi\,\frac{\chi_0 Dq^2}{\omega+iDq^2}, \tag{29}$$

where χ_0 is the static magnetic susceptibility, and the spin diffusion coefficient for two-dimensional Heisenberg magnets is[24] $D=(1/3)(2\pi)^{1/2}Ja^2[s(s+1)]^{1/2}$ (J is the intralayer exchange parameter and s is the spin). Strictly speaking, the superconducting currents screen the long-wavelength part of the exchange and electromagnetic interactions, renormalizing the parameters of the magnetic subsystem.[25] However, since we are considering the paramagnetic temperature range and in what follows we shall be interested in an order-of-magnitude estimate, we shall neglect this circumstance.

Let us consider the spectrum of small-amplitude electromagnetic excitations

$$\varphi(x,t)=\varphi_0\exp[i(Qx-\Omega t)],\quad |\varphi_0|\ll 1, \tag{30}$$

propagating with wave vector Q and frequency Ω along a Josephson junction. From Eq. (27), taken together with Eqs. (28) and (29), in the nondissipative limit ($\beta=0$) and in the absence of a transport current and an external field, we obtain the following dispersion relation for $\hat{\Omega}=\hat{\Omega}(\hat{Q})$:

$$\hat{\Omega}^2=1+\frac{2}{\pi}l\hat{Q}^2I(\hat{Q}\hat{\Omega}), \tag{31}$$

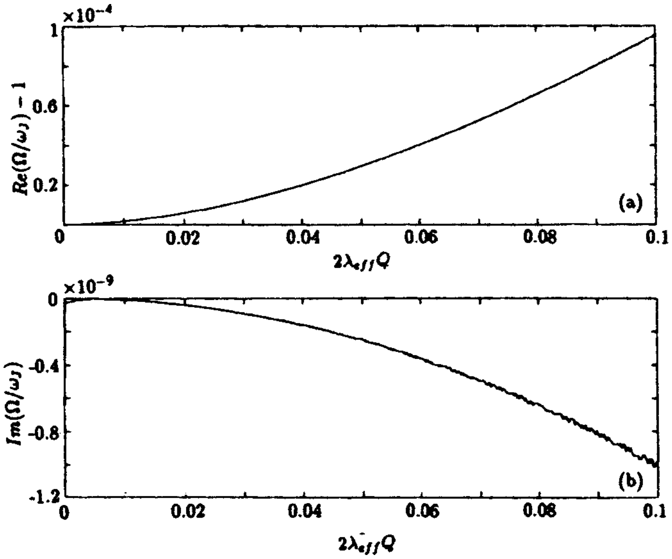

FIG. 1.

where

$$I(\hat{Q},\hat{\Omega})=\int_0^\infty dx\left[1+\hat{Q}\cosh x+\frac{4\pi\chi_0\hat{Q}^2\cosh^2 x}{b+\hat{Q}^2\cosh^2 x}\right]^{-1}, \tag{32}$$

and we have introduced the dimensionless quantities $\hat{Q}=2\lambda_{\text{eff}}Q$, $\hat{\Omega}=\Omega/\omega_J$, and the notation $l=l_J/2\lambda_{\text{eff}}$; $b=-i\eta\hat{\Omega}$; $\eta=\omega_J/\Omega_{\text{eff}}$; $\Omega_{\text{eff}}=D/(2\lambda_{\text{eff}})^2$. For $\chi_0=0$ (for a nonmagnetic superconductor) Eqs. (31) and (32) lead to the well-known spectrum, calculated in Ref. 17, of small-amplitude electromagnetic waves in the long- and short-wavelength regions. The frequency $\hat{\Omega}$ is a real function of the wave vector $\hat{Q}$, and there is no damping of the modes in the nondissipative limit. A different situation is observed for a magnetic superconductor with $\chi_0\neq 0$. The typical value for antiferromagnets is $\chi_0 \propto 10^{-3}$–10^{-5}. Numerical analysis showed that for $\chi_0\propto 10^{-3}$–10^{-4}, comparable to the susceptibility of the copper subsystem of HTSC materials, the implicit (with respect to $\hat{\Omega}$) equation (31), taken together with Eq. (32), gives a complex solution $\hat{\Omega}=\hat{\Omega}(\hat{Q})=\operatorname{Re}\hat{\Omega}(\hat{Q})+i\operatorname{Im}\hat{\Omega}(\hat{Q})$ with a small negative imaginary part satisfying the condition

$$|\operatorname{Im}\hat{\Omega}(\hat{Q})|/\operatorname{Re}\hat{\Omega}(\hat{Q})\ll 1. \tag{33}$$

This indicates the presence of damping of small-amplitude electromagnetic excitations as a result of the influence of the magnetic subsystem. Growing solutions are not found. Figure 1 shows the electromagnetic-wave spectrum, renormalized by the magnetic subsystem, and the damping decrement in a Josephson junction for the long-wavelength region $\hat{Q}\ll 1$ for $\chi_0=10^{-3}$, $l=10^{-2}$, and $\eta=10^3$. Figure 2 shows for the same values of the parameters the spectrum and damping decrement of small-amplitude electromagnetic waves in the short-wavelength region $\hat{Q}\gg 1$.

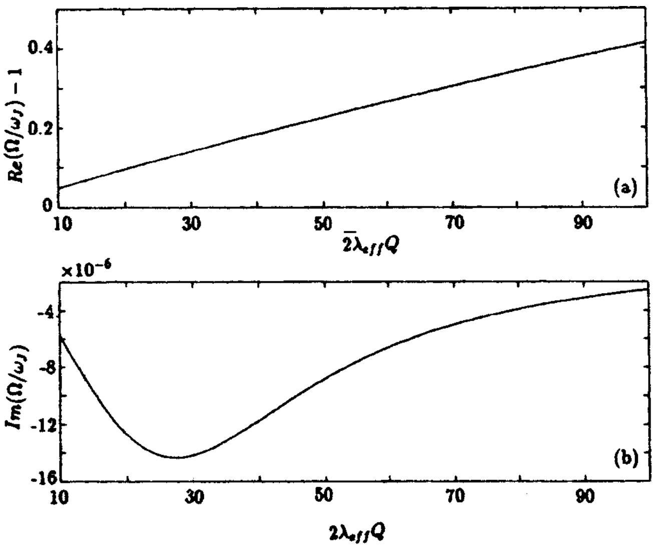

FIG. 2.

We are deeply grateful to the participants of Yu. V. Medvedev's seminar for critical remarks, A. S. Zel'tser for assisting in the numerical calculations, and V. N. Krivoruchko, Yu. E. Kuzovlev, Yu. G. Pashkevich, and A. É. Filippov for helpful discussions, interest, and encouragement.

*e-mail: medvedev@host.dipt.donetsk.ua

---

[1] A. I. Buzdin, L. N. Bulaevskiĭ, M. K. Kulich, and S. V. Panyukov, Usp. Fiz. Nauk **144**, 597 (1984) [Sov. Phys. Usp. **27**, 927 (1984)].
[2] A. I. Buzdin and L. N. Bulaevskiĭ, Usp. Fiz. Nauk **149**, 45 (1986) [Sov. Phys. Usp. **29**, 412 (1986)].
[3] Yu. A. Izyumov, N. M. Plakida, and Yu. N. Skryabin, Usp. Fiz. Nauk **159**, 621 (1989) [Sov. Phys. Usp. **32**, 1060 (1989)].
[4] M. B. Maple and O. Fischer (Eds.), *Superconductivity in Ternary Compounds II*, Springer-Verlag, New York, 1982; Mir, Moscow, 1985, p. 392.
[5] D. M. Ginsberg (Ed.), *Physical Properties of High-Temperature Superconductors I*, World-Scientific Publishers, 1989; Mir, Moscow, 1990, Ch. 4, p. 6.
[6] Yu. M. Aliev, V. P. Silin, and S. A. Uryupin, Sverkhprovodimost' **5**, 228 (1992) [Superconductivity **5**, 230 (1992)].
[7] A. Gurevich, Phys. Rev. B **46**, 3187 (1992).
[8] Yu. M. Aliev, V. P. Silin, and S. A. Uryupin, JETP Lett. **57**, 193 (1993).
[9] Yu. M. Aliev and V. P. Silin, Zh. Éksp. Teor. Fiz. **104**, 2526 (1993) [JETP **77**, 142 (1993)].
[10] Yu. M. Aliev and V. P. Silin, Phys. Lett. A **117**, 259 (1993).
[11] V. P. Silin, JETP Lett. **58**, 701 (1993).
[12] G. L. Alfimov and V. P. Silin, Zh. Éksp. Teor. Fiz. **106**, 671 (1994) [JETP **79**, 369 (1994)].
[13] V. P. Silin, JETP Lett. **60**, 460 (1994).
[14] Yu. M. Ivanchenko and T. K. Soboleva, JETP Lett. **51**, 114 (1990).
[15] Yu. M. Ivanchenko and T. K. Soboleva, Phys. Lett. A **147**, 65 (1990).
[16] Yu. M. Ivanchenko and T. K. Soboleva, Fiz. Tverd. Tela (Leningrad) **32**, 2029 (1990) [Sov. Phys. Solid State **32**, 1181 (1990)].
[17] R. G. Mints and I. B. Snapiro, Phys. Rev. B **51**, 3054 (1995).

[18] I.O. Kulik and I. K. Yanson, *The Josephson Effect in Superconducting Tunneling Structures*, Israel Program for Scientific Translations, Jerusalem, 1972; Nauka, Moscow, 1970.
[19] Yu. E. Kuzovlev and A. I. Lomtev, Zh. Éksp. Teor. Fiz. **111**, 1803 (1997) [JETP **84**, 986 (1997)].
[20] A. I. Lomtev, Zh. Éksp. Teor. Fiz. **113**, 2256 (1998) [JETP **86**, 1234 (1998)].
[21] E. M. Lifshitz and L. P. Pitaevskiĭ, *Statistical Physics*, Pergamon Press, New York [Russian original, Nauka, Moscow, 1978, Part 2, Ch. 5].
[22] H. Umezawa, H. Matsimoto, and M. Tatiki, *Thermo Fields Dynamics and Condensed States*, Elsevier, New York, 1982; Mir, Moscow, 1985, Chap. 11.
[23] B. I. Halperin and P. C. Hohenberg, Phys. Rev. **188**, 898 (1969).
[24] P. M. Richards and M. B. Salamon, Phys. Rev. B **9**, 32 (1974).
[25] A. I. Buzdin, JETP Lett. **40**, 956 (1984).

Translated by M. E. Alferieff

JETP LETTERS VOLUME 69, NUMBER 2 25 JAN. 1999

The de Haas–van Alphen effect in quasi-two-dimensional materials

P. D. Grigoriev
*L. D. Landau Institute of Theoretical Physics, Russian Academy of Sciences, 142432 Chernogolovka, Moscow Region, Russia**

I. D. Vagner
Grenoble High Magnetic Field Laboratory MPI-FRF and CNRS, BP 166 F-38042 Grenoble Cedex 09, France

(Submitted 19 November 1998; resubmitted 17 December 1998)
Pis'ma Zh. Éksp. Teor. Fiz. **69**, No. 2, 139–144 (25 January 1999)

We calculate the amplitude of magnetization oscillations for a quasi-two-dimensional electron system. In the two-dimensional case the behavior of this amplitude as a function of magnetic field and temperature differ completely from the conventional Lifshitz–Kosevich formula valid for three-dimensional metals. Previously only the ideal two-dimensional case has been considered, and the difference of the shape of the Fermi surface from cylindrical has not been taken into account. We obtain the general formula for the envelope of magnetization oscillations as a function of magnetic field, temperature, and the strength of the warping of the Fermi surface. This problem is important because of the great amount of interest in heterostructures and quasi-two-dimensional organic metals which has arisen in recent years. © *1999 American Institute of Physics.* [S0021-3640(99)01102-0]

PACS numbers: 71.18.+y

1. Introduction

The de Haas–van Alphen (dHvA) effect is very important for investigating the properties of metals, since it gives information about the Fermi surface and the cyclotron mass of electrons in these compounds. This effect was suggested in 1930 by L. D. Landau[1] and was first measured by de Haas and van Alphen in the same year.[2] Calculation of the magnetization as a function of magnetic field and temperature for an arbitrary electronic spectrum in three-dimensional metals was carried out in 1955 by Lifshitz and Kosevich.[3] Those authors assumed the chemical potential to be constant, which is a very good approximation in the three-dimensional (3D) case but is not valid for two dimensions. This difference arises because in three dimensions the spectrum of electrons is continuous (due to the *z* component of momentum) and the Fermi surface is intersected by many Landau levels (LLs). Therefore the chemical potential is approximately equal to the Fermi energy and does not oscillate with changing magnetic field. In a two-dimensional (2D) system the electron spectrum has gaps (between LLs), and the chemical potential (which is the minimum energy of a particle to be added to the system) is pinned to the highest occupied Landau level. When this LL becomes completely filled, the chemical potential jumps to the next LL. Such a jump has been detected by magnetization measurements in several single-layer, high-mobility 2D-electron-gas AlGaAs–GaAs heterostructures.[4] Thus the chemical potential in two dimensions oscillates strongly with varying magnetic field and must not be treated as a constant. This fact changes the amplitude and the form of magnetization oscillations completely.

Experimentally a significant departure from the conventional Lifshitz–Kosevich formula[3] has been observed in the number of the charge-transfer salts based on the molecule bis(ethylenedithio)tetrathiafulvalene (BEDT-TTF; Refs. 5–7) and in heterostructures.[4] A theoretical study of dHvA oscillations in the ideal 2D case (with a cylindrical Fermi surface and without Landau level broadening) has been performed by Vagner *et al.*[8] in order to explain dHvA measurements made on 2D GaAs/$\mathrm{Al}_x\mathrm{Ga}_{1-x}\mathrm{As}$ heterojunctions and graphite intercalation compounds. An analytical study of the 2D dHvA effect with broadened Landau levels at zero temperature $(T=0)$[9] and quite thorough numerical calculations[10] for a wide temperature region have been made, but in those papers the influence of warping of the Fermi surface on the magnetization oscillations is disregarded. That approximation is correct only if the size of warping is much smaller than LL broadening and temperature. In this paper we consider the opposite case, when this warping energy W is bigger than the scattering broadening of the LLs but less (not much less!) than the distance between LLs. The analytical formula for the amplitude of the magnetization oscillations is derived for an arbitrary ratio $W/2kT$. Since the magnetic-field, warping-energy, and temperature dependence of the amplitude of the dHvA effect contain information about the warping of the Fermi surface and the effective mass, our formula will be very useful for obtaining these parameters from experiment for many quasi-2D compounds.

2. Chemical potential

In order to calculate the magnetization we need first to obtain the expression for chemical potential $\mu(B)$. Let us write the number of particles as a sum over all LLs with a Fermi distribution function f_n:

$$N=\frac{ga}{2\pi\hbar}\sum_{n=0}^{\infty}\int_0^{\frac{2\pi\hbar}{a}} f_n dp_z, \tag{1}$$

where g is the degeneracy of a LL, a is the lattice constant in the z direction (the 2D layer separation in heterostructures), and N is the number of particles in one layer. The chemical potential is situated between the two LLs with energies $\hbar\omega_c(n_F-\frac{1}{2})$ and $\hbar\omega_c(n_F+\frac{1}{2})$, where $\omega_c=eB/m^*c$ is the cyclotron frequency. Since we assume $\hbar\omega_c\gg kT$, only these two Landau levels make contribution to thermodynamics. We can therefore set $f_n=1$ for all $n<n_F-1$ and $f_n=0$ for all $n>n_F$:

$$N=(n_F-1)g+\frac{ga}{2\pi\hbar}\int_0^{\frac{2\pi\hbar}{a}}(f_{n_F-1}+f_{n_F})dp_z. \tag{2}$$

The electron energy is given by $E=\hbar\omega_c(n+\frac{1}{2})+E_z$, where n is the number of the LL and the term $E_z=(W/2)(1-\cos(p_z a/\hbar))$ gives the dependence of the energy on the momentum along the z axis. For the ideal 2D case $W=0$, and $W\neq 0$ takes into account the warping of the Fermi surface. Later for convenience we shall use another expression for E_z:

$$E_z=(W/2)\cos(p_z a/\hbar). \tag{3}$$

The difference between expression (3) and the previous one consists solely of shifting the zero of energy by a constant $W/2$ (which of course does not change any physical result) and the shifting of the zero of the quasi-momentum p_z by $\pi\hbar/a$ (and that makes no difference because of the subsequent integration over the full period of p_z). Substituting the expression for $f_n=1/[1+\exp(E-\mu/kT)]$ into Eq. (2), we get

$$\begin{aligned}\frac{N}{g}-(n_F-1)=\frac{1}{2\pi}\int_0^{2\pi}&\frac{dy}{1+\exp(X_F-\alpha)\exp[(W/2kT)\cos y]}\\ &+\frac{1}{2\pi}\int_0^{2\pi}\frac{dy}{1+\exp(X_F+\alpha)\exp[(W/2kT)\cos y]},\end{aligned} \tag{4}$$

where $y=p_z a/\hbar$, $X_F=(\hbar\omega_c n_F-\mu)/kT$, and $\alpha=\hbar\omega_c/2kT$. In order to calculate the integral we will use the condition

$$\exp(-\alpha+W/2kT\pm X_F\ll 1 \tag{5}$$

which, as will be shown later, even for $W\sim\hbar\omega$ is equivalent to $\sqrt{\alpha}\gg 1$ and is usually fulfilled in the experiments. One can therefore expand Eq. (4) in the small parameter (5), keeping only first two terms:

$$\begin{aligned}\frac{N}{g}-(n_F-1)&=\frac{1}{2\pi}\int_0^{2\pi}\left[1-e^{X_F-\alpha}\exp\left(\frac{W}{2kT}\cos y\right)+e^{-X_F-\alpha}\exp\left(\frac{-W}{2kT}\cos y\right)\right]\mathrm{d}y\\ &=1-e^{-\alpha}\cdot 2\sinh X_F\cdot I_0\left(\frac{W}{2kT}\right),\end{aligned} \tag{6}$$

where $I_0(W/2kT)$ is the modified Bessel function of argument $W/2kT$. Now we have

$$N/g-n_F=\tilde{n}=-e^{-\alpha}\cdot 2\sinh X_F\cdot I_0(W/2kT). \tag{7}$$

Later we shall use the notation $\tilde{n}=N/g-n_F$. Equation (7) can be easily solved with respect to the chemical potential:

$$\sinh X_F=-\frac{\tilde{n}e^{\alpha}}{2I_0\left(\frac{W}{2kT}\right)}\Rightarrow\mu=\hbar\omega_c n_F+kT\sinh^{-1}\left(\frac{\tilde{n}e^{\alpha}}{2I_0\left(\frac{W}{2kT}\right)}\right). \tag{8}$$

Let us examine the limiting cases of the expression obtained for μ. For this purpose we need the asymptotic form of the modified Bessel function:

$$I_0(x)=1+\frac{x^2}{4}+\cdots,\quad x\ll 1, \tag{9}$$

$$I_0(x)=\exp(x)\cdot\sqrt{1/2\pi x},\quad x\gg 1. \tag{10}$$

For $W/2kT \ll 1$, formula (8) coincides with the expression for the chemical potential without warping of the Fermi surface:[8]

$$\mu = \hbar\omega_c n_F - kT \ln[(-\tilde{n}\cosh\alpha + \sqrt{1+\tilde{n}^2\sinh^2\alpha})/(1+\tilde{n})].$$

To show this let us simplify this expression using $\tilde{n}e^{\alpha} \gg 1$: $\mu \simeq \hbar\omega_c n_F - kT\ln(\tilde{n}e^{\alpha}/(1-\tilde{n}))$. Taking into account the identity $\sinh^{-1}x = \ln(x+\sqrt{1+x^2})$ and the inequality $\tilde{n}e^{\alpha} \gg 1$, we can rewrite formula (8) in the form $\mu = \hbar\omega_c n_F - kT\ln(\tilde{n}e^{\alpha})$. Thus in the limit $\tilde{n} \ll 1/\sqrt{\alpha}$ these formulas coincide.

3. Thermodynamic potential and magnetization

For calculating the thermodynamic potential we use its definition:

$$\Omega = -kT\frac{ga}{2\pi\hbar}\int_0^{\frac{2\pi\hbar}{a}}\sum_{n=0}^{\infty}\ln\left(1+\exp\left[\frac{\mu - E_n(p_z)}{kT}\right]\right)dp_z. \tag{11}$$

The calculation of the sum and integral is analogous to that done for the chemical potential.

Expanding in the same small parameter $\exp(-\alpha + W/2kT \pm X_F) \ll 1$ and separating the contribution from the last two LLs, we get

$$\Omega = g\sum_{n=0}^{n_F-2}\left(\hbar\omega_c\left(n+\frac{1}{2}\right)-\mu\right)+\frac{gkT}{2\pi}$$
$$\times\int_0^{2\pi}\left[\left(X_F - \alpha + \frac{W}{2kT}\cos y\right) - e^{X_F-\alpha}\exp\left(\frac{W}{2kT}\cos y\right)\right]dy + \frac{gkT}{2\pi}$$
$$\times\int_0^{2\pi}\left[-e^{-X_F-\alpha}\exp\left(\frac{-W}{2kT}\cos y\right)\right]dy.$$

After taking the integrals and sum we finally obtain

$$\Omega = g[(n_F^2/2)\hbar\omega_c - \mu n_F] - gkTe^{-\alpha}\cdot 2\cosh X_F \cdot I_0(W/2kT). \tag{12}$$

It is easy to check that in the limit $W/2kT \ll 1$ and $\tilde{n} \ll 1$ this formula coincides with the expression for the thermodynamic potential in the 2D case of ideally cylindrical Fermi surface[8]

$$\Omega = g\left[\frac{n_F{}^2}{2}\hbar\omega_c - \mu n_F + \frac{1}{2}\hbar\omega_c - kT\ln(2\cosh X_F + 2\cosh\alpha)\right]$$

(for proving this one should use $\cosh X_F \simeq |\tilde{n}|e^{\alpha}/2I_0(W/2kT) \ll \cosh\alpha$). The free energy

$$F = \Omega + \mu N = g\left\{\frac{n_F{}^2}{2}\hbar\omega_c + \left(\frac{N}{g} - n_F\right)\mu - kTe^{-\alpha}\cdot 2\cosh X_F \cdot I_0\left(\frac{W}{2kT}\right)\right\}. \tag{13}$$

Now we can calculate the magnetization

$$M = -\frac{\partial F}{\partial B} = -\frac{\partial F}{\partial\omega_c}\frac{e}{m^* c} - \frac{\partial F}{\partial g}\frac{S}{\Phi_0} - \frac{\partial F}{\partial\mu}\frac{\partial\mu}{\partial B} \tag{14}$$

(where $S-$ is the area of the sample and Φ_0- is the magnetic flux quantum). Now one only has to take this derivative accurately.

Since $g\hbar e/m^*c=\hbar\omega_c S/\Phi_0$ we get

$$M=\frac{S}{\Phi_0}\hbar\omega_c\left\{-n_F\tilde{n}+\frac{n_F}{2\alpha}\sinh^{-1}\left(\frac{\tilde{n}e^{\alpha}}{2I_0(W/2kT)}\right)+e^{-\alpha}\cdot I_0\left(\frac{W}{2kT}\right)\cosh X_F\cdot\left(-1+\frac{1}{\alpha}\right)\right\}. \tag{15}$$

This is the expression for the magnetization in the presence of warping of the Fermi surface. The only restriction on the magnitude W of the warping is that it must be not greater than energy difference between LLs.

Formula (15) is valid only in the narrow region

$$\tilde{n}\ll I_0(W/2kT)e^{-W/2kT}\simeq\min\{\sqrt{kT/\pi W},1\}, \tag{16}$$

where the condition (5): $\exp(-\alpha+W/2kT\pm X_F)\simeq\tilde{n}e^{W/2kT}/I_0(W/2kT)\ll 1$ is satisfied. What we are interesting in is the envelope of the magnetization oscillations, i.e., the amplitude of these oscillations as a function of magnetic field, temperature, and the size of the warping, because experimentally only this amplitude is detected. To calculate this amplitude one needs only the values of the maxima and minima of the magnetization oscillations. Thus if these extrema of the magnetization fall into these narrow regions of $\tilde{n}$ or B, then we can use formula (15) to calculate the envelope. As will be shown later, these extrema of $M(B)$ occur at $\tilde{n}\simeq 1/2\alpha$, so that the condition (16) is usually satisfied (this restriction for $W\sim\hbar\omega_c$ is equivalent to $\sqrt{\alpha}\gg 1$).

Let us turn to the calculation of the envelope of $M(B)$. Since $|\sinh X_F| =|-\tilde{n}e^{\alpha}/2I_0(W/2kT)|\gg 1$, then $\cosh X_F\simeq|\sinh X_F|=|\tilde{n}|e^{\alpha}/2I_0(W/2kT)$, and the expression for the magnetization (15) can be replaced by

$$M=\frac{SE_F}{\Phi_0}\left\{-\tilde{n}\left(1+\frac{1}{n_F}\right)+\frac{1}{2\alpha}\sinh^{-1}\left(\frac{\tilde{n}e^{\alpha}}{2I_0(W/2kT)}\right)\right\}, \tag{17}$$

where $E_F=\hbar\omega_c n_F$ is the Fermi energy of the electrons in the absence of a magnetic field. In order to find the amplitude of the magnetization oscillations one has to differentiate (17) with respect to B. Taking into account that $n_F(B)=\text{const}$ for each interval of B where the extrema occur, one gets:

$$\frac{\partial M}{\partial B}\approx\frac{\hbar\omega_c}{B}\frac{gn_F}{B}\left\{n_F+\frac{3}{2}-\frac{n_F}{2\alpha}\frac{1}{|\tilde{n}|}\right\}=0\Rightarrow\tilde{n}_{\text{ex}}=\pm\frac{1}{2\alpha}\frac{n_F}{n_F+3/2}. \tag{18}$$

The values B_{ex} of magnetic field at which the magnetization M has extrema are given by

$$B_{\text{ex}}=B^*\left(1\pm\frac{1}{2\alpha(n_F+3/2)}\right). \tag{19}$$

To obtain the envelope of the magnetization one should substitute the extremal values of $\tilde{n}_{\text{ex}}$ into (17) :

$$M_{\pm}=\pm\frac{SE_F}{2\Phi_0}\left\{\frac{1}{\alpha}\sinh^{-1}\left(\frac{e^{\alpha}}{4\alpha I_0(W/2kT)}\,\frac{n_F}{n_F+3/2}\right)-\frac{1}{\alpha}\,\frac{n_F+1}{n_F+3/2}\right\}. \tag{20}$$

All of the above calculations have been made for spinless electrons. To generalize them one should replace all $\hbar\omega_c$ in the resulting formula by the real distances between energy levels with the spin splitting taken into account. These distances will depend periodically on the magnetic field, and this period in the energy scale is equal to the LL separation. If the spin–orbit interaction is weak compared to the cyclotron energy, the spin-up states add one level between each two LLs with spin down no matter what is the ratio of spin-splitting energy to the distance between LLs (we assume that the g factor of the electrons does not depend on the magnetic field). In special cases when the spin-splitting energy is just n times the distance between LLs (to the precision of the temperature or LL broadening), formula (20) acquires only a factor of 2, because the effect of spin on the magnetization oscillations in this case is only to increase the degeneracy of the LLs by a factor of two. Since the temperature and LL broadening are usually not very small, such a situation is not rare. The envelope for the magnetization oscillations in this case becomes:

$$M_{\pm}=\pm\frac{SE_F}{\Phi_0}\left\{\frac{1}{\alpha}\sinh^{-1}\left(\frac{e^{\alpha}}{4\alpha I_0(W/2kT)}\,\frac{n_F}{n_F+3/2}\right)-\frac{1}{\alpha}\,\frac{n_F+1}{n_F+3/2}\right\}. \tag{21}$$

In the limit $W/2kT\ll 1$ and $n_F\gg 1$ this formula coincides with the previous one, obtained for the ideal 2D case:[8]

$$M_{\pm}=\pm\frac{SE_F}{\Phi_0}\left[1-\frac{1}{\alpha}\ln(2\alpha)-\frac{1}{\alpha}\right], \tag{22}$$

which is valid when the number n_F of filled LLs is large.

In the opposite case of large warping formula (20) becomes

$$M_{\pm}=\pm\frac{SE_F}{\Phi_0}\left[1-\frac{W}{\hbar\omega_c}+\frac{1}{\alpha}\ln\left(\frac{\sqrt{kT\cdot\pi W}}{\hbar\omega_c}\right)-\frac{1}{\alpha}\right]. \tag{23}$$

This formula differs substantially from the ideally 2D one (Eq. (22)). The amplitude of the oscillations depends approximately linearly on the size of the warping W.

4. Discussion

The formula (20) obtained here differs drastically from the 3D Lifshitz–Kosevich behavior. Instead of the exponential dependence on temperature of the 3D case, $M\sim\exp(-2\pi^2Tcm^*/e\hbar H)$, here the amplitude of the magnetization oscillations instead has a logarithmic dependence (Eq. (23)). The form of the oscillations in two dimensions is also dissimilar to the 3D case. Instead of smooth, nearly sinusoidal oscillations, where one may retain only the first few harmonics in the Lifshitz–Kosevich formula, in the 2D case we have a sawtooth form. The maxima and minima of the magnetization are separated by $\Delta\tilde{n}=n_F/\alpha(n_F+3/2)$ (see Eq. (18)), so the jumps are very sharp if $\alpha\gg 1$, i.e., if the temperature and LL broadening are much less than the cyclotron energy. This result has experimental confirmation.[4] Therefore, considering only the first few harmonics of the the magnetization oscillations becomes a bad approximation for obtaining the effective electron masses and other parameters of 2D compounds. The use of the conventional Lifshitz–Kosevich formula for processing the experimental data for quasi-2D materials may thus lead to incorrect results.

For many BEDT-TTF salts the effective mass m^* determined from the dHvA and Shubnikov–de Haas effects is found to be larger than the band mass m_b. This difference has been attributed to mass enhancement due to many-body renormalization.[11] Singleton *et al.*[12] have reported cyclotron resonance measurements indicating a cyclotron mass m_{CR} smaller by a factor of 5 than m^* on the closed orbit in the salt KHg(SCN)$_4$. They concluded that the transport mass is enhanced mainly by electron-electron interactions, whereas m_{CR} is independent of these short-range interactions, and the electron–phonon interactions may play only a minor role in the mass enhancement. Although the carrier on the relevant open orbit is also thought to be strongly correlated, direct evidence has not been obtained yet.[13] In this context it would be interesting to obtain the effective mass of these quasi-2D compounds from dHvA effect using our formula (20).

The authors thank A. M. Dyugaev for a helpful discussion. This work was supported by the Russian Fund for Fundamental Research under Grant 96-02-18168 and the INTAS-RFBR (Grant 95-553).

*e-mail: pashag@itp.ac.ru

---

[1] D. Schoenberg, Proc. R. Soc. London, Ser. A **170**, 341 (1939).
[2] W. J. de Haas and P. M. van Alphen, Leiden Commun. A **212**, 215 (1930); Proc. R. Acad. Sci. Amsterdam **33**, 1106 (1930).
[3] L. M. Lifshitz and A. M. Kosevich, Zh. Éksp. Teor. Fiz. **29**, 730 (1956) [Sov. Phys. JETP **2**, 636 (1956)].
[4] S. A. J. Wiegers, M. Specht, L. P. Levy *et al.*, Phys. Rev. Lett. **79**, 3238 (1997).
[5] N. Harrison, A. House, I. Deckers *et al.*, Phys. Rev. B **52**, 5584 (1995).
[6] P. S. Sandhu, G. J. Athas, J. S. Brooks *et al.*, Surf. Sci. **361-362**, 913 (1996).
[7] V. N. Laukhin, A. Audouard, H. Rakoto *et al.*, Physica B **211**, 282 (1995).
[8] K. Jauregui, V. I. Marchenko, and I. D. Vagner, Phys. Rev. B **41**, R12922 (1990).
[9] K. Jauregui, W. Joss, V. I. Marchenko, and I. D. Vagner, in *High Magnetic Fields in Semiconductor Physics III*, edited by H. K. V. Lotsch, Vol. 101 of Springer Series in Solid-State Sciences, Springer-Verlag, Berlin, 1992, p. 668.
[10] N. Harrison, R. Bogaerts, S. J. Blundell *et al.*, Phys. Rev. B **54**, 9977 (1996).
[11] N. Toyota, E. W. Fenton, T. Sasaki, and M. Tachiki, Solid State Commun. **72**, 859 (1989).
[12] J. Singleton, F. L. Pratt, M. Doporto *et al.*, Phys. Rev. Lett. **68**, 2500 (1992).
[13] T. Sasaki and N. Toyota, Phys. Rev. B **49**, 10120 (1994).

Published in English in the original Russian journal. Edited by Steve Torstveit.

JETP LETTERS VOLUME 69, NUMBER 2 25 JAN. 1999

Synthesis, structure, and formation mechanism of boron nitride nanotubes

T. S. Bartnitskaya, G. S. Oleĭnik, A. V. Pokropivnyĭ,*
and V. V. Pokropivnyĭ
*Institute of Materials Science, Ukrainian National Academy of Sciences,
252028 Kiev, Ukraine*

(Submitted 2 December 1998)
Pis'ma Zh. Éksp. Teor. Fiz. **69**, No. 2, 145–150 (25 January 1999)

The structure and mechanism of formation and growth are investigated for two forms of BN nanotubes produced by carbothermal synthesis. © *1999 American Institute of Physics.* [S0021-3640(99)01202-5]

PACS numbers: 81.05.Je, 81.05.Zx, 81.05.Ys

1. The synthesis of fullerenes and advances in high-resolution electron microscopy and nanotechnologies have in recent years generated great interest in carbon nanotubes (C-NTs) (see reviews[1,2]). They were synthesized by S. Iijima in 1991,[3] but they had been observed a comparatively long time ago in the products of the high-temperature decomposition of hydrocarbons, and chrysotile and halloysite microtubes have been observed even under natural conditions.[4] The fact that the electronic properties of NTs depend strongly on the chiral angle and the diameter[5] makes them promising as superconductors, molecular switches, and elements of three-dimensional integrated circuits. The high strength and flexibility of NTs under compression, stretching, bending, and twisting[6] give them unique possibilities for use as tips for atomic-force and scanning tunneling microscopes,[7] nanowhiskers, nanofibers of composite materials, and nanogears.[8] The similarity of the phase diagrams of C and BN (Ref. 9) suggests the existence of boron nitride analogs of fullerenes and nanotubes. Multilayer particles (onions) and nanotubes of boron nitride were recently obtained by the arc-discharge method.[10–12] It is interesting that they were observed in Refs. 13 and 14, but they were not investigated in detail at the time.

2. Boron nitride nanotubes (BN-NTs) were synthesized by carbothermal reduction of ultradisperse amorphous boron oxide with simultaneous nitriding at temperature 1100–1450 °C by reactions that can be summarized as $B_2O_3+3B_4C+7N_2=14BN+3CO$. The investigations were performed by molecular-dynamics simulation, transmission electron microscopy (TEM), and x-ray spectral microanalysis.

3. The most characteristic types of BN-TNs were found to be the following. 1) Cylindrical (Fig. 1). These NTs possess several forms: rectilinear (Fig. 1a), helical, smoothly curved or kinked, in the form of concretions along the outer surface, trillings, (Fig. 1b), and other forms (Fig. 1c). Most NTs terminate in a hemispherical cap at one or both ends (Fig. 2b). 2) NTs with a bamboo structure in the form of a succession of joined variable-diameter cylindrical NTs with caps or multilayer particles (onions) at the nodes

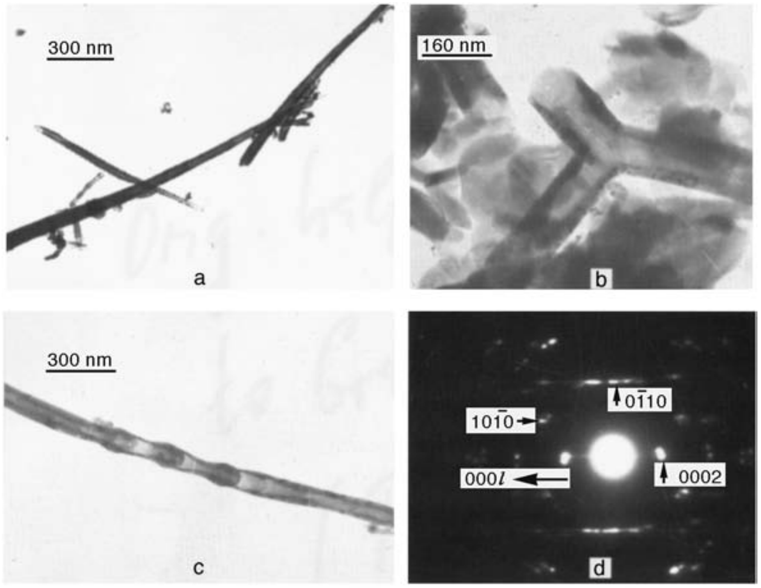

FIG. 1. Electron-microscope image of cylindrical BN nanotubes: a — rectilinear NTs; b — triple joint of NTs; c — change in the forms of growth of NTs; d — electron microdiffraction pattern from the fragment of a cylinder marked by an arrow in Fig. 1b.

(Fig. 2b). They often form bundles and clusters. 3) Nanotubes in the form of a combination of truncated cones, one inserted into another (Fig. 2c).

X-ray spectral analysis shows that NTs contain carbon. The quantity of carbon, as estimated from concretions of NTs, does not exceed 0.1 mass %. In the case of the NTs

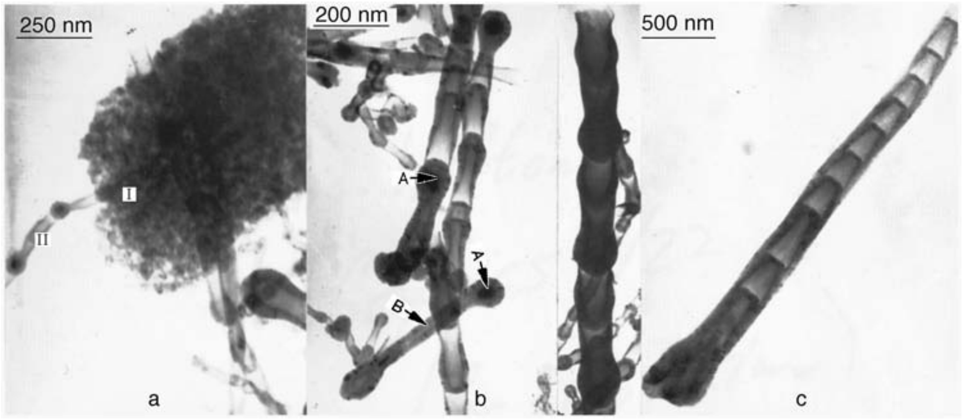

FIG. 2. Electron-microscope images of BN-NTs with the bamboo structure (a, b) and in the form of nested truncated cones (c): a — NT formed by growth in the solid (I) and gas (II) phases; b — concretions of NTs (A — carbon-enriched formations, B — cylindrical NT capped at both ends).

with the bamboo structure, the caps or onions contain carbon-enriched formations (Fig. 2b).

Electron microdiffraction patterns from individual NTs of all types indicated above always contain a series of strong $00l$ reflections (Fig. 1d). Comparing with the electron-microscope image shows that the long axes of the NTs coincide with the a axis of the graphitic BN, and their cylindrical surfaces are formed by the basal planes (0001). The characteristic features of other reflections in the electron microdiffraction patterns from NTs (on the basis of an analysis of the electron microdiffraction patterns from tubes consisting of natural minerals[5]) indicates that the BN-NTs consist of a set of coaxial cylinders. The a axes of the cylinders are most often nonparallel. This is indicated by the splitting of the $00l$ reflections in Fig. 1d. Apparently, the type and orientation of individual NTs in multilayer NTs can be very diverse because of the weak van der Waals bonds. The caps are open onions. Rings of point reflections 002 can be seen in the electron microdiffraction patterns from them. The rings indicate that the caps and onions are formed by the basal layers.

We found the minimum diameter of the NTs to be 10–20 nm and the maximum diameter to be 500 nm. As the outer diameter increases, the form factor (length to diameter ratio) increases. It equals 3–5 for tubes with the minimum diameter and 10–30 and more for tubes with the maximum diameter.

All types of NTs of various scales appear under the same conditions (temperature, nitrogen pressure). Often, the same NT contains fragments of tubes of different types, indicating a mechanism whereby one form of growth passes successively into another.

4. The atomic structure of the NTs (Fig. 3) was modeled by the molecular-dynamics method. A generator program was developed for this purpose. The program consisted of the following steps: 1) building up a planar hexagonal network with a fixed length L and perimeter P; 2) determination of the chiral angle $\theta=30^\circ-\tan^{-1}((n-m)/(n+m)3^{1/2})$ and identity period (distance between coincidence sites) $T=a(3(n^2+m^2+nm))^{1/2}$ according to the prescribed chiral numbers n and m, $a=0.14457$ nm; 3) rotation of axes by the angle θ: $x'=x\cdot\sin\theta+y\cdot\cos\theta$, $y'=x\cdot\cos\theta-y\cdot\sin\theta$; 4) cutting out a $P\times L$ rectangular sheet, where the perimeter P must be a multiple of T: $P=kT$; 5) calculation of the radius of the NT $R=P/2\pi$; 6) rolling up the sheet in the (x,z) plane, perpendicular to the y axis of the NT in accordance with the cylindrical transformation $x''=R\cdot\cos\psi$, $z''=R\cdot\sin\psi$, where $\psi=2\pi x'/P$. The BN-NTs can be constructed not only from a hexagonal network $(3:6^3)$ (Figs. 3d–3f) but also from a $(3:4,8^2)$ network[15] consisting of squares and octagons (Fig. 3g).

The covalent interaction B–N in graphitic BN was described using a new interatomic potential obtained by the embedded-atom method, $\varphi(r)=W\cdot\ln^2[\xi\rho(r)/\rho_0]/(r/r_k)^t-\varphi_0$, which automatically satisfies the condition $\varphi(r_0)=\varphi_0$, where $\varphi_0=-2.2$ eV is the equilibrium value of the potential at the nearest-neighbor distance $r_0=0.14457$ nm. The electron density $\rho(r)$ of hybridized sp^2 bonds can be expressed in terms of the parametrized atomic wave functions of nitrogen, which are given in Ref. 9. Its total value at the point r_0 is $\rho_0=0.282971$. The parameters of the potential $W=1.083426$ eV, $t=2.5668$, $\xi=0.245388$ were obtained by adjusting the binding energy, the lattice constant, and the bulk modulus of the basal plane. The energy of the NT is $U=\frac{1}{2}\Sigma\varphi(r_{ij})$. The relaxation energy is negligible, so that $U\simeq N_b\varphi_0$. The formation energy is $E_f=U$

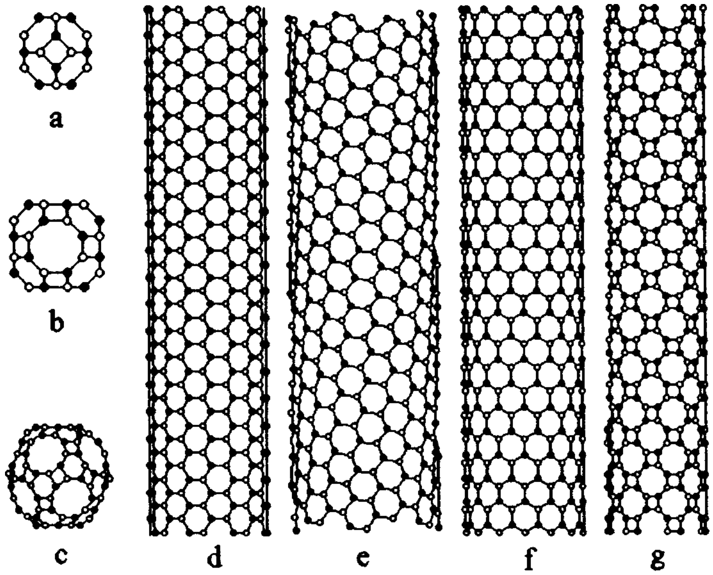

FIG. 3. Structure of BN molecules in BN-NTs with different configurations (N_a — number of atoms, N_b — number of interatomic bonds, θ — chiral angle, D — diameter, E_c/L — binding energy per unit length): a — $B_{12}N_{12}$ molecule; b — $B_{24}N_{24}$ molecule; c — $B_{60}N_{60}$ molecule; d — armchair NT ($\theta=30°$, $D=1.10$ nm, $N_a=640$, $N_b=944$, $E_c/L=17.1$ eV/nm); e — chiral NT ($n=7, m=11, \theta=22.7°, D=1.253$ nm, $N_a=653, N_b=960, E_c/L=10.7$ eV/nm); f — zigzag NT ($\theta=0°$, $D=1.116$ nm, $N_a=644$, C $N_b=952$, $E_c/L-13.5$ eV/nm); g — zigzag shaped NT rolled from a $(3:4,8^2)$-sheet ($D=1.257$ nm, $N_a=672$, $N_b=994$, $E_c/L=8.9$ eV/nm).

$-\frac{3}{2}N_a\varphi_0$. The linear binding energy was calculated as the difference of the energies of the broken bonds of equiatomic configurations of a tube and graphitic sheet per unit length $E_c/L \simeq \Delta N_b \varphi_0/L$. The atomic structure and binding energy of BN-NTs with the typical configurations is presented in Figs. 3d–3f. The figures also show analogs of fullerenes — $B_{12}N_{12}$, $B_{24}N_{24}$, and $B_{60}N_{60}$ molecules, the halves of which (Figs. 3a–3c) can serve as caps and growth centers of NTs. The fact that the $B_{12}N_{12}$ molecules, when packed in a simple cubic lattice, form a zeolite-type crystal, for example, with lattice parameter $A=0.554$ nm and density $\delta=2915$ kg/m^3, which are close to the parameters of the intermediate BN phase $A=0.565$ nm and $\delta=2760$ kg/m^3 (Ref. 16), serves as indirect proof of the existence of such structures.

5. Let us now analyze the mechanism of formation and growth of BN-NTs taking into account: a) the nonequilibrium conditions of synthesis and subsequent cooling, b) the building blocks (B and N atoms, BN rings, a small number of C atoms and their clusters formed as a result of gas-phase reactions, for example, $B_2O_3+3CO+N_2=2BN+3CO_2$), c) physicochemical processes (deposition from the gas phase, migration, crystallization), and d) electron-microscope data and the results of computer simulation of the mechanisms leading to the synthesis of BN-NTs.[17,18]

BN-NTs are formed in both the gas and solid phases (Fig. 2a). Growth of NTs occurs during deposition from the gas phase and surface migration of B and N atoms to the open ends or steps of a NT, as well as incorporation of BN clusters in the open or closed ends. Settling on onion or tube surfaces, the BN clusters stick and form growth centers. The growth of most NTs starts from the surface of concretions of BN nanoparticles (Fig. 2a). The growth centers most often appear on the surface of the onions, and less often on the NTs themselves (Fig. 2b). The structure and composition of these centers determine the internal structure of the tubes (long axis, chirality, layering). Secondary NTs, triple joints of NTs (Fig. 1b) and/or nanoparticles in the form of onions with the formation of concretions and bundles of tubes (Fig. 2b) often start to grow on the cylindrical surfaces of NTs. The NTs grow from onions with both open and closed shells. In the first case, the NTs grow as a continuation of the onion by deposition on a prismatic plane of the type (1120) or (1100), while in the second case the nucleus of a cylinder forms in the basal plane of the surface of an onion. When the thickness of the walls changes gradually, long NTs grow, and when the wall thickness increases rapidly, the NTs close. If the wall thickness increases, a convex cap with positive curvature in the direction of growth forms at the end; if the wall thickness decreases, a concave cap forms. Such caps become centers of new NTs, whose growth likewise is interrupted by the formation of onions, and so on. Such a successive change in forms of growth (NT → onion → NT → onion) leads to the formation of a bamboo structure (Fig. 2a and 2b). Growth of cylindrical tubes stops either when the free end is closed by an onion or by strong thinning of the wall in the direction of growth. When growth occurs in the form of nested truncated cones, the thickness of the walls within one cone remains essentially unchanged, but the outer diameter decreases in the direction of growth (Fig. 2c). For all forms of NTs, the outer diameter characteristically decreases in the direction of growth (Fig. 2c).

Nanotubes with the armchair configuration (Fig. 3d) grow preferentially to zigzag tubes (Fig. 3f),[17] since their binding energy is higher (Fig. 3). This is explained by the fact that the atoms at the tips of the latter are all of one kind. An equal concentration of the deposited B and N atoms in the case of the armchair BN-NTs leads to uniform growth, while in the case of zigzag tubes it leads to the appearance of weak homopolar B–B or N–N bonds, which in turn leads to the formation of metastable pentagons of the type B_3N_2, an amorphous tip, and the termination of growth.[17]

The thickening and narrowing of multilayer tubes are explained by the nonuniform growth of individual layers and the formation of cylindrical terraces. The formation of caps and cones of multilayer NTs is explained by disruptions of the hexagonal packing and the formation of five- and seven-membered rings. As molecular-dynamics calculations show, C_7 rings lead to the expansion of C-NTs, while C_5 rings lead to contraction and formation of sharp closed cones.[18] We note that neither we nor Chopra *et al.*[11] nor Loiseau *et al.*[12] observed sharp cones at the tips of BN-NTs. Instead, caps with flat faces at an angle of 90° to the axis of the NT were observed. Such valence angles are possible in BN molecules (Fig. 3a–c) and in a $(3:4,8^2)$ network of tubes in Fig. 3g. The formation of B_3N_4 heptagons together with B_3N_2 pentagons can lead to the formation of negative curvature fullerenes, which were predicted and named shwartzons in Ref. 19. The triple junction of tubes in Fig. 2b shows that they exist.

BN-NTs are often terminated by amorphous particles with the intermediate composition BNC because of nonequilibrium conditions. Growth in the solid phase occurs as the particles crystallize. On cooling after synthesis, a temperature gradient arises from the surface to the center of the particles. This gradient leads to decomposition of the solid solution BNC and the formation of precipitates with elevated carbon content inside the onion, which can be seen in TEM photographs in the form of beads or nodes of a bamboo structure (Fig. 2). Some of the growth stages considered above agree with the growth mechanism proposed in Ref. 20 for C-NTs.

Some of the forms of BN-NTs, including that with the bamboo structure, have also been observed for C-NTs obtained under conditions of pyrolysis and in an arc discharge in the presence of impurities.[21,22] However, there are no nodes in pure BN-NTs obtained in an arc discharge in complete absence of carbon.[12] Therefore the bamboo structure of NTs is determined not by the production method, but rather by the influence of the impurities which promote a change in the forms of growth in the sequence NT → onion → NT → onion, and so on.

It can be expected that the presence of diatomic basal layers and an ionic component of the interatomic bonds B^+–N^- in BN-NTs, as compared with C-NTs, will expand the possibilities of obtaining alternative layered structures and will give new properties and applications.

*e-mail: pokr@ipms.kiev.ua

---

[1] A. V. Eletskiĭ, Usp. Fiz. Nauk **167**, 945 (1997).
[2] Yu. E. Lozovik and A. M. Popov, Usp. Fiz. Nauk **167**, 751 (1997).
[3] S. Iijima, Nature (London) **354**, 56 (1991).
[4] G. S. Gritsaenko, B. B. Zvyagin, R. V. Boyarskaya *et al.*, *Methods of Electronic Microscopy of Minerals*, Nauka, Moscow, 1968.
[5] J. B. Wildoer, L. C. Venema, A. G. Rinzler *et al.*, Nature (London) **391**, 59 (1998).
[6] B. I. Yakobson, C. J. Brabec, and J. Bernhole, Phys. Rev. Lett. **76**, 2511 (1996).
[7] H. Dai, J. H. Hafner, A. G. Rinzler *et al.*, Nature (London) **384**, 147 (1996).
[8] J. Han, Al Globus, R. Jaffe, and G. Deardorff, Nanotechnology **8**, 95 (1997).
[9] A. V. Kurdyumov, V. G. Malogolovets, N. V. Novikov *et al.*, *Handbook of Polymorphic Modifications of Carbon and Boron Nitride* [in Russian], Metallurgiya, Moscow, 1994.
[10] L. Boulanger, B. Andriot, M. Caucheiter, and F. Willaime, Chem. Phys. Lett. **234**, 227 (1995).
[11] N. G. Chopra, R. J. Luyken, K. Cherry *et al.*, Science **269**, 966 (1995).
[12] A. Loiseau, F. Willaime, N. Demoncy *et al.*, Phys. Rev. Lett. **76**, 4737 (1996).
[13] T. Ya. Kosolapova, T. S. Bartnitskaya, G. S. Oleĭnik, *et al.*, Preprint No. 5 [in Russian], Institute of Applied Mechanics, Ukrainian Academy of Sciences, Kiev, 1985.
[14] T. S. Bartnitskaya, T. Yu. Kosolapova, A. V. Kurdyumov *et al.*, J. Less-Common Met. **117**, 253 (1986).
[15] I. V. Stankevich, M. V. Nikerov, and D. A. Bochvar, Usp. Khim. **53**, 1101 (1974).
[16] A. V. Kurdyumov and A. N. Pilyankevich, in *Boron: Production, Structure, and Properties* [in Russian], Nauka, Moscow, 1974, p. 181.
[17] X. Blase, A. De Vita, J. C. Charlier, and R. Car, Phys. Rev. Lett. **80**, 1666 (1998).
[18] C. J. Brabec, F. Maiti, C. Roland, and J. Bernholc, Chem. Phys. Lett. **236**, 150 (1995).
[19] G. E. Scuseria, Chem. Phys. Lett. **195**, 534 (1992).
[20] X. F. Zang, X. B. Zang, G. Van Tendeloo *et al.*, J. Cryst. Growth **130**, 368 (1994).
[21] M. Endo, K. Takeuchi, S. Igarachi *et al.*, J. Phys. Chem. Solids **54**, 1841 (1993).
[22] Y. Saito, T. Yoshikawa, M. Okuda *et al.*, J. Phys. Chem. Solids **54**, 1849 (1993).

Translated by M. E. Alferieff

JETP LETTERS VOLUME 69, NUMBER 2 25 JAN. 1999

Quasielastic neutron scattering by diffusive adsorbed hydrogen as a possible cause of the energy spreading of ultracold neutrons during long storage in traps

Yu. N. Pokotilovskii*
Frank Laboratory of Neutron Physics, Joint Institute for Nuclear Research,
141980 Dubna, Moscow Region, Russia

(Submitted 17 November 1998)
Pis'ma Zh. Éksp. Teor. Fiz. **69**, No. 2, 81–86 (25 January 1999)

Small cooling and heating of ultracold neutrons during long storage in traps have been observed in recent experiments. It is shown that quasielastic neutron scattering due to the diffusive motion of hydrogen at the surface of adsorbed hydrogenous contaminants on the surface may be a possible cause of the spreading of the energy of ultracold neutrons during long storage in traps. © *1999 American Institute of Physics.* [S0021-3640(99)00102-4]

PACS numbers: 28.20.Cz, 29.25.Dz

1. Ultracold neutrons (UCNs) can be stored in a material trap if they have energies less than the boundary energy for the trap material.[1] The latter is usually about $(1-3)\times10^{2}$ neV, which corresponds to neutron velocities of $\sim(4-7)$ m/s. There is a widespread opinion that UCNs bounce perfectly elastically from the walls of the trap, provided that they survive the wall encounter. The UCN loss probability per reflection is usually $\sim10^{-5}-10^{-3}$, depending on the material, its temperature, and, what is the most important in the majority of experiments, the presence of hydrogenous contaminants on the surface of the wall. The main causes of UCN losses in material traps are inelastic scattering, with the acquisition of energy of the order of the wall temperature ($10^{-3}-10^{-1}$ eV) and the subsequent escape from the trap, and neutron capture by the nuclei of the wall.

Recently two experimental groups observed a small energy change in UCNs during long storage in closed traps.

The UCN energy increase was observed[2,3] in a stainless steel chamber for a primary energy of stored UCNs in the range from 0 to $\simeq100$ neV. The results were described in Ref. 3 as an approximate doubling of the UCN energy with a probability $\sim10^{-5}$ per encounter with the wall of the trap during a storage time of 200 s. The finding of Ref. 2 was essentially an inexplicable and abnormal subbarrier UCN transmission through a thick (56 μm) beryllium foil, exceeding by many orders of magnitude the quantum-mechanical tunneling transmission. This effect of UCN anomalous transmission through foils was confirmed in Ref. 4 for 10 μm copper foils, with a comment that, most probably, this transmission should be attributed to an imperfect cleaning of the incident UCN

© 1999 American Institute of Physics

spectrum to remove neutrons of higher energies. This effect was not observed,[4] however, for thicker beryllium and 12-μm stainless steel foils. This anomalous transmission was then confirmed in a subsequent experiment[3] with aluminum foils, and, what is most important, it was demonstrated that the cause of this transmission is an increase in the UCN energy during the storage time. No explanation of the observed effects has been given before now.

On the other hand, according to the experiments of the second experimental group (Ref. 5), performed in a somewhat different way, UCN cooling and heating were observed, with a UCN energy transfer ~ 15 neV and with a probability per UCN reflection in the range of $3\times 10^{-4}-10^{-3}$ for several investigated materials: Ni, Cu, C, brass, and Be.

Suspicions about the possibility of small changes in the UCN energy in reflections on the trap walls were voiced many times long ago but without indicating any physical mechanism (see, for example, Ref. 6). The effect of possible undesirable wall sound vibrations was estimated in Ref. 7. The possible effect of the low-frequency part of the phonon spectrum of solids and the very questionable existence of low-frequency vibrating clusters in disordered solids were considered in Ref. 8.

Some special experiments were previously undertaken to search for small UCN energy changes during long storage. The authors[9] reported that for UCNs in the energy range of (6–28) neV, in copper traps with a measured loss coefficient of $\sim 10^{-3}$, they observed an overall negative shift of the UCN spectrum $\simeq$(2–3) neV after 140 s of UCN storage in the trap. But since there can hardly be any reason for a negative UCN energy change, in reporting their result they stated that the neutron energy change per reflection did not exceed 7×10^{-2} neV.

It is shown in this paper that the results obtained in the experiments[2,3,5] may be explained by the diffusive motion of hydrogen atoms in significant hydrogenous contaminants on the surface of the traps.

It must be mentioned that the way by which the quantitative conclusions were obtained in all the publications cited is approximate. Therefore, the scenario proposed in the present work cannot be an exact interpretation of these experiments but may only serve as an indication of the physical processes leading to the observed phenomena and as order-of-magnitude estimates of the observed effects.

2. The ordinary problem of UCN traps is significant hydrogenous contamination of the inner surface of the traps. The experiments[2,3] demonstrate very short experimental lifetimes for UCNs in a stainless steel chamber in comparison with the results obtained for traps that were cleaned and outgassed at high temperature in vacuum, and with calculations for a clean surface. It is possible to estimate, with high certainty, the UCN loss coefficient η per collision with the walls of the chamber from the measured storage time, size of the chamber, and the UCN spectrum.[2,3] Simple estimation gives $\eta\approx(3-4)\times 10^{-3}$, and this estimate is confirmed by a Monte Carlo simulation of the evolution of the UCN density in a chamber with the geometry of Ref. 3. The calculated loss coefficient for stainless steel is $\eta\simeq 10^{-4}$, which means that the experimental loss coefficient is 30–40 times larger than it must be for the clean stainless steel surface. According to Refs. 2 and 3 the chamber was not outgassed at high temperature in vacuum. In this case, such a large difference can be attributed to surface hydrogenous contamination, most probably adsorbed water, as has been confirmed in numerous experiments.[1]

Calculation for a quantum mechanical potential consisting of the stainless steel barrier and the water layer at the surface shows that the large UCN loss coefficient in Refs. 2 and 3 may be explained by hydrogenous layer $\geqslant 100$ Å thick adsorbed on or dissolved near the surface.

Hydrogen diffusion in this thick surface water layer may not differ very much from that in bulk water at room temperature, where the diffusion coefficient is $D \simeq 1.8 \times 10^{-5}$ cm^2/s. The assumption that diffusion in a thick, physically adsorbed water layer is not as rapid as in liquid water but more like that in ice does not basically change the proposed picture, because it is known from macroscopic measurements (confirmed by the neutron experiments[10]) that the diffusion coefficient in water changes only by approximately a factor of three in the range (–20, 20) °C. The hydrogen diffusion coefficients measured by quasielastic neutron scattering in water adsorbed on silica surfaces were found to be in the range $(2-8.5) \times 10^{-6}$ cm^2/s, depending on the degree of hydration.[11]

On the other hand, hydrogen dissolved in metals has in some cases a large diffusion constant. For example, the diffusion coefficient of atomic hydrogen in α-Fe at room temperature is as large as $D \approx 1.4 \times 10^{-5}$ cm^2/s or even more, depending on the particular experiment.[12]

In many cases hydrogen absorbed from the atmosphere or from a low vacuum absorbs dissociatively. In real experiments with UCNs hydrogen may be present on the surface in many different forms, with a variety of diffusion coefficients.

Generally the metal surface is covered with an oxide layer. There is very little information on hydrogen diffusion in oxides. Studies show that the microstructure and microchemistry of the underlying metal or alloy can affect the characteristics of the oxide and in turn the diffusion of hydrogen through the oxide. In certain cases the oxide layer may be a homogeneous medium for hydrogen diffusion, but in most cases it is heterogeneous and may contain extremely fine interconnected cracks and pores undetected by conventional microanalytical techniques. These cracks and pores are good sites for adsorbed hydrogenous contamination of the subsurface layer that is of importance in UCN experiments.

3. The total neutron quasielastic scattering cross section for the hydrogen atom is

$$\sigma_{\mathrm{qel}} = 4\pi b_{\mathrm{inc}}^2 (E/E_0)^{1/2} \simeq 80b,$$

where b_{inc} is the hydrogen incoherent scattering length. The inelastic neutron upscattering in the room temperature water (and in many different hydrogen containing compounds[13]) behaves as $\sigma_{\mathrm{inel}} \simeq (3-7)b \times 2.2 \times 10^5 / v_{\mathrm{UCN}}$ (cm/s). For a UCN energy $\simeq 50$ neV, the ratio $\sigma_{\mathrm{qel}}/\sigma_{\mathrm{inel}} \gtrsim 1.6 \times 10^{-2}$, decreasing with decreasing UCN energy, e.g., inelastic UCN upscattering dominates over quasielastic scattering and is the main mechanism of the UCN losses. For this particular stainless steel barrel, the probability per wall encounter of quasielastic scattering due to diffusive motion of surface hydrogen is less than $\sim 10^{-4}$. Indeed, the value reported in Ref. 3 for the probability of UCN heating with energy doubling in the case of a stainless steel chamber, $\approx 10^{-5}$, is more than two orders of magnitude lower than the measured total loss probability ($\sim 4 \times 10^{-3}$) in this experiment. More-accurate recent processing of the experimental data of Ref. 3 yielded much lower values for the probability of doubling of the UCN energy in a reflection:

between1) $\sim 5\times 10^{-7}$ and $\sim 10^{-6}$. Thus it seems that the small UCN heating and cooling due to diffusive motion of hydrogen, while interesting in itself, is not the main cause of anomalous UCN losses in material traps.

It is not yet clear whether diffusion scattering may dominate at lower temperatures, where the ''Gatchina anomaly''[14] takes place: it may happen in the case of abnormally high hydrogen diffusion at low temperatures.

At small changes in the neutron wave vector κ, the spreading of the scattering function (HWHM) is[15]

$$\delta E = \hbar \kappa^2 D. \tag{1}$$

For a primary UCN energy of $\simeq 50$ neV and a value of D equal to that in water, this gives $\delta E \simeq 3$ neV, and so for $\Delta E = \delta E \times n^{1/2}$, where $n \simeq 250$ is the number of collisions, we have $\Delta E \simeq 50$ neV. This scenario is confirmed by the observation in Ref. 3 that the energy gain during storage increases with the energy of the primary neutrons.

For simplicity, the spectrum of quasielastically scattered neutrons can be calculated using the classical diffusion model, which works well at the conditions $\kappa^2\langle R^2\rangle/6 \ll 1$ and $\kappa^2 D\tau_0 \ll 1$, where $\langle R^2\rangle$ is the mean squared radius of the vibrations of the hydrogen atoms and τ_0 is the mean time of vibration before a jump to another site in the diffusion process.[15] These conditions are satisfied very well even at UCN energies after upscattering as large (in comparison with the incident UCN energies) as 10 μeV, which is far outside the measurement conditions of the experiments.[2,3] In contrast to typical quasielastic neutron scattering experiments, where the energy distribution of the scattered neutrons is studied at fixed κ or the probability of the elastic scattering is studied as a function of κ or temperature, in the cited experiments with UCNs the scattering angle is not determined, and the energy change is accumulated as a result of many scattering events. When the expression for the differential cross section for quasielastic scattering in the classical limit[15]

$$\frac{d^2\sigma_{\mathrm{qel}}}{d\Omega\, d\epsilon} = \frac{b_{\mathrm{inc}} k}{\pi\hbar k_0}\,\frac{\kappa^2 D}{(\epsilon/\hbar)^2 + (\kappa^2 D)^2} \tag{2}$$

is integrated over solid angle, one obtains the differential quasielastic scattering cross section as a function of energy change ϵ:

$$\frac{d\sigma_{\mathrm{qel}}}{d\epsilon} = 4\pi b_{\mathrm{inc}}^2 \frac{a}{E_0} \ln\left[\frac{d^2 + b^2((1+d)^{1/2}+1)^4}{d^2 + b^2((1+d)^{1/2}-1)^4}\right], \tag{3}$$

where $a = \hbar/16\pi MD$, M is the neutron mass, $b = 2MD/\hbar$, and $d = \epsilon/E_0$, and E_0 is the incident UCN energy.

This cross section is an asymmetric function about $\epsilon = 0$, with the upscattering cross section dominating. Results of calculations of the differential cross section and probability of UCN quasielastic scattering due to diffusive motion of hydrogen atoms (the ratio of the quasielastic scattering to the total UCN loss probability at a wall encounter) are shown in Fig. 1 for different values of the diffusion coefficient. Computations show that the mean energy transfer $\langle\epsilon\rangle$ is much greater than the value of δE given by Eq. (1) in the energy range where the classical diffusion model is applicable. For the case of adsorbed hydrogen with a diffusion coefficient equal to that in water to water, the probability for

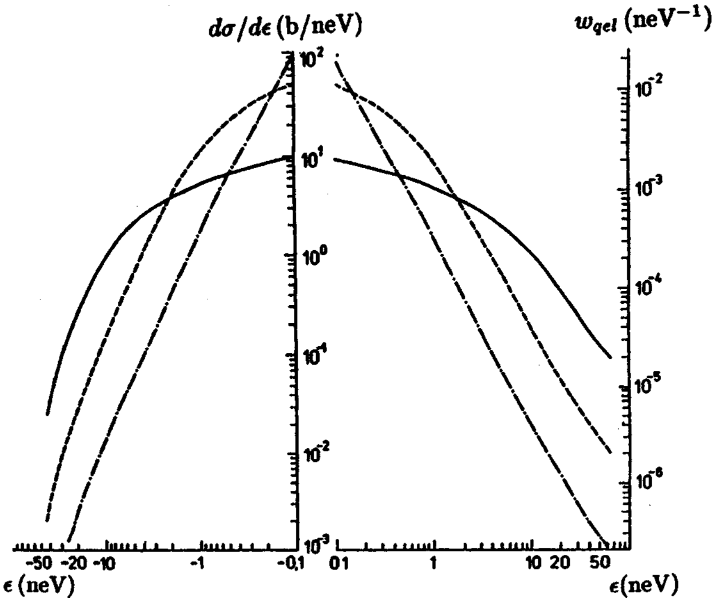

FIG. 1. Differential cross section $d\sigma/d\epsilon$ (b/neV) and relative (to the total loss) probability w_{qel} (neV^{-1}) of quasielastic UCN scattering due to diffusive motion of hydrogen atoms for different values of the diffusion coefficient D: solid line — $D = 1.85\times 10^{-5}$ cm^2/s; dashed line — $D = 1.85\times 10^{-6}$ cm^2/s; dot-and-dash line — $D = 1.85\times 10^{-7}$ cm^2/s. Incident neutron energy 50 neV.

UCNs with energy $E_0 = 50$ neV to acquire an energy $\epsilon > E_0$ in a quasielastic scattering event is about 5%, which, in combination with a probability of quasielastic scattering relative to inelastic scattering of $\approx 1.6\times 10^{-2}$ and a reflection probability of 4×10^{-3} fits the results of Ref. 3 quite well. The corrected$^{1)}$ value of the probability of doubling of the UCN energy in reflection, $\sim 5\times 10^{-7} - 10^{-6}$, needs a significantly lower adsorbed hydrogen diffusion coefficient than in liquid water. It is even more favorable for the proposed hypothesis of UCN quasielastic scattering on diffusive adsorbed hydrogen as a possible cause for small UCN heating and cooling during storage in traps.

According to the proposed scenario, the neutron spectrum after a UCN collision with a wall containing hydrogen contaminants is not the result of a ''doubling'' of the incident UCN energy, but is a broad, smooth distribution with a long tail at large energies, described by Eq. (3).

An additional important confirmation of this scenario is the observation of proportionality or at least a strong correlation between the probabilities of weak heating and the inelastic scattering of UCNs to the thermal energy range.[5] Both effects are proportional to the extent of hydrogen contamination of the surface.

For clean solid surfaces or at low temperatures, the observed effect of UCN heating,[3,5] according to our hypothesis, must be reduced or disappear.

*e-mail: pokot@nf.jinr.ru

1) E. V. Lychagin, private communication.

---

[1] A. Steyerl, *Springer Tracts in Modern Physics* **80**, 57 (1977); R. Golub and J. M. Pendlebury, Rep. Prog. Phys. **42**, 439 (1979); V. K. Ignatovich, *The Physics of Ultracold Neutrons*, Oxford, Clarendon, 1990 [Russian original, Nauka, Moscow, 1986]; R. Golub, D. J. Richardson, and S. Lamoreaux, *Ultracold Neutrons*, Bristol, Adam Hilger, 1991.

[2] V. E. Varlamov, P. Geltenbort, V. V. Nesvizhevsky *et al.*, JETP Lett. **66**, 336 (1997).

[3] V. V. Nesvizhevsky, P. Geltenbort, A. V. Strelkov, and P. Iaydjiev, ILL Annual Report 1997, p. 62; JINR Commun. P3-98-79, Dubna, 1998.

[4] Al. Yu. Muzychka, Yu. N. Pokotilovski, and P. Geltenbort, JETP Lett. **67**, 459 (1998).

[5] S. Arzumanov, L. Bondarenko, S. Chernyavsky *et al.*, in *Proceedings of the International Seminar on Interaction of Neutrons with Nuclei ISINN-6: ''Neutron Spectroscopy, Nuclear Structure, Related Topics,''* Dubna, 13–16 May 1998, p. 108; L. Bondarenko, E. Korobkina, V. Morozov *et al.*, ILL Experimental Report No. 3-14-44 (1997).

[6] I. M. Frank, JINR Preprint P3-7810, Dubna, 1974; Lecture at the II School on Neutron Physics, Alushta, April 2–19, 1974, p. 19.

[7] A. S. Gerasimov, V. K. Ignatovich, and M. V. Kazarnovsky, JINR Preprint P4-6940 [in Russian], Dubna, 1973.

[8] V. K. Ignatovich, JINR Preprint P4-8687 [in Russian], Dubna, 1975.

[9] Yu. Yu. Kosvintsev, Yu. A. Kushnir, and V. I. Morozov, Zh. Éksp. Teor. Fiz. **77**, 1277 (1979) [Sov. Phys. JETP **50**, 642 (1979)].

[10] J. Texeira, M. C. Bellisent-Funal, S. H. Chen, and A. J. Dianoux, Phys. Rev. A **31**, 1913 (1985).

[11] A. A. Tumanov and V. I. Zarko, Physica B **198**, 97 (1994).

[12] G. Alefeld and J. Völkl (Eds.), *Hydrogen in Metals*, Vol. 1, Springer-Verlag, 1978; Mir, Moscow, 1981.

[13] K. Knopf and W. Waschkowski, J. Neutron Res. **5**, 147 (1997).

[14] V. P. Alfimenkov, V. V. Nesvizhevsky, A. P. Serebrov *et al.*, LNPI Preprint No. 1729, Gatchina, Russia (1991); JETP Lett. **55**, 84 (1992).

[15] M. Bée, *Quasielastic Neutron Scattering*, Adam Hilger, Bristol, 1988.

Published in English in the original Russian journal. Edited by Steve Torstveit.

JETP LETTERS VOLUME 69, NUMBER 2 25 JAN. 1999

The decay $\phi \to \eta' \gamma$

V. M. Aul'chenko, M. N. Achasov, A. V. Bozhenok, A. D. Bukin,
D. A. Bukin, S. V. Burdin, I. A. Gaponenko, V. B. Golubev, T. V. Dimova,
S. I. Dolinskiĭ, V. P. Druzhinin, M. S. Dubrovin,* V. N. Ivanchenko,
P. M. Ivanov, A. A. Korol', S. V. Koshuba, A. A. Mamutkin,
E. V. Pakhtusova, S. I. Serednyakov, V. A. Sidorov, Z. K. Silagadze,
Yu. V. Usov, V. V. Sharyĭ, and Yu. M. Shatunov
Institute of Nuclear Physics, Siberian Branch of the Russian Academy of Sciences,
Novosibirsk State University, 630090 Novosibirsk, Russia

(Submitted 21 December 1998)
Pis'ma Zh. Éksp. Teor. Fiz. **69**, No. 2, 87–91 (25 January 1999)

A search for the process $e^+e^- \to \phi(1020) \to \eta'(958)\gamma$ in the decay channel $\eta' \to \pi^+\pi^-\eta$, $\eta \to \gamma\gamma$ was made in an experiment at the VEPP-2M e^+e^- collider with the SND detector. Analysis confirms the occurrence of $\phi \to \eta'\gamma$ decay with probability $B(\phi \to \eta'\gamma) = (6.7^{+3.4}_{-2.9}) \times 10^{-5}$. © *1999 American Institute of Physics.* [S0021-3640(99)00202-9]

PACS numbers: 13.65.+i, 13.25.Jx

In the last few years, rare ϕ meson decays with probability 10^{-4}–10^{-5} have become accessible for study in experiments performed at the VEPP-2M e^+e^- collider[1] with the SND and KMD-2 detectors.[2–8] One such process is the rare radiative decay $\phi \to \eta'\gamma$. The quark model predicts its probability to be in the range $B(\phi \to \eta'\gamma) = (0.7–1.0) \times 10^{-4}$. Thus far the decay $\phi \to \eta'\gamma$ has been observed with probability $B(\phi \to \eta'\gamma) = (1.35^{+0.55}_{-0.45}) \times 10^{-4}$ in one experiment with the KMD-2 detector.[7,8] In the present work, the existence of this decay is confirmed on the basis of an analysis of the SND data.

The experiment was performed in 1996–1997 with the SND detector in the VEPP-2M e^+e^- collider. The SND detector[9] is a universal nonmagnetic detector based on a three-layer spherical calorimeter consisting of 1630 NaI(Tl) crystals. The energy resolution of the calorimeter for photons can be described as $\sigma_E/E = 4.2\% \sqrt[4]{E(\mathrm{GeV})}$, and the angular resolution is $\sim 1.5°$. The solid angle of the calorimeter is 90% of 4π. A system of two cylcindrical drift chambers with a solid angle of 95% of 4π is used to measure the charged-particle angles. The azimuthal and polar angles are measured with accuracies of 0.4° and 2°, respectively. The data sample for the e^+e^- interactions was collected by repeated scanning of the energy interval $2E_0 = 980–1060$ MeV at 14 energy points. The corresponding total integrated luminosity was $\Delta L = 4.4\ \mathrm{pb}^{-1}$, and the number of ϕ mesons produced was 8.3×10^6. The total integrated luminosity was measured to within 3% for the processes $e^+e^- \to e^+e^-$ and $e^+e^- \to \gamma\gamma$ at large angles ($27° < \vartheta < 153°$).

The decay $\phi \to \eta'\gamma$ is studied in the process

$$e^+e^- \to \phi \to \eta'\gamma, \quad \eta' \to \pi^+\pi^-\eta, \quad \eta \to \gamma\gamma. \tag{1}$$

The background processes which impede the search for $\phi \to \eta'\gamma$ decay are

$$e^+e^- \to \phi \to \eta\gamma, \quad \eta' \to \pi^+\pi^-\pi^0, \tag{2}$$

$$e^+e^- \to \phi \to \pi^+\pi^-\pi^0, \tag{3}$$

$$e^+e^- \to \omega\pi^0 \to \pi^+\pi^-\pi^0\pi^0. \tag{4}$$

The basic problem in analyzing the process (1) lies in the fact that the reaction (2) gives a similar final state, and its cross section is two orders of magnitude larger. The processes (3) and (4) likewise have a similar state and can contribute to the process under study.

The following conditions were used for preliminary selection of events:

— number of charged particles $N_{cp}=2$; number of neutral particles $N_\gamma=3$;

— parameter characterizing the degree of energy–momentum conservation, $\chi^2_E<50$;

— minimum angle of emergence of particles relative to the beams $\theta_{\min}>27°$;

— spatial angle between the tracks $\alpha_{\pi\pi}<145°$;

— total energy release normalized to the energy in the center-of-mass system, $E_{\text{tot}}/2E_0<0.8$;

— normalized energy release for neutrals $E_{NP\text{tot}}/2E_0>0.4$.

The limit on the parameter $\alpha_{\pi\pi}$ makes it possible immediately to exclude the background from the process $e^+e^- \to \phi \to K_SK_L$, $K_S \to \pi^+\pi^-$ ($K_L \to$neutral particles) and the possible background from elastic e^+e^- scattering and higher-order QED processes, for example, $e^+e^- \to e^+e^-\gamma\gamma$. A total of 21103 events satisfying these conditions were found.

Analysis of the kinematics of the reaction (1) shows that among the three photons the recoil photon is always hardest $E_{\gamma3} \simeq 60$ MeV, while the photons from the decay $\eta \to \gamma\gamma$ have energies in the range 170 MeV $<E_{\gamma1}$, $E_{\gamma2}<440$ MeV. The photons are enumerated in order of decreasing energy. In the background process (2), among the three photons the recoil photon is hardest $E_{\gamma1} \simeq 362$ MeV, and the photons from the decay $\pi^0 \to \gamma\gamma$ have energies in the range 12 MeV $<E_{\gamma2}$, $E_{\gamma3}<364$ MeV. It should be noted that the probability of formation of a photon with energy close to the limits of the indicated intervals is low, in accordance with the phase volume of such configurations of events. For this reason, there is practically no combinatorial background for these processes, even when the finite resolution of the detector is taken into consideration.

The distribution of selected events over the recoil mass $m_{\text{rec}1}$ of the photon with highest energy and over the invariant mass m_{23} of less energetic photons were analyzed first. It was shown that a sharp peak at $m_{\text{rec}1} \sim m_\eta$ and $m_{23} \sim m_{\pi^0}$ from the reaction (2) stands out against the background of a wide distribution of events from the processes (3) and (4). An estimate of the expected number of all background events calculated by simulation[10] agrees well with the experimental data. The relative probability of the decay was estimated from the distributions to be $B(\phi \to \eta\gamma) = 1.20 \pm 0.03\%$, where only the

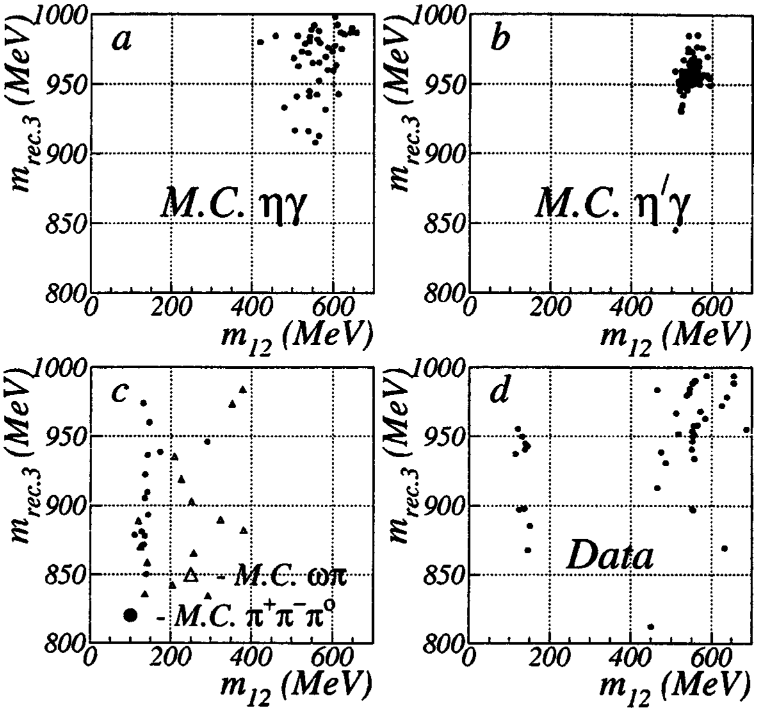

FIG. 1. Two-dimensional distribution of experimental (d) and simulated (a–c) events over the recoil mass m_{rec3} with the lowest energy and over the invariant mass m_{12} of the hardest photon pair in the search for $\phi \rightarrow \eta' \gamma$ decay. The number of simulated events is not normalized.

statistical error is given. The result obtained is only 5% less than the tabulated value,[11] confirming that there are no large systematic errors in the selection of events and in the determination of the detection efficiency. Further, the condition

$$\left(\frac{m_{\mathrm{rec1}} - m_{\eta}}{50} \right)^2 + \left(\frac{m_{23} - m_{\pi^0}}{35} \right)^2 > 1,$$

where the tripled resolutions (3σ in MeV) with respect to the corresponding masses of the η and π^0 mesons appear in the denominators, is used to exclude events due to the process (2). The kinematic features of the process under study are used to suppress the background events more effectively: The sum of the energies of the three photons is greater than 607 MeV; the energy of each photon from $\eta \rightarrow \gamma\gamma$ decay exceeds 170 MeV. This permits using the conditions

$$E_{NP\mathrm{tot}}/2E_0 > 0.5 \quad \text{and} \quad E_{\gamma 2}/E_0 > 0.45,$$

which decrease the contribution from the processes (3) and (4) by more than a factor of 20. Moreover, the condition

$$\zeta < 0,$$

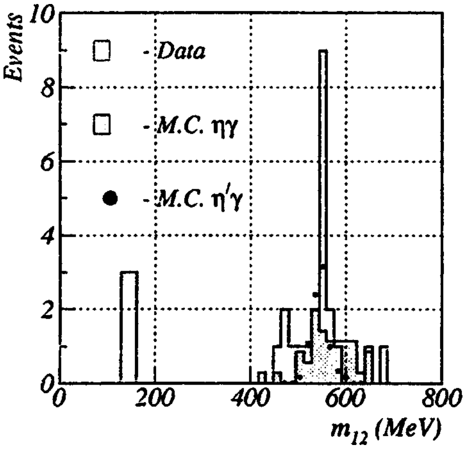

FIG. 2. Distribution of experimental and simulated events over the invariant mass of the photon pair with the highest energy in the search for $\phi \to \eta' \gamma$ decay.

which guarantees the quality of the photon showers in the calorimeter[12] on the basis of the transverse energy distribution, was used. After all of the conditions enumerated above were applied, the number of events decreased to 367.

The distribution of events over any of the invariant masses m_{13}, m_{23}, and m_{12} of the photon pairs shows that the events are concentrated near the π^0-meson mass, confirming their background nature. The conditions

$$|m_{13} - m_{\pi^0}| > 35\,\text{MeV} \quad \text{and} \quad |m_{23} - m_{\pi^0}| > 35\,\text{MeV}$$

were used to exclude such events. The second restriction strengthens the condition used to suppress events from the process $\phi \to \eta\gamma$.

The two-dimensional distribution of the 28 remaining events over the recoil mass $m_{\text{rec}3}$ of the photon with the minimum energy and the invariant mass m_{12} of the hardest photon pair are shown in Fig. 1d. Similar distributions for the simulated events of the desired and background processes are shown in Figs. 1a–c (the number of simulated events is not normalized). The simulation demonstrates (Fig. 2b) that the expected events of the desired process are clustered near $m_{\text{rec}3} \simeq m_{\eta'}$ and $m_{12} \simeq m_{\eta}$. The events of the background process (2) are distributed over a wider mass interval (Fig. 1a). To show the expected contribution from the processes (3) and (4), the events in Fig. 1c were selected without restrictions on the parameter $E_{\gamma 2}/E_0$. Nonetheless, they lie in the range $m_{12} < 400$ MeV and are well distinguishable from the events under study. The experimental distributions in Fig. 1d agree well with the hypothesis of a sum of the contributions from the processes (1), (2), and (3). The projection of the two-dimensional distribution on the m_{12} axis is shown in Fig. 2. The computed contributions from the desired process (1) for $B(\phi \to \eta' \gamma) = 10^{-4}$ and the main background process (2) are likewise shown in Fig. 2. Besides the peak at the η-meson mass, the background events of the process (3) form a peak at the π^0 mass. Figure 3 shows a second projection of the two-dimensional distribution on the $m_{\text{rec}3}$ axis with the additional condition

$$|m_{12} - m_{\eta}| < 35\,\text{MeV}.$$

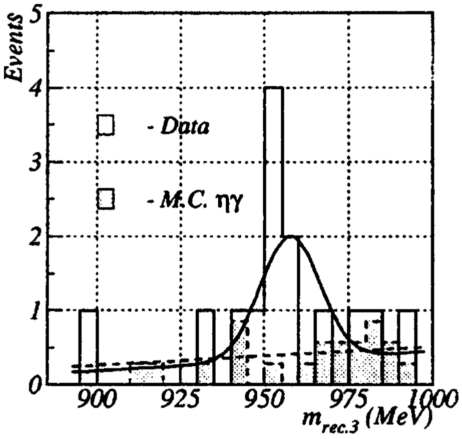

FIG. 3. Distribution of experimental and simulated events over the recoil mass of the photon with the lowest energy in the search for $\phi\to\eta'\gamma$ decay. The shaded histogram and the dashed line show the computed contribution from the background process $e^+e^-\to\eta\gamma$, $\eta\to\pi^+\pi^-\pi^0$ (2) and its approximation by a linear function. The histogram and the smooth curve show the distribution of experimental events and its optimal approximation.

The peak at the η'-meson mass confirms the existence of $\eta'\gamma$ decay. The histogram and the smooth curve in Fig. 3 show the distribution of 14 experimental events and their optimal approximation by a sum of a linear function and a Gaussian distribution with fixed parameters $m_{\eta'}=957.5$ MeV and $\sigma_{m_{\eta'}}=6.2$ MeV, obtained by simulating the process (1). The shaded histograms and the dashed line show the computed contribution from process (2) and its approximation by a linear curve. The difference in the background estimated from the experimental data and simulation does not exceed 0.6 events in the interval $m_\eta\pm 20$ MeV (2.6 and 3.2 events, respectively). The number of useful events in the peak is $N_{\eta'\gamma}=5.2^{+2.6}_{-2.2}$. The detection efficiency of the final state is $\epsilon_{\eta'\gamma}=5.5\pm 0.6\%$. From the tabulated values[11] of $B(\eta'\to\eta\pi^+\pi^-)$ and $B(\eta\to\gamma\gamma)$ we obtained $B(\phi)$. The systematic error is determined by the accuracy of the calculation of the detection efficiency for the selection conditions enumerated above and is approximately 15%.

The value obtained for the probability is approximately two times lower than the KMD-2 result,[7,8] but it is consistent with the latter because of the large measurement errors. The result obtained agrees with the predictions of the quark model.[13]

This work is partially supported by the Russian Fund for Fundamental Research (Grants Nos. 96-02-19192 and 97-02-18563) as well as by STP Integration (Grant No. 274).

*e-mail: M.S.Dubrovin@inp.nsk.su

---

[1] G. M. Tumaikin, in *Proceedings of the 10th International Conference on High Energy Particle Accelerators,* Serpukhov, 1977, Vol. 1, p. 443.
[2] S. I. Serednyakov, in *Proceedings of the HADRON-97 Conference,* 1997, p. 26.
[3] M. N. Achasov *et al.*, Phys. Lett. B **438**, 441 (1998).

[4] M. N. Achasov *et al.*, Phys. Lett. B **440**, 442 (1998).
[5] M. N. Achasov *et al.*, Preprint Budker INP 97-78, Novosibirsk, 1997; http://xxx.lanl.gov/abs/hep-ex/9710017.
[6] M. N. Achasov *et al.*, Preprint Budker INP 98-65, Novosibirsk, 1998; http://xxx.lanl.gov/abs/hep-ex/9809013.
[7] R. R. Akhmetshin *et al.*, Phys. Lett. B **415**, 445 (1997).
[8] R. R. Akhmetshin *et al.*, to be published in *Proceedings of the 29th International Conference on High-Energy Physics (ICHEP 98)*, Vancouver, Canada, 23–29 July 1998.
[9] V. M. Aulchenko *et al.*, in *Proceedings of the Workshop on Physics and Detectors for DAΦNE*, Frascati, Italy, April 9–12, 1991, p. 605.
[10] A. D. Bukin *et al.*, Preprint BudkerINP 92-93 (1992).
[11] Particle Data Group, Phys. Rev. D **54**, 536 (1996).
[12] A. V. Bozhenok, V. N. Ivanchenko, and Z. K. Silagadze, Nucl. Instrum. Methods A **379,** 507 (1996).
[13] P. J. O'Donnell, Rev. Mod. Phys. **53**, 673 (1981).

Translated by M. E. Alferieff